J Adv Ceram

Review

High-entropy ceramics: From paradigm formation to ordered development

Lei Su[1,2], Hongjie Wang[2,3,✉], Yanchun Zhou[4,✉]

Cite this article: Su L, Wang H, Zhou Y. *J Adv Ceram* 2026, **15**(6): 9221301. https://doi.org/10.26599/JAC.2026.9221301

ABSTRACT: High-entropy ceramics (HECs), defined as single-phase inorganic solid solutions comprising five or more principal elements in equimolar or near-equimolar ratios, have emerged as a frontier and hotspot in materials science over the past decade. Their expansive compositional space and diverse crystal structures open up new avenues for the design and performance regulation of ceramic materials. Initially, focused on proving the feasibility of entropy-stabilized phases, the field rapidly expanded into a vast, complex landscape of nonequimolar, multianionic, and medium-entropy compositions. This exploratory "great chaos" successfully validated the concept across diverse ceramic families and unlocked extraordinary properties, including ultrahigh temperature stability, exceptional radiation tolerance, ultralow thermal conductivity, and superior energy storage density. The realization of performance-tailored HECs fundamentally depends on rational compositional design and precise control of preparation processes, core challenges that remain at the heart of current research. However, a clear "scissors gap" has emerged between the rapid accumulation of experimental data and the lag in theoretical frameworks and data comparability. This review synthesizes a decade of research to chart a crucial transition "from chaos to order". It formulates emerging design paradigms for targeted applications such as oxidation-resistant ultrahigh temperature ceramics (UHTCs), thermal barrier coatings, durable nuclear materials, and high-performance energy storage and conversion materials. The analysis highlights the shift from discovery to quantitative efforts integrating computational thermodynamics, advanced characterization, and machine learning (ML). Despite remarkable progress, significant bottlenecks persist in processing, standardized characterization, and scaling from powder to component. The future roadmap emphasizes establishing robust structure–property relationships, fostering community-wide data standards, and advancing rational, physics-, and artificial intelligence (AI)-guided design to systematically realize the immense technological potential of HECs.

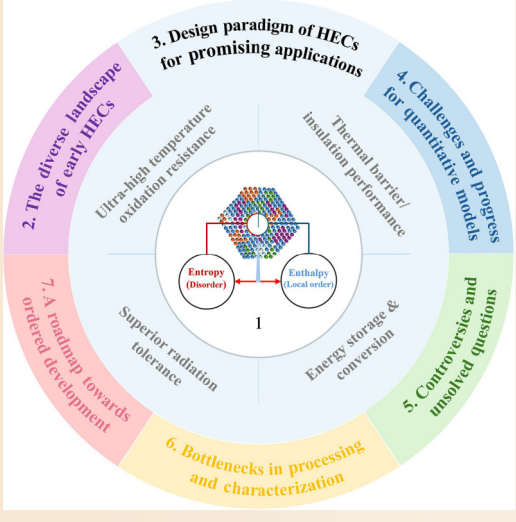

KEYWORDS: high-entropy ceramics (HECs); enthalpy; paradigm formation; rational design; ordered development

1 Introduction

The field of materials science has witnessed the meteoric rise of high-entropy ceramics (HECs) over the past decade [1–4]. Defined as single-phase inorganic solid solutions comprising five or more principal elements in equimolar or near-equimolar ratios, HECs leverage the profound high-entropy effect to stabilize unprecedented multication configurations within classic ceramic crystal structures [1–6]. This paradigm shift has unlocked a vast, largely unexplored compositional space, promising a new frontier for designing materials with tailored properties [1,2,6]. The initial phase of HEC research has been phenomenally successful, conclusively proving the existence of these materials and demonstrating their exceptional potential in areas ranging from ultrahigh temperature ceramics (UHTCs), thermal barrier coatings, and wear-resistant components to efficient energy storage dielectrics and robust catalysts [7–12]. However, this success has given rise to a period of "great chaos" [13–15].

In compositional design, the initial paradigm of equimolar five-component design has rapidly expanded into a vast and complex landscape. This now includes nonequimolar ratios [16–18], medium-entropy configurations [19–21], multiprincipal element systems [15,22,23], and multianionic compounds (such as carbonitrides [24–27] and borocarbides [28,29]). The frontier has

[1] State Key Laboratory for Mechanical Behavior of Materials, Xi'an Jiaotong University, Xi'an 710049, China. [2] Shaanxi Laboratory of Advanced Materials, Xi'an Jiaotong University, Xi'an 710049, China. [3] State Key Laboratory for Porous Metals, Xi'an Jiaotong University, Xi'an 710049, China. [4] Suzhou Laboratory, Suzhou 215000, China.

✉ Corresponding authors. E-mail: H. Wang, hjwang@xjtu.edu.cn; Y. Zhou, yczhou@alum.imr.ac.cn

Received: February 28, 2026; Revised: April 16, 2026; Accepted: April 16, 2026

even extended to intricate systems incorporating engineered vacancies or interstitial elements [30–34]. This explosion of possibilities has led to an exponentially growing design space. However, this abundance highlights a critical challenge: the lack of robust and universally applicable screening principles. The field often relies on trial-and-error approaches, and the thermodynamic and kinetic rules governing the formation and stability of these complex compositions, especially under nonequilibrium processing conditions, remain inadequately defined. While configurational entropy is a key design parameter, thermodynamic stability often involves a balance of enthalpy and entropy, and many reported "high-entropy" phases may be metastable. This complexity is further amplified when pursuing specific functionalities, where the interplay between entropy and targeted property metrics is not yet quantitatively understood.

In structural control, the early focus on achieving single-phase solid solutions has given way to a more sophisticated and deliberate approach to microstructure engineering. Researchers are now actively constructing multiphase architectures (e.g., high-entropy matrices with tailored secondary phases) [35–38], nanocomposites [39,40], graded structures [41–43], and porous morphologies [44–48]. Concurrently, the fundamental understanding of the "high-entropy" structure has deepened profoundly. Investigation has moved beyond the concept of "lattice distortion" to probe atomic-scale phenomena such as local chemical ordering, the formation of specific chemical clusters, and their complex coupling with various defect types [49–55]. This intricate hierarchy of structure, from atomic-scale ordering to nanoscale phase separation and microscale composites, creates a "kaleidoscope" of microstructures. A significant challenge lies in precisely controlling these multilevel structures and, more importantly, deconvoluting their individual contributions to the final material properties [56–58].

In performance mechanisms, the field is currently dominated by qualitative and often overlapping conceptual descriptions to explain enhanced properties. Terms such as "high-entropy effect", "lattice distortion", "sluggish diffusion kinetics", and "cocktail effect" are frequently invoked. However, there is a severe shortage of quantitative, universal "structure–property" relationship models that can reliably predict performance [59–64]. When a property improvement is observed, it becomes exceptionally difficult to isolate and conclusively prove which specific mechanism is the dominant contributor. For instance, is the enhanced strength primarily due to severe lattice distortion, the solution strengthening from various elements, or perhaps the nanoscale precipitates? This ambiguity stems from the complex intertwining of these effects and the current limitations in both experimental characterization and computational modeling to decouple them, creating a significant bottleneck for rational design.

The field of HECs is thus at a critical inflection point, confronting its "original sins" and facing the urgent need to transition from simply proving existence to systematically establishing order. This review aims to navigate this crucial transition from proving existence to systematically establishing order. To achieve this, we will formulate reproducible paradigms, champion a quantitative leap in understanding, directly confront key controversies, and provide a definitive performance map. By synthesizing a decade of research into this "from chaos to order" roadmap, this review serves to guide the rational design and systematic development of high-entropy ceramics for the coming decade. Section 2 describes the early exploratory phase and the challenges that emerged. Section 3 formulates design paradigms for key application areas. Section 4 discusses quantitative efforts in thermodynamics, kinetics, and machine learning (ML). Section 5 addresses controversies and unresolved questions. Section 6 analyzes the processing and characterization bottlenecks. Section 7 presents a roadmap for future ordered development.

2 Diverse landscape of early HECs

The inaugural phase of HEC research was characterized by explosive growth and exploratory fervor [1–6]. This period successfully validated the core concept across virtually every major ceramic family—from oxides [4,65–68] and carbides [69–71] to borides [72,73], nitrides [74,75], and silicides [76,77]. However, this success fostered a landscape of immense diversity and complexity that, while rich in potential, also sowed the seeds of contemporary challenges. This formative era is critically examined here, focusing on the rapid expansion of the composition space, the deepening yet incomplete understanding of atomic-scale structure, and the emerging dilemma of qualitative, often ambiguous, performance descriptions.

2.1 Vast expansion of composition space

The initial paradigm for HECs was elegantly simple: five or more principal cations in equimolar ratios occupying a single sublattice within a known ceramic structure (e.g., rock-salt [4], perovskite [78], fluorite [79]), stabilized by configurational entropy. The validation of this concept in (Mg,Co,Ni,Cu,Zn)O served as a powerful proof-of-principle [4,80–83]. However, the field rapidly evolved beyond this original blueprint, embarking on a multifaceted expansion of compositional space that vastly increased both its complexity and potential [1–3,84–96] (Fig. 1).

The first and most straightforward expansion was the shift from strict equimolarity to nonequimolar or "nonideal" compositions. Researchers quickly realized that while the maximum configurational entropy occurs at equimolarity, practical property optimization often necessitates deviation [13,15–18,97–99]. Tailoring mechanical properties [100,101], catalytic activity [102–104], or optical band gaps [105,106] required fine-tuning individual element concentrations. This led to the exploration of medium-entropy compounds (with 3 or 4 principal elements) and high-entropy compositions with deliberately skewed ratios [15,19–21,49,107–113]. While this provided a powerful knob for property adjustment, it fundamentally complicated phase stability predictions. The stabilizing entropic contribution is reduced in such cases, placing greater emphasis on accurately modeling often unfavorable enthalpy terms.

A more profound expansion occurred through the engineering of the anion sublattice. The early focus on cation disorder naturally progressed to introducing disorder among anions. This gave rise to multianionic systems such as high-entropy oxynitrides [114,115], oxycarbides [93], carbonitrides [25–27,116], and borocarbides [28,29]. In these systems, not only cations but also anions (C, N, O, and B) randomly occupy their respective sublattice sites. This dramatically enlarges the design space and introduces new mechanisms for property control, such as modulating bond covalency, electronic structure, and defect chemistry. The anion sublattice is no longer a passive spectator but an active participant in the entropy-stabilization process, as it can deform to accommodate cationic size mismatches. This "reciprocal" character of many ceramics, with independently disorderable cation and anion sublattices, represents a unique and powerful feature of HECs compared to their metallic counterparts.

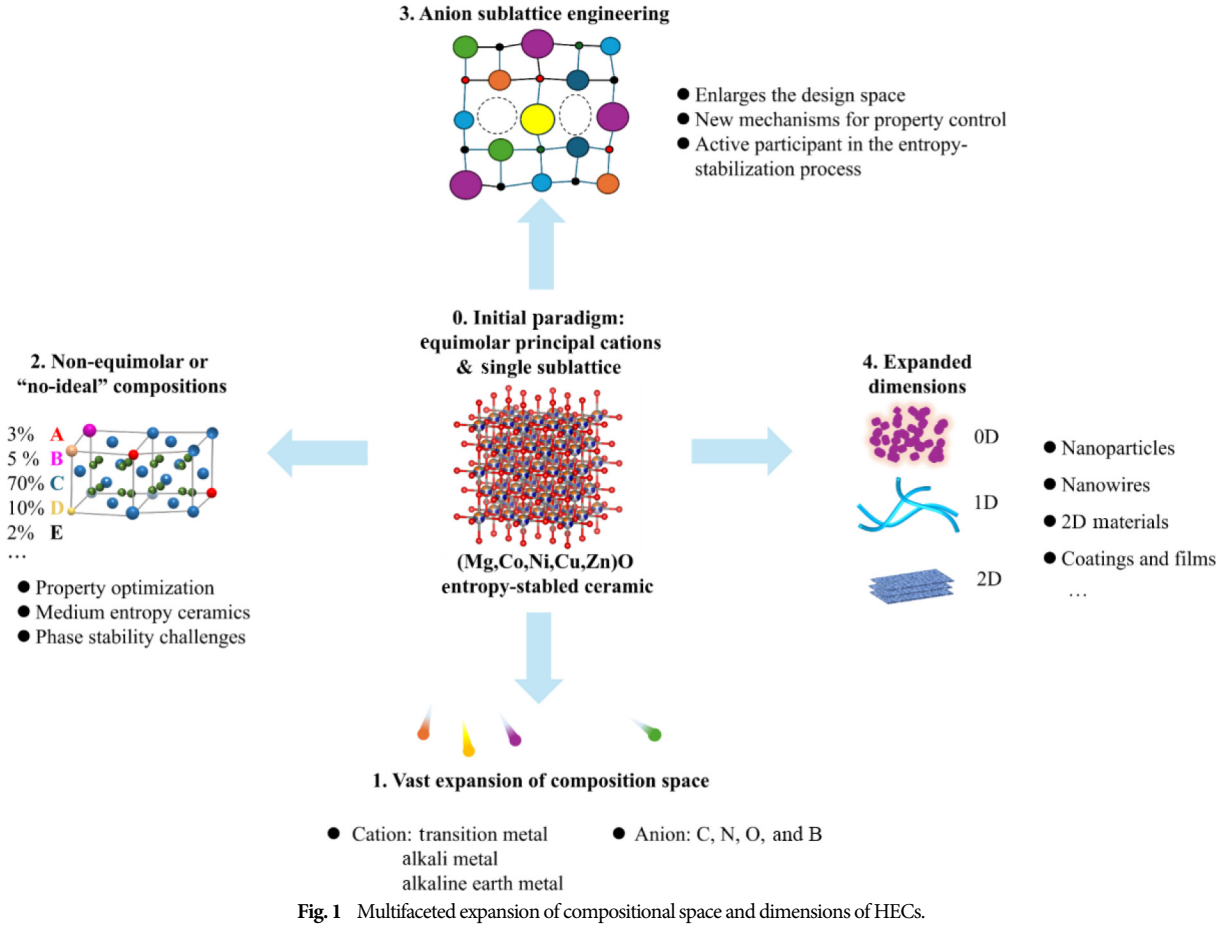

Fig. 1 Multifaceted expansion of compositional space and dimensions of HECs.

Concurrently, the field expanded dimensionally. While bulk synthesis via methods such as spark plasma sintering (SPS) and other sintering approaches dominated early works [117–120], the development of thin-film and coating techniques rapidly followed [121–124]. Magnetron sputtering, pulsed laser deposition, and other vapor deposition methods enabled the synthesis of high-entropy nitride, carbide, and oxide coatings with exceptional hardness, wear resistance, oxidation resistance, and functional properties [125–127]. Thin-film synthesis often operates under nonequilibrium conditions, allowing access to metastable single-phase compositions or amorphous structures not achievable in bulk. Furthermore, exploration extended to low-dimensional forms, such as nanoparticles synthesized by solution combustion or flame spray pyrolysis, and the nascent investigation of potential one-dimensional (1D) and two-dimensional (2D) HECs, promising novel electronic and catalytic properties [128–136].

This breathtaking expansion, from equimolar cations to tunable multianionic systems, from bulk to coatings and nanoparticles, successfully demonstrated the universality of the high-entropy concept across the ceramic kingdom. It transformed the field from a study of a specific phenomenon in rock–salt oxides into a vast new playground for materials design. However, this "combinatorial explosion" also created a central paradox: An exponentially growing design space was confronted by the near-absence of robust, predictive screening tools. The field transitioned from testing a clear hypothesis to navigating a vast, uncharted territory largely through empirical, trial-and-error approaches. This lack of guiding principles for compositional selection in such a complex parameter space became a primary bottleneck, highlighting the urgent need for advanced computational and data-driven approaches.

2.2 Deepening structural understanding

As shown in Fig. 2, the early confirmation of HECs relied heavily on X-ray diffraction (XRD) to verify the formation of a single-phase solid solution with the parent crystal structure and the absence of secondary phase peaks. While this was a necessary first step, it provided only a spatially and chemically averaged picture, masking the rich atomic-scale complexity inherent to these disordered systems. As research progressed, the structural understanding of HECs evolved significantly, moving beyond the simplistic "single-phase" label to grapple with the nuanced reality of local chemical environments.

The primary focus shifted to investigating and characterizing local chemical ordering, clustering, and short-range order (SRO) [137–140]. The ideal configurational entropy model assumes a perfectly random distribution of cations. In reality, enthalpy-driven preferences for certain local neighborhoods can lead to SRO or the formation of specific chemical clusters [13,137,141–144]. Advanced characterization techniques, such as extended X-ray absorption fine structure, neutron pair distribution function (PDF) analysis, and especially aberration-corrected scanning transmission electron microscopy (AC-STEM) with spectroscopic mapping, began to reveal this hidden order [52,141,145–149]. For example, in the prototypical (Mg,Co,Ni,Cu,Zn)O, studies revealed tendencies for Cu to induce specific local Jahn–Teller distortions and potential clustering [150–152]. The discovery that local order can exist within a long-range disordered framework was pivotal, as such SRO can significantly influence properties such as mechanical performance, magnetic coupling, dielectric response, and other properties [146,148,153–156].

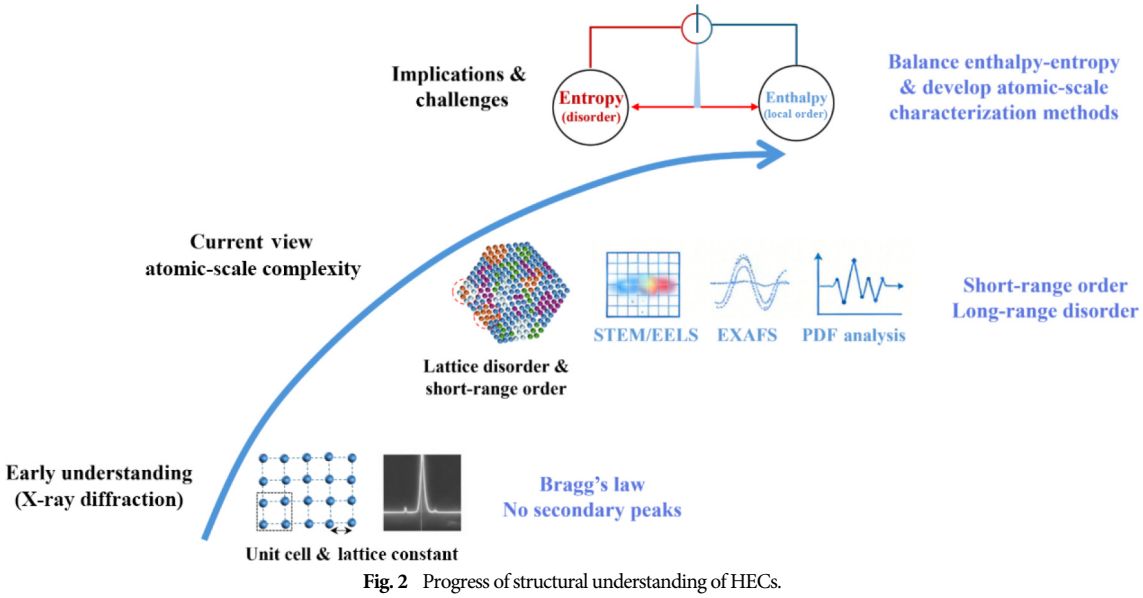

Fig. 2 Progress of structural understanding of HECs.

Closely related is the quantification of microscopic lattice distortion [52,53,68,140,157–163]. The severe lattice distortion postulated as a core effect was initially a theoretical concept. Experimentally, it manifests as broadening of XRD peaks and can be quantified more precisely using advanced diffraction and PDF analysis [157,158,161] as well as AC-STEM [52]. The distortion arises from the different ionic sizes, bonding preferences, and electronic configurations of the mixed cations, straining the ideal lattice. In oxides, the pliable oxygen sublattice can absorb some strain via local polyhedral distortions, but significant local bond length variations persist [52,157,158,164–167]. In rigid, strongly bonded carbides, nitrides or borides, the distortion might be more constrained, potentially leading to different strengthening mechanisms [159,160,168,169]. Research efforts focused on correlating the degree of lattice distortion, often estimated from the variance in ionic radii, with macroscopic properties such as hardness and thermal conductivity have been made [157,160,162,167,169].

This journey from simple "single-phase" verification to the investigation of SRO, clusters, and lattice distortion represented a critical maturation in the field's structural understanding. HECs are not merely "blurred" versions of simple ceramics but possess a unique hierarchical structure: a long-range crystalline order and short-range nonrandom chemical correlations, within which the sublattice exhibits a complex landscape of local distortions. However, this deeper understanding also revealed greater complexity. The interplay between entropy (favoring disorder) and enthalpy (favoring specific local arrangements) creates a delicate balance. Furthermore, the precise characterization of these atomic-scale features, especially in multicomponent systems, remains technically challenging. The field thus found itself with a more sophisticated, yet also more complicated, view of HEC structure, making the task of deconvoluting specific structural contributions to properties even more formidable.

2.3 Dilemma of adjectivized performance descriptions

The explosive growth in reported HEC compositions and properties was accompanied by a pervasive linguistic trend, the reliance on qualitative, overarching concepts to explain enhanced performance. Terms such as the "high-entropy effect", "severe lattice distortion", "sluggish diffusion", and the "cocktail effect" became ubiquitous in the literature (Fig. 3). While useful as a heuristic shorthand to describe the novel physical context of these materials, their overuse and imprecise application evolved into a significant epistemological dilemma, directly impacting data comparability and hindering mechanistic understanding.

The high-entropy effect is often invoked as a catch-all explanation for any property deviation from the rule-of-mixtures, be it positive or negative. This conflates thermodynamics (entropy stabilization of the phase) with its various kinetic and structural consequences (distortion, diffusion). Sluggish diffusion kinetics, for instance, is a hypothesized kinetic effect arising from a rough, multicomponent energy landscape for migrating species, but direct, conclusive experimental evidence distinguishing it from other rate-limiting steps can be elusive. The cocktail effect suggests synergistic property enhancements greater than the linear average, but it often serves as a descriptive label rather than a hypothesis with a testable atomic-scale mechanism.

This adjectivization of explanations creates two major problems. First, it obscures specific mechanisms. When a high-entropy carbide shows exceptional hardness, is it primarily due to lattice distortion (solid-solution strengthening), the prevention of dislocation motion by disparate atomic sizes, the stabilization of a nanograined microstructure, or a combination thereof? The blanket term "high-entropy effect" does not help differentiate. Second, and more practically, it severely compromises data comparability. Performance metrics (hardness, thermal conductivity, and catalytic activity) are highly sensitive to synthesis route, densification, grain size, porosity, and testing methodology. Without standardized reporting of these critical microstructural and processing parameters, reported property data for even nominally similar compositions can vary widely, making it difficult to discern intrinsic material behavior from extrinsic artifacts. This variability is evident in the broad ranges of properties reported for similar compositions across different studies.

This dilemma highlighted the growing gap between empirical discovery and fundamental understanding. It underscored the need for a more rigorous, quantitative language, one that seeks to disentangle overlapping effects, mandates comprehensive microstructural reporting, and aims to establish predictive structure–property relationships rather than merely describing outcomes with attractive but imprecise terminology (Fig. 3). This

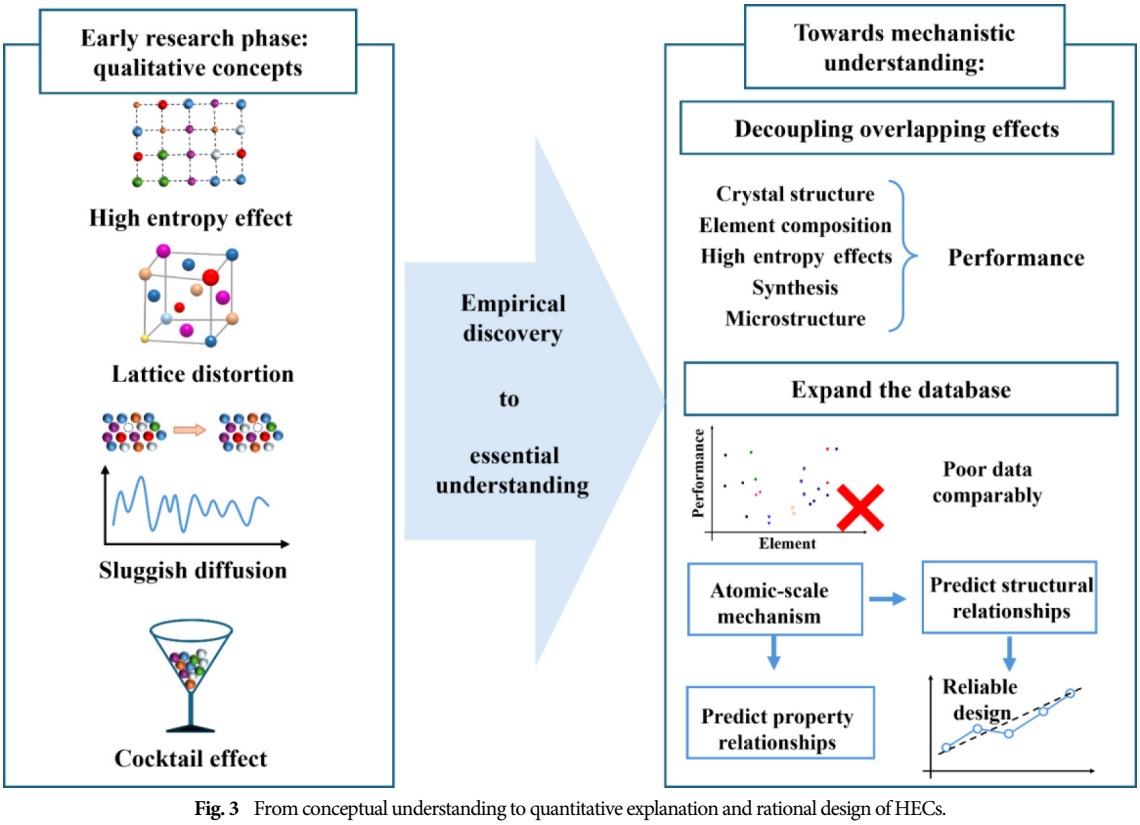

Fig. 3 From conceptual understanding to quantitative explanation and rational design of HECs.

recognition marked a turning point, fuelling the drive toward quantitative and computational efforts and the search for effective theoretical descriptors.

3 Paradigm formulation: Emerging paths toward rational design

3.1 Ultrahigh-temperature oxidation resistance

The oxidation resistance of traditional UHTCs, such as ZrB_2 and HfC, relies on the formation of single, high-melting-point oxides (e.g., ZrO_2, HfO_2) or low-viscosity glass phases (e.g., borosilicate) [170,171]. However, under ultrahigh temperatures (> 2000 °C) and high-speed gas flow scouring, these oxide layers are prone to volatilization, spallation, or destructive phase transformations. The core of the HEC design strategy not only enhances the thermodynamic stability, mechanical properties, and tunable thermal conductivity of the bulk material but also, more crucially, reprograms the oxidation process of the materials [69,171–173]. The goal is no longer merely to resist oxidation but to actively design the oxidation pathway so that the material *in-situ* generates a complex, multilayered, self-healing, and highly stable multifunctional oxide protective layer under extreme environments [172,173]. This protective layer typically consists of a high-melting-point complex oxide skeleton and a low-melting-point filler phase, working synergistically to block oxygen diffusion, resist mechanical scouring, and suppress component volatilization [174,175].

3.1.1 Intrinsic mechanisms for enhanced oxidation/ablation resistance in high entropy UHTCs

***In situ* construction of complex oxide protective layers.** (1) Skeleton formation. Elements such as Hf, Zr, Ta, and Nb tend to form high-melting-point complex oxide skeletons, such as $(Hf,Zr)_6(Ta,Nb)_2O_{17}$ (pyrochlore structure), $(Zr,Hf)TiO_4$, and Ti-doped $(Hf,Zr)O_2$ solid solutions [173,176,177]. This skeleton provides mechanical support against the shear force of high-speed gas flow. (2) Liquid phase filling and self-healing. Oxides of elements such as Ti, Si, B (TiO_2, SiO_2, and B_2O_3) or their eutectics with other oxides form a suitably viscous liquid phase at high temperatures [178,179]. This liquid phase infiltrates the pores and microcracks of the skeleton via capillary action, achieving dynamic self-healing and significantly hindering the inward diffusion channels for oxygen [180,181]. (3) Gradient structure and synergistic effect. The oxide layer typically exhibits a gradient in chemical composition and phase from the exterior to the interior, consisting of an outer dense oxide layer, a middle solid-liquid mixture layer, and an inner oxygen-diffusion/reaction layer [182,183]. In high-entropy UHTCs, component segregation and rapid diffusion are largely suppressed, allowing this gradient structure to remain stable during prolonged ablation [184].

Thermodynamic and kinetic control. The chemical potentials of elements in a high-entropy solid solution are similar, slowing down the rapid selective oxidation and volatilization (e.g., TiO (g)) of the thermodynamically most oxidizable elements (e.g., Ti) [185]. All elements act "collectively" to participate in building the protective layer by suppressing preferential oxidation and element volatilization [186,187]. Severe lattice distortion significantly reduces the diffusion rates of metal cations and oxygen ions, thereby lowering oxidation kinetics and leading to slower, denser growth of the protective layer [188,189]. The design of oxidation-resistant refractory high-entropy materials is fundamentally guided by thermodynamic principles, most effectively visualized through Ellingham diagrams, which plot oxide stability vs. temperature [185–187]. As shown in Fig. 4, for Group IV, V, and VI transition metals, clear periodic trends emerge: Group IV elements (Hf, Zr, and Ti) form the most stable, high-melting oxides, Group V oxides are less stable with lower melting points, and Group VI elements form volatile oxides detrimental to scale integrity [186]. Ellingham diagrams predict strong preferential

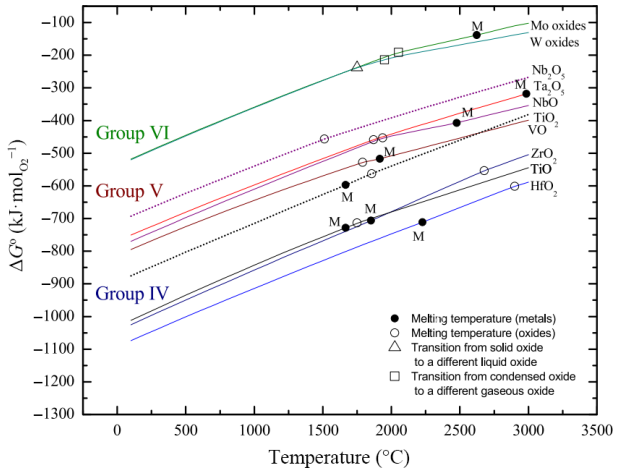

Fig. 4 Ellingham diagrams illustrate Gibbs free energy change per mole of O_2 for oxides of refractory metals from groups IV, V, and VI. Solid dots mark the melting points of metals, while open dots indicate those of oxides. Reproduced with permission form Ref. [186], © Acta Materialia Inc., 2020; Ref. [187], © Elsevier Ltd. 2018.

oxidation in multiprincipal component materials, as differences in Gibbs free energy among constituent oxides are substantial [185]. In the $(Hf_{0.2}Zr_{0.2}Ti_{0.2}Ta_{0.2}Nb_{0.2})C$ and $(Hf_{0.2}Zr_{0.2}Ti_{0.2}Ta_{0.2}Nb_{0.2})B_2$ systems, Group IV elements preferentially oxidize, dominating the scale, while the substrate is enriched in the less reactive Group V elements Ta and Nb [185,186]. Configurational entropy contributes minimally to the free energy of the reaction and is insufficient to override this thermodynamic hierarchy [185]. Oxidation kinetics and gaseous products also influence scale morphology. For carbides, CO (g) formation creates porous oxides; for diborides, liquid B_2O_3 seals pores, yielding denser, more protective Group IV-rich scales [186]. Ultimately, preferential depletion of key elements can destabilize the underlying solid solution, potentially forming secondary phases and compromising desired multiprincipal element characteristics [185].

3.1.2 Design strategies for oxidation/ablation-resistant high entropy UHTCs

High-melting-point element combination and screening. The foundation is selecting transition metal carbides/borides with extremely high melting points (HfC, ZrC, TaC, NbC, TiC, HfB_2, ZrB_2, etc.). First-principles calculations and the calculation of phase diagrams (CALPHAD) method are used to predict solid solution formability, phase stability, and elastic properties, screening for combinations that can form single-phase cubic rock salt (carbides) or hexagonal (borides) structures, such as the classic quinary system $(Ti_{0.2}Zr_{0.2}Hf_{0.2}Nb_{0.2}Ta_{0.2})C$ [190–192].

Medium-entropy and nonequimolar design for performance tuning. Moving beyond equimolar ratios, element proportions are adjusted ("medium-entropy" or nonequimolar high-entropy design) to precisely control oxidation behavior [193]. For example, increasing the Hf/Zr ratio enhances oxide skeleton stability; increasing the Ti ratio provides more liquid-phase TiO_2 to promote self-healing (Fig. 5(a)); adding Ta can suppress the formation of oxygen vacancies in $(Zr,Hf)O_2$ and form $(Hf,Zr)_6Ta_2O_{17}$, improving the viscosity and stability of the oxide layer to reduce oxygen diffusion channels at high temperatures [194,195] (Figs. 5(b) and 5(c)). One work shows that the nonequimolar design of $(Hf_{1/2}Zr_{1/3}Ti_{1/6})C$ achieves the optimal balance between skeleton and liquid phase, demonstrating ablation performance superior to its equimolar counterpart [196].

Carbon/boron stoichiometry control. For high-entropy carbides, the carbon vacancy concentration is a key design parameter. Deviating from stoichiometry (C/TM < 1) can (1) lower synthesis temperature and promote single-phase solid solution formation [197,198]. (2) Alter oxidation kinetics, potentially forming an oxycarbide transition layer initially as an oxygen diffusion barrier [199]. Operation within a precise "carbon window" is required to avoid precipitation of detrimental secondary phases (e.g., graphite or free metal) [200,201]. (3) Influence the degree of lattice distortion and electronic structure, thereby tuning the hardness and toughness [202,203].

Addition of Si/SiC. This is one of the most widely adopted strategies. During oxidation, the SiO_2 glass phase is generated through the oxidation of SiC. This liquid phase effectively seals cracks and pores, heals defects, and combines with the high-entropy oxide skeleton, significantly increasing the density and viscosity of the oxide layer to resist gas flow scouring [204–206]. Furthermore, SiC acts as a second phase to refine matrix grains and can improve the thermal conductivity of the materials to lower the surface temperature and thus increase the thermal stability [207,208].

Addition of rare earth elements (Y, La, Sc, etc.). Rare earth doping brings the "reactive element effect". The addition of Y has been proven to promote the formation of dense, adherent Al_2O_3 or Cr_2O_3 scales (in alloys); in high-entropy ceramics, it aids in forming more stable complex oxides, inhibits oxide layer spallation, and may promote the formation of amorphous oxide layers acting as effective oxygen diffusion barriers [209–211].

Introduction of Cr, Mo, W, etc. Cr addition can increase hardness (solid solution strengthening) and form Cr_2O_3 or complex chromates upon oxidation, aiding protection [212,213]. Oxides of Mo and W (e.g., WO_3), while potentially volatile, see their volatilization suppressed within the high-entropy system and can act as high-melting-point particles enhancing oxide layer stability, as reported for the $(Ti_{0.2}Zr_{0.2}Hf_{0.2}Ta_{0.2}Mo_{0.2})B_2$ [195] (Fig. 5(d)) and (Hf,Ta,Zr,W)C systems exhibiting excellent oxidation resistance [214,215].

Partial nitride substitution. Partially substituting C with N to form high-entropy carbonitrides (e.g., $(Ta_{0.2}Hf_{0.2}Zr_{0.2}Ti_{0.2}Nb_{0.2})C_{0.8}N_{0.2}$)) can further reduce thermal conductivity, increase hardness, and improve oxidation/ablation resistance by forming more complex oxide–nitride hybrid layers [216,217].

Dual-phase/multiphase HECs. Designing HEC-high-entropy boride (HEC-HEB) dual-phase ceramics, e.g., the (Hf,Nb,Ta,Ti,Zr)C-(Hf,Nb,Ta,Ti,Zr)B_2 system, allows the phases to pin each other, inhibiting grain growth and achieving fine-grain strengthening. During oxidation/ablation, the two phases can synergistically form a tougher, more complex oxide protective layer [218,219].

Fiber-reinforced composites. Combining a high-entropy ceramic as a matrix or coating with continuous carbon fibers (C_f) to prepare C_f/HEC or C_f/HEC-SiC composites. The fiber-reinforced composites show exceptional fracture toughness and damage tolerance, wherein the high-entropy matrix/coating provides ultrahigh temperature protection [220,222].

Metal-ceramic composites (cermets). Replacing traditional Co/Ni binders with high-entropy alloys (HEAs; e.g., CoCrFeNiCuMn, AlCoCrFeNi) and combining them with high-entropy ceramic or carbonitride powders. The high-entropy alloy binder typically offers better high-temperature strength, oxidation resistance, and compatibility with the ceramic phase, enabling materials with both high hardness and improved toughness for applications such as cutting tools and wear-resistant parts [223–225].

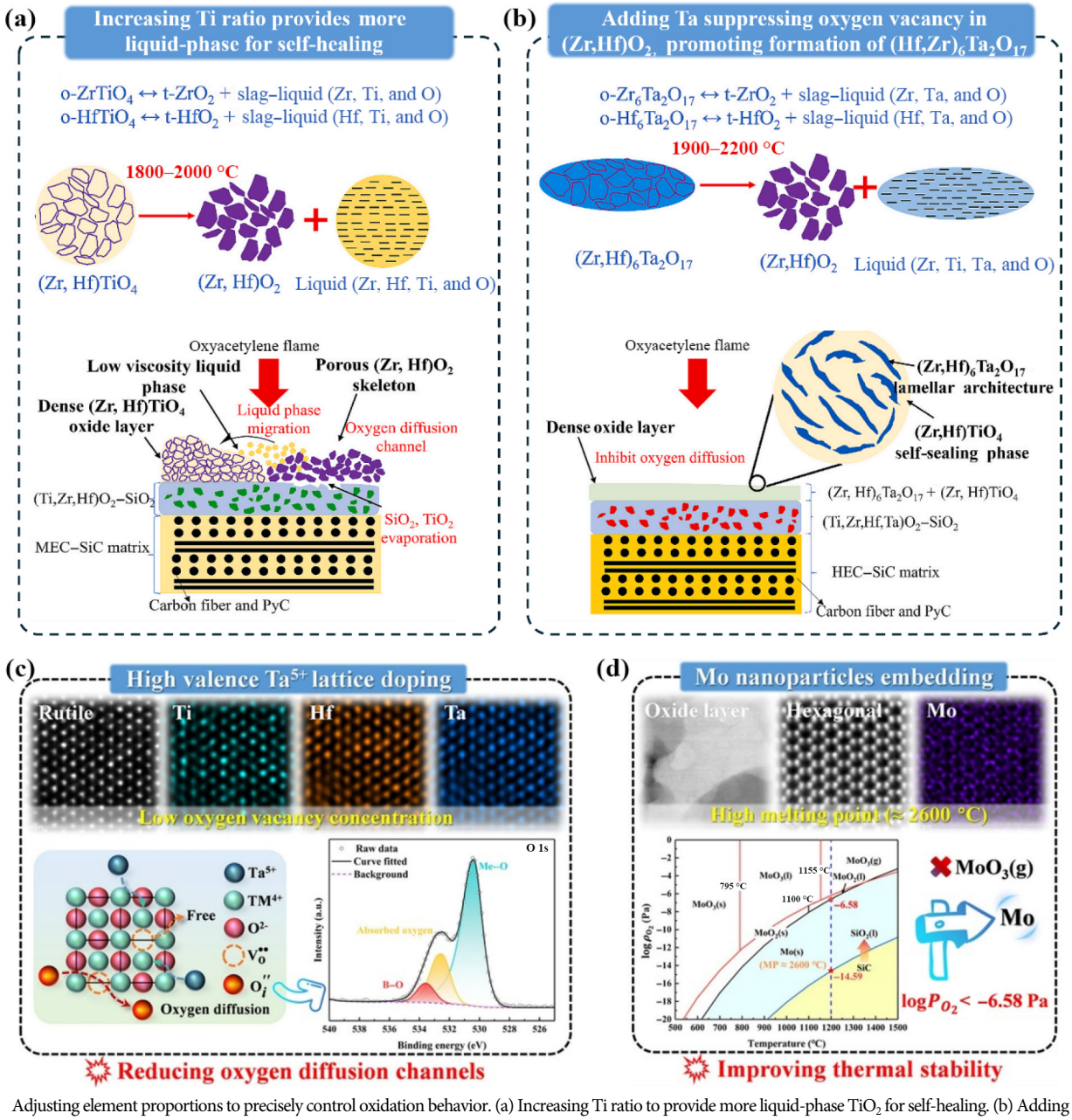

Fig. 5 Adjusting element proportions to precisely control oxidation behavior. (a) Increasing Ti ratio to provide more liquid-phase TiO_2 for self-healing. (b) Adding Ta to suppress formation of oxygen vacancies in $(Zr,Hf)O_2$ and form $(Hf,Zr)_6Ta_2O_{17}$. Reproduced with permission from Ref. [194] for (a, b), © Elsevier Inc. 2025. (c) Adding Ta to reduce oxygen diffusion channels. (d) Adding Mo to act as high-melting-point particles enhancing oxide layer stability. Reproduced with permission from Ref. [195] for (c, d), © Published by Elsevier Ltd., on behalf of The editorial office of Journal of Materials Science & Technology 2026.

3.1.3 Desired multilevel, systematic, integrated engineering approach

Table 1 summarizes the design strategies illustrated above. The design strategy for ablation/oxidation-resistant high-entropy UHTCs is thus a multilevel, systematic material–process–performance–mechanism integrated engineering approach. It starts with atomic-scale compositional design, proceeds through controlled synthesis and microstructure, and ultimately aims to construct a dynamic, adaptive, and robust oxide protection system *in-situ* formed under service conditions [226]. Further research on interface engineering and the design of tougher oxide layers with long-term stability is needed [227]. Moreover, materials may face simultaneous high-temperature oxidation, high-speed particle erosion, thermochemical ablation, and severe thermal shock. A thermal expansion mismatch between the oxide protective layer and the substrate can lead to delamination. Design strategies must comprehensively consider these coupled factors [228]. More in-depth *in situ* studies are still required on the amorphous/crystalline transition during early-stage oxidation, the formation sequence and growth kinetics of complex oxide phases, and the volatilization and phase equilibrium mechanisms at extreme temperatures (> 3000 °C) [229].

3.2 Thermal barrier/insulation performance

The relentless pursuit of higher operating temperatures in gas turbines, aerospace engines, and energy conversion systems has exposed the limitations of traditional thermal barrier coating (TBC) materials such as yttria-stabilized zirconia (YSZ) [12]. Their susceptibility to phase degradation, sintering, and limited thermal insulation efficiency above 1200 °C necessitates a paradigm shift. Enter high-entropy oxide ceramics (HEOCs), a disruptive class of

Table 1 Design strategies for oxidation/ablation resistance in high-entropy UHTCs

Design strategy	Added elements/phase	Mechanism	Oxide layer structure	Property enhancement	Ref.
High-melting-point skeleton	Hf, Zr, Ta, and Nb	Form complex oxides (e.g., $(Hf,Zr)_6(Ta,Nb)_2O_{17}$)	Support skeleton layer	↑ Erosion resistance	[173,176,177]
Liquid-phase self-healing	Ti, Si, and B	Form TiO_2, SiO_2, B_2O_3 liquid to fill cracks	Densification layer	↓ Oxygen diffusion	[178–180]
Nonstoichiometry control	C/TM < 1	Carbon vacancies promote solid solution, forming oxycarbide	Gradient transition layer	↓ Oxidation rate	[197–199]
SiC addition	SiC particles/whiskers	Generate SiO_2 glass, composite with oxide skeleton	Composite dense layer	↑ Ablation resistance, ↑ Thermal conductivity	[204–206]
Rare-earth doping	Y, La, and Sc	Reactive element effect, inhibits oxide spallation	Adhesion-enhanced layer	↑ Cyclic oxidation life	[209–211]
Cr/Mo/W addition	Cr_3C_2, Mo, and W	Form high-melting oxides or complex chromates	Strengthened skeleton layer	↑ Hardness, ↑ Stability	[212–214]
Partial nitride substitution	N replaces C	Form carbonitrides, lower thermal conductivity, and increase hardness	Complex mixed layer	↑ Oxidation resistance	[216,217]
Dual-phase design	HEC-HEB	Grain boundary pinning, inhibits growth	Synergistic oxide layer	↑ Strength-toughness	[218,219]
Fiber reinforcement	C_f	Toughening, damage tolerance	Fiber + matrix	↑ Fracture toughness	[220–222]

materials born from the extension of the high-entropy alloy concept to the ceramic realm [4]. For thermal insulation, this is revolutionary. The resulting severe lattice distortion from mixing cations of different sizes and masses creates a crystalline structure that behaves like a phonon glass [157]. Phonons, the primary heat carriers in insulating ceramics, are scattered at multiple scales by point defects, strained bonds, and disordered lattices, leading to dramatic reductions in thermal conductivity [230]. Furthermore, the sluggish diffusion effect inherent to these complex compositions grants exceptional resistance to grain growth and phase decomposition at extreme temperatures [84]. The synergistic interaction of the combined elements often yields properties superior to any of the constituent oxides [9]. Thus, HEOCs are not mere incremental improvements but represent a fundamentally new design space, enabling the co-optimization of ultralow thermal conductivity, high thermal expansion coefficients, robust mechanical properties, and outstanding environmental stability in a single material, paving the way for next-generation ultrahigh-temperature technologies [231].

3.2.1 *Core design principles*

Entropy maximization and phase stabilization. The cornerstone is maximizing the configurational entropy (ΔS_{conf}) on a cation sublattice. For an equimolar, n-component solid solution, $\Delta S_{conf} = R\ln(n)$, where R is the gas constant. This term can outweigh a positive enthalpy of mixing (ΔH_{mix}) at elevated temperatures, making the Gibbs free energy ($\Delta G = \Delta H - T\Delta S$) negative and stabilizing a single-phase solid solution [4,232]. The prototypical example is (Mg,Co,Ni,Cu,Zn)O, where five distinct divalent cations coexist on a single rock-salt lattice [4]. For thermal barrier oxides, the strategy is applied to fluorite (e.g., $(Hf,Zr,Ce,Y,Yb)O_2$) [67], pyrochlore (e.g., $(La,Nd,Sm,Eu,Gd)_2Zr_2O_7$) [84], and perovskite (e.g., $(Sr,Ca,Ba,La,Pb)TiO_3$) [233] structures. The selection of cations must balance entropy maximization with other critical factors, such as ionic charge compatibility and radius, to ensure solubility and avoid charge ordering, which would reduce the effective configurational entropy [232].

Lattice distortion engineering. Severe lattice distortion is the primary engine for phonon scattering (Figs. 6(a)–6(c)) [157]. This arises from the significant mismatch in ionic radii among the constituent cations occupying the same crystallographic site. This distortion manifests as local strain fields, bond–length disorder, and deviations from ideal bond angles, all of which dramatically increase phonon scattering [68]. The degree of distortion can be quantified by a size disorder parameter, δ_r. A larger δ_r, achieved by combining cations such as large La^{3+} (1.16 Å) with small Yb^{3+} (0.985 Å), correlates strongly with lower lattice thermal conductivity (Fig. 6(d)) [234]. This distortion disrupts the harmonicity of the lattice, scattering the medium- to high-frequency phonons (acoustic branch) that carry a significant portion of the heat [157,230]. As shown in Figs. 6(c) and 6(e), the resulting thermal conductivity often exhibits an "amorphous-like" temperature dependence, plateauing at high temperatures instead of following the traditional $1/T$ relationship, indicating that the phonon mean free path has been reduced to its lower limit [235].

Mass contrast and phonon scattering: In addition to size mismatch, a large variance in atomic masses among the constituent cations introduces mass disorder scattering (Figs. 6(e) and 6(f)) [235]. Phonons propagating through a lattice are scattered by fluctuations in atomic mass, with the scattering efficiency proportional to the variance [157,234]. By intentionally combining light (e.g., Y, Al) and heavy (e.g., Hf, Ta, W) elements, designers can create a powerful mass contrast effect. This mechanism is particularly effective for scattering high-frequency optical phonons. The mass disorder parameter, δ_M, is a key descriptor for predicting thermal conductivity suppression. Often, the most effective HEOCs for thermal insulation are those that maximize both size (δ_r) and mass (δ_M) disorder simultaneously, creating a multifaceted phonon scattering landscape that operates across the entire phonon spectrum [157,234].

Charge disorder and oxygen vacancies: Introducing cations with different valences (aliovalent doping) is a sophisticated strategy to further engineer properties. For example, substituting a divalent cation (Ca^{2+}) for a tetravalent cation (Zr^{4+}) in a fluorite structure necessitates the creation of oxygen vacancies for charge compensation [236]. These vacancies serve as potent point defect scatterers for phonons. Moreover, they can pin domain boundaries, enhance sintering resistance, and in some cases, be manipulated to tune electrical properties [237]. However, the design must be careful, as excessive oxygen vacancy concentration can sometimes promote undesirable ionic diffusion or phase instability [232]. The goal is to achieve a controlled level of charge disorder that augments phonon scattering without compromising other critical attributes, such as oxidation resistance or mechanical integrity [67].

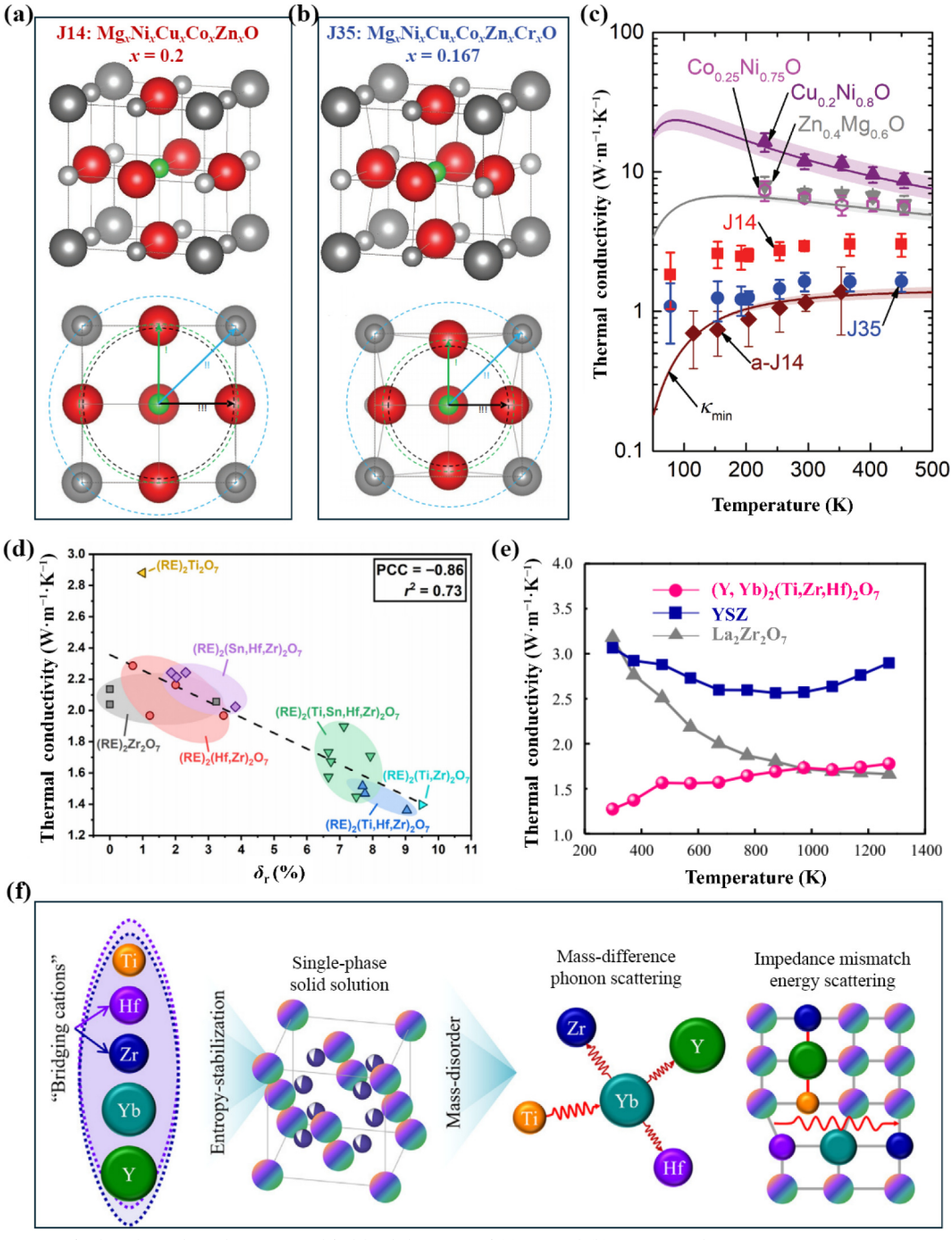

Fig. 6 Design strategies for low thermal conductivity. Modified local distortion of (a) J14 and (b) J35. J14 and J35 represent $Mg_xNi_xCu_xCo_xZn_xO$ (x = 0.2) and $Mg_xNi_xCu_xCo_xZn_xCr_xO$ (x = 0.167), respectively. (c) Temperature-dependent thermal conductivity of J14 and J35. Reproduced with permission from Ref. [157] for (a–c), © WILEY-VCH Verlag GmbH & Co. KGaA, Weinheim 2018. (d) Size disorder-dependent thermal conductivity in HECs. Reproduced with permission from Ref. [234], © Acta Materialia Inc. 2020. (e) Comparison of temperature-dependent thermal conductivity between HEC and other ceramics. (f) Illustration of mechanisms of low thermal conductivity in HEC. Reproduced with permission from Ref. [235] for (e, f), © The Authors 2021.

3.2.2 Thermal barrier/insulation performance optimization

3.2.2.1 The choice of crystal structures

The choice of crystal structure provides the foundational framework upon which high-entropy design principles are applied, with fluorite, pyrochlore, and perovskite being the most prominent for thermal barrier applications.

Fluorite-structured HEOCs. The fluorite structure (AO_2, with A in 8-fold coordination) is highly tolerant to cation disorder and oxygen nonstoichiometry, making it an ideal host for high-entropy engineering [232]. Systems such as $(Hf,Zr,Ce,RE)O_2$, where RE represents a mix of rare-earth elements (Y, Yb, Gd, etc.), are exemplary [15,232]. The intrinsic oxygen vacancies from RE^{3+} substitution into the A^{4+} site further depress the thermal conductivity. These materials often exhibit excellent phase stability up to 1600 °C, good fracture toughness, and thermal expansion coefficients ($(10–12)\times10^{-6}$ K^{-1}) superior to YSZ [79,232]. Their compositional flexibility allows for fine-tuning; for instance, incorporating Si^{4+} or Ti^{4+} can modify sintering behavior and mechanical properties [238]. Their relatively simple cubic structure also facilitates deposition as coatings via plasma spray techniques.

Pyrochlore-structured HEOCs ($A_2B_2O_7$). Pyrochlores, particularly rare-earth zirconates ($RE_2Zr_2O_7$), are leading TBC candidates due to their naturally low thermal conductivity and high-temperature capability [239]. High-entropy design transforms them from single-RE systems to multi-RE solid solutions such as $(La_{0.2}Nd_{0.2}Sm_{0.2}Eu_{0.2}Gd_{0.2})_2Zr_2O_7$ [84]. The key is maintaining the average A-site to B-site cation radius ratio (r_A/r_B) within the pyrochlore stability range (~1.46–1.80) [240]. This structure offers two cation sites (A and B), and high entropy can be engineered on one or both. HE pyrochlores demonstrate remarkable properties: thermal conductivity as low as 0.76 $W·m^{-1}·K^{-1}$ [84], enhanced fracture toughness from solid solution strengthening [90], and superb resistance to calcium–magnesium–alumina–silicate (CMAS) corrosion due to the formation of dense, multication apatite reaction layers [241].

Perovskite-structured HEOCs (ABO_3). While traditionally explored for dielectric and catalytic applications, high-entropy perovskites have emerged as promising thermoelectric and protective coating materials [242]. The design typically involves high-entropy mixing on the A-site (e.g., Sr, Ca, Ba, La, Pb) in titanates or manganates [233,243]. The large lattice distortion and strain from A-site disorder effectively suppress the lattice thermal conductivity to glass-like levels (< 2 $W·m^{-1}·K^{-1}$) [233,244]. Furthermore, the B-site can be simultaneously engineered with transition metals to tailor electronic transport for thermoelectric applications or to enhance environmental resistance [242]. Their mechanical properties and thermal expansion can be tuned over a wide range, offering versatility for specific substrate matching [243].

Dual-phase and composite HEOCs. Pushing beyond single-phase design, researchers are exploring dual-phase or composite HEOCs. For example, compositions at the boundary of the pyrochlore–fluorite transition can yield nanocomposite microstructures [7]. Alternatively, introducing a second phase (e.g., Al_2O_3 fibers or a different HEOC) can enhance toughness, further reduce thermal conductivity through interfacial scattering, or improve erosion resistance. This approach adds another dimension to the design toolkit, allowing for the creation of hierarchical architectures that optimize multiple properties concurrently [245].

3.2.2.2 Optimization strategies based on properties

Achieving the target profile for a thermal barrier material requires simultaneous optimization of several conflicting properties. High-entropy design provides unique pathways to resolve these trade-offs.

Thermal conductivity reduction. The paramount goal is to minimize the lattice thermal conductivity (κ_{ph}). HEOCs achieve ultralow κ_{ph}, often between 1.0 and 1.8 $W·m^{-1}·K^{-1}$ at room temperature, through engineered multiscale phonon scattering (Fig. 6) [157,230,234]. This is realized by leveraging atomic-scale point defects (from cation size/mass disorder), nanoscale strain fields and dislocations (from severe lattice distortion), and microscale grain boundaries (stabilized by sluggish diffusion), complemented by oxygen vacancies from aliovalent doping [67,230]. The synergistic combination of these scattering mechanisms suppresses κ_{ph} across the full phonon spectrum, driving it near the theoretical amorphous limit and ensuring that it remains low even at temperatures exceeding 1200 °C [235].

Thermal expansion coefficient matching. A major flaw of many advanced TBC candidates (e.g., $La_2Zr_2O_7$) is a low TEC and thermal contraction in the medium temperature range, causing stress and delamination. High-entropy engineering provides an effective strategy to systematically tailor the TEC [79]. By designing the A-site cation composition, introducing larger rare-earth ions (e.g., Nd^{3+} and Sm^{3+}) and promoting the formation of a disordered fluorite structure over an ordered pyrochlore, the lattice anharmonicity and expansibility are enhanced [79,246]. For instance, a series of high-entropy $(5RE_{0.2})_2Ce_2O_7$ fluorite oxides achieved high TECs of $(11.92–12.11)\times10^{-6}$ K^{-1} (above 673 K), which are comparable to those of $La_2Ce_2O_7$ but with significantly reduced thermal contraction in the critical 473–673 K range [79]. Furthermore, tuning the Ce^{4+} content in $(La_{0.2}Sm_{0.2}Er_{0.2}Yb_{0.2}Y_{0.2})_2Ce_xO_{3+2x}$ allowed the TEC to be tailored over a wide range from 9.04×10^{-6} to 13.12×10^{-6} K^{-1}, demonstrating the remarkable flexibility of this approach [247]. Consequently, high-entropy rare-earth zirconates and cerates frequently exhibit TECs of $(10.5–11.5)\times10^{-6}$ K^{-1}, significantly higher than their single–cation counterparts and much better matched to nickel-based superalloy substrates (~14×10^{-6} K^{-1}) than YSZ [38]. This enhanced TEC matching, combined with low thermal conductivity, positions them as promising candidates for next–generation TBCs [79,246–250].

Mechanical property enhancement. Solid solution strengthening leads to improved mechanical performance [9]. The random strain field from lattice distortion effectively pins dislocations, increasing the hardness and yield strength. While the fracture toughness (K_{IC}) of ceramics is challenging to drastically improve, some HE pyrochlores and fluorites show K_{IC} values between 1.5 and 2.5 $MPa·m^{1/2}$, superior to many single-component oxides [85,90]. This enhancement is attributed to crack deflection and microcracking induced by the complex local stress fields. The high elastic modulus is typically retained, leading to a high "stiffness-to-conductivity" ratio (E/κ), a key figure of merit for TBCs [157].

Environmental and chemical stability. Service life depends on resistance to degradation. HEOCs excel here due to the sluggish diffusion effect, which drastically reduces the rates of elemental segregation, grain growth, and reaction kinetics [84]. In CMAS attack, the multication composition leads to the precipitation of a complex, stable sealing layer (e.g., Ca-apatite with multiple REs) that is more resistant to further melt infiltration [90,241]. Their high configurational entropy also translates to excellent phase stability, with many compositions showing no decomposition or phase separation after hundreds of hours at 1400–1500 °C [84].

3.2.3 Path forward for HEOC thermal barriers

Despite remarkable progress, the field of HEOCs for thermal barriers is nascent and faces significant challenges that point toward exciting future research directions [13]. While empirical rules (size/mass disorder) are helpful, a precise, *ab initio* prediction of which multicomponent combinations will form stable single phases remains difficult. The true role of configurational entropy vs. enthalpy and the nature of short-range order need deeper theoretical and experimental investigation [232,49]. Many high-performing compositions rely heavily on scarce and expensive rare–earth elements (e.g., Yb, Lu). Exploring high-entropy systems based on more abundant and cheaper elements (e.g., Al, Si, Mg, Fe) is crucial for large-scale industrial adoption [251].

Reproducibly synthesizing and processing multicomponent powders with perfect homogeneity is challenging. Scaling up wet–chemical methods or controlling plasma spray parameters for complex HEOCs requires significant process optimization. The brittleness of ceramics, although improved, remains a fundamental limitation [13]. The vast compositional space of HEOCs is ideally suitable for ML-guided discovery. Algorithms

trained on existing data can predict new stable compositions and even suggest those with targeted property profiles (e.g., minimum κ, maximum TEC), dramatically accelerating the innovation cycle [252].

Beyond equimolar and high entropy, research is expanding into "compositionally complex ceramics (CCCs)", which include medium-entropy (3–4 cations) and nonequimolar compositions [7]. These may offer optimized properties at lower cost and complexity. Exploring entropy engineering on the anion site (e.g., oxynitrides, oxyfluorides) is another frontier [77]. The next generation may move beyond passive insulation. Designing HEOCs that combine ultralow κ with specific functional properties such as high emissivity for radiative cooling, self-healing capabilities through controlled oxidation, or tailored electrical conductivity for embedded sensors could create intelligent, multifunctional thermal protection systems [253]. Integrating HEOCs with additive manufacturing (AM) (three-dimensional (3D) printing) could enable the fabrication of complex, graded, or porous structures with optimized thermal and mechanical performance [254]. The development of robust protocols for depositing HEOCs as durable, thick coatings via advanced thermal spray or hybrid processes is essential for commercialization [255].

The development of high-entropy oxide ceramics represents a paradigm shift in the design of advanced thermal barrier and insulation materials. By strategically harnessing the stabilizing power of configurational entropy and the phonon-scattering effects of severe lattice distortion and mass contrast, researchers have demonstrated the feasibility of creating single-phase materials that successfully reconcile what was once a series of trade-offs: ultralow thermal conductivity alongside high temperature stability, suitable thermal expansion, and enhanced mechanical and environmental durability [12,84,247]. From rare-earth zirconates and fluorites to complex perovskites, this material design strategy has opened a vast new compositional space to explore. While challenges in predictive design, cost, and processing persist, the pathway forward is illuminated by the integration of computational tools, high–throughput experimentation, and advanced manufacturing [252,256]. As these efforts converge, high-entropy oxide ceramics are poised to transition from laboratory curiosities to enabling materials for the next generation of hyperefficient jet engines, gas turbines, and hypersonic vehicles, marking a true revolution in high-temperature technology [231,257].

3.3 Superior radiation-tolerance structural components and highly durable waste immobilization matrices

The advent of HECs represents a paradigm shift in materials design for extreme nuclear environments [231]. By incorporating multiple principal cations into a single-phase crystal structure, HECs leverage chemical complexity, lattice distortion, and configurational entropy to achieve properties unattainable in conventional ceramics [34,231]. This strategy aims to outline a multifaceted design framework for developing HECs with exceptional radiation tolerance for two critical nuclear applications: (1) structural components in advanced reactors (e.g., fuel cladding, core components) and (2) immobilization matrices for high-level radioactive waste (HLW).

3.3.1 Foundational principles and mechanisms of radiation tolerance in HECs

Chemical complexity and lattice distortion. The superior performance of HECs under irradiation stems from core principles derived from their disordered structure. The random distribution of multiple elements with different atomic radii and electronegativities creates severe lattice distortion. This distortion increases the activation energy for defect migration, leading to sluggish diffusion kinetics. As noted in multiple studies, this slows down the evolution of irradiation-induced defects (e.g., dislocation loops, voids) and retards processes such as helium bubble coalescence. For instance, in $(Zr_{0.2}Ti_{0.2}Nb_{0.2}Ta_{0.2}W_{0.2})C$, the high entropy-induced lattice distortion contributes to smaller, uniformly distributed He bubbles and suppressed defect aggregation compared to ZrC (Fig. 7(a)) [258].

Phase stability and resistance to amorphization. The high configurational entropy of mixing stabilizes single-phase solid solutions against decomposition under irradiation. Furthermore, chemical disorder can elevate the critical temperature and dose for irradiation-induced amorphization. While some high-entropy pyrochlores amorphized at doses comparable to simple pyrochlores [259], others, such as $(Sm_{0.2}Eu_{0.2}Gd_{0.2}Dy_{0.2}Er_{0.2})_2Hf_2O_7$, maintained crystallinity at very high doses (120 dpa) where single-component analogs may amorphize (Fig. 7(b)) [260]. The key is the selection of constituents that promote a disordered yet stable lattice.

Defect engineering and recombination. Chemical complexity influences the formation and recombination energies of point defects (vacancies, interstitials). First-principles calculations on high-entropy carbides suggest that introducing disorder in the anion sublattice (e.g., forming carbonitrides) can significantly enhance Frenkel pair recombination compared to disorder only in the cation sublattice, thereby improving defect recovery (Fig. 7(c)) [261]. This highlights the importance of designing disorder across all sublattices.

Synergistic effects in waste forms. For waste immobilization, high-entropy pyrochlores ($A_2B_2O_7$) can incorporate a wide spectrum of radionuclides (simulating diverse HLW) into a single, stable phase. The combined effects of chemical complexity and lattice distortion (1) inhibit cation diffusion, leading to exceptionally low normalized leaching rates (e.g., 10^{-7} to 10^{-9} $g{\cdot}m^{-2}{\cdot}d^{-1}$ for $(Nd_2(Ti_{0.25}Zr_{0.25}Hf_{0.25}Sn_{0.25})_2O_7)$) (Fig. 7(d)) [262], and (2) enhance tolerance to atomic displacement damage, often undergoing a controlled order–disorder (pyrochlore-to-fluorite) transition instead of amorphization (Fig. 7(e)) [263,264].

3.3.2 Material-specific design strategies

3.3.2.1 High-entropy carbides for structural components

Focusing on refractory transition metal carbides (Ti, Zr, Hf, Nb, Ta, W, V, and Mo), systems such as $(Ti_{0.25}Zr_{0.25}Nb_{0.25}Ta_{0.25})C$, $(Hf_{0.2}Zr_{0.2}Ta_{0.2}Nb_{0.2}Ti_{0.2})C$, and $(Cr_{0.2}Nb_{0.2}Ta_{0.2}Ti_{0.2}W_{0.2})C$ show outstanding phase stability under heavy-ion and He-ion irradiation [265–267]. Studies on $(Ti_{0.25}Zr_{0.25}Nb_{0.25}Ta_{0.25})C$ reveal that irradiation-induced lattice expansion decreases with temperature due to dynamic annealing, and He bubbles remain nanosized and uniformly distributed without preferential segregation to grain boundaries at high temperatures [268]. Computational screening suggests that tailoring the formation enthalpy can be a key indicator for designing rock salt-structured carbides with low Frenkel pair recombination barriers, directly linking thermodynamics to radiation tolerance [261]. Compositions such as $(Zr_{0.2}Ti_{0.2}Nb_{0.2}Ta_{0.2}W_{0.2})C$ demonstrate reduced He bubble coarsening and more complete lattice parameter recovery postannealing compared to binary ZrC, attributed to sluggish diffusion and stress dispersion [258]. HECs such as $(Hf_{0.2}Nb_{0.2}Ta_{0.2}Ti_{0.2}Zr_{0.2})B_2$ can exhibit superior recovery of hardness and elastic modulus at high irradiation fluences

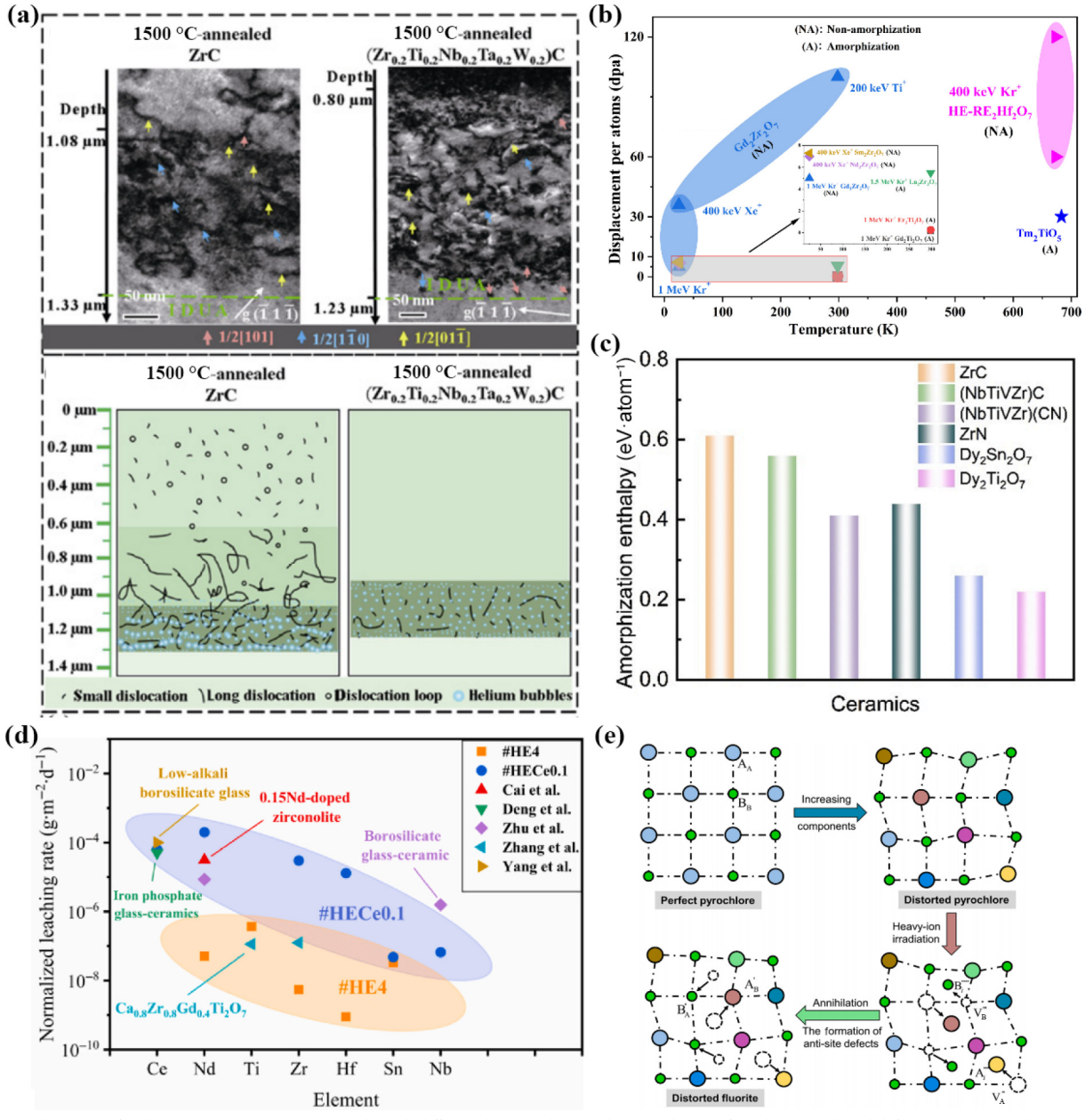

Fig. 7 Mechanisms of radiation tolerance in HECs. (a) Sluggish diffusion kinetics slowing down evolution of irradiation-induced defects in $(Zr_{0.2}Ti_{0.2}Nb_{0.2}Ta_{0.2}W_{0.2})C$. Reproduced with permission from Ref. [258], © The Author(s) 2023. (b) Radiation-induced amorphization doses of single-component materials and HE-$RE_2Hf_2O_7$ at different conditions. Reproduced with permission from Ref. [260], © Published by Elsevier Ltd. on behalf of The editorial office of Journal of Materials Science & Technology 2023. (c) Disorder in anion sublattice significantly enhances Frenkel pair recombination compared to disorder only in the cation sublattice. Reproduced with permission from Ref. [261], © Acta Materialia Inc. 2024. Chemical complexity and lattice distortion (d) inhibit cation diffusion, leading to exceptionally low normalized leaching rates and (e) enhance tolerance to atomic displacement damage and undergo a controlled order–disorder (pyrochlore-to-fluorite) transition instead of amorphization. Reproduced with permission from Ref. [262] for (d), © Elsevier Ltd. and Techna Group S.r.l. 2024; Ref. [264] for (e), © Elsevier Ltd. 2022.

compared to their quaternary subsets, indicating a role for chemical disorder in preserving mechanical properties [269].

Maximize lattice distortion via multiprincipal cation selection. Severe lattice distortion, induced by the atomic size mismatch of four or more different transition metals, increases the intrinsic energy landscape. This raises activation barriers for point defect (vacancy, interstitial) migration and dislocation glide, thus slowing defect aggregation, void growth, and helium bubble coalescence. The study on $(Zr_{0.2}Ti_{0.2}Nb_{0.2}Ta_{0.2}W_{0.2})C$ demonstrated that its high-entropy-induced distortion resulted in smaller, more uniformly distributed He bubbles and a lower residual lattice expansion after annealing compared to binary ZrC [258]. The sluggish diffusion impeded bubble coarsening and defect recovery. Similarly, $(Hf_{0.2}Nb_{0.2}Ta_{0.2}Ti_{0.2}Zr_{0.2})B_2$ showed superior recovery of mechanical properties at high fluence, attributed to the complex energy landscape hindering damage evolution [269].

Employ computational screening for phase stability and defect energetics. Prior to synthesis, *ab initio* calculations were used to predict thermodynamic stability (negative mixing enthalpy, high formation energy) and defect properties. Key computational descriptors include formation enthalpy (correlated with Frenkel pair recombination energy in rock salt structured ceramics) and vacancy/interstitial formation/migration energies. ML models trained on such data can rapidly predict properties such as lattice distortion and amorphization resistance. First-principles work by Li *et al.* [261] revealed that for high-entropy

carbides, disorder on the anion sublattice (creating carbonitrides) significantly improves defect recombination over cation-only disorder. They proposed formation enthalpy as a key screening parameter. Another study used ML to directly predict lattice distortion in HE-MAX (M is a transition metal, A is Group A element, and X is carbon, nitrogen, or boron) phases, linking it to amorphization resistance for rapid screening [270].

Validate irradiation response across operational temperature spectra. Radiation damage is highly temperature-dependent due to thermal annealing. A robust material must perform across a range from reactor start-up (near room temperature (RT)) to operating temperatures (hundreds of °C). Testing must evaluate (a) defect cluster evolution (loop density/size), (b) helium behavior (bubble nucleation, distribution, swelling), and (c) phase stability at relevant temperatures. Zhang *et al.* [268] systematically irradiated $(Ti_{0.25}Zr_{0.25}Nb_{0.25}Ta_{0.25})C$ with He ions from RT to 700 °C. They found that lattice expansion decreased with rising temperature due to dynamic annealing, and He bubbles remained nanosized and intragranular even at 700 °C, demonstrating favorable high-temperature behavior. Conversely, $(W_{0.2}Ti_{0.2}V_{0.2}Nb_{0.2}Ta_{0.2})C$ showed a reduced defect density and the formation of a defect-denuded zone when irradiated at 650 °C compared to RT, highlighting temperature-activated recovery [271].

Prioritize single-phase stability and resistance to phase decomposition. Under irradiation, chemical driving forces can cause precipitation or decomposition, creating weak interfaces and accelerating failure. A single-phase solid solution stabilized by high configurational entropy is more likely to remain homogeneous, avoiding detrimental secondary phases that can act as sinks for deleterious elements such as He or sites for accelerated corrosion. The magnetron-sputtered $(Cr_{0.2}Nb_{0.2}Ta_{0.2}Ti_{0.2}W_{0.2})C$ film maintained a single-phase structure after heavy-ion irradiation to 10 dpa at 573 K, with no signs of amorphization or decomposition, showing excellent phase stability under irradiation [265]. In contrast, studies on multilayer coatings showed that metallic CrFeCoNi sublayers were less stable and prone to interlayer diffusion under irradiation compared to their nitride counterparts, underscoring the importance of phase and chemical stability [272].

3.3.2.2 High-entropy oxides for waste immobilization

The critical factor is managing cation size disorder. Successful single-phase synthesis, as in $(La_{0.2}N_{0.2}Sm_{0.2}Eu_{0.2}Gd_{0.2})_2Zr_2O_7$, requires careful selection of A- and B-site cations with compatible ionic radii to avoid secondary phase formation (e.g., monoclinic phases) [262,273]. Introducing larger B-site cations, such as Zr^{4+}, can stabilize the pyrochlore structure [273]. High-entropy pyrochlores exhibit leaching rates orders of magnitude lower than those of conventional materials. This is due to synergistic effects: (a) Compositional complexity increases lattice potential energy and (b) reduced oxygen vacancy concentration slows cation migration [274]. Zirconate-based high-entropy pyrochlores ($A_2Zr_2O_7$) generally show superior radiation resistance compared to titanate-based pyrochlores, undergoing a reversible pyrochlore-to-fluorite transformation rather than amorphization [264,275]. Compositions such as $(Gd_{0.2}Sm_{0.2}Dy_{0.2}Er_{0.2}Yb_{0.2})_2Ti_2O_7$ demonstrate suppressed helium bubble generation and coalescence due to chemical disorder [276]. The A- and B-sites can be engineered to directly host specific radionuclides (e.g., actinides at the A-site, fission products at the B-site). The $Eu_2B_2O_7$ (B = Ti, Zr, Hf, Sn, Nb, Ce) system exemplifies the ability to incorporate multiple simulated waste elements [277].

Engineering cation selection and size disorder to achieve dense, single-phase fabrication. The primary challenge is synthesizing a fully dense, single-phase ceramic from a complex mixture. The cationic radius ratio (r_A/r_B) is critical, but the tolerance window may differ from that of conventional pyrochlores due to configurational entropy. The goal is to minimize the formation of secondary phases (e.g., monoclinic) that compromise chemical durability and mechanical integrity. Liu *et al.* [273] systematically investigated Ti-based high-entropy pyrochlores and found that certain large A-site cations had low solubility, leading to a monoclinic secondary phase. They successfully suppressed this by introducing Zr^{4+} at the B-site, adjusting the crystal structure to achieve a pure pyrochlore phase. Zhang *et al.* [262] identified that size disorder was the critical factor, successfully synthesizing single-phase $Nd_2(Ti_{0.25}Zr_{0.25}Hf_{0.25}Sn_{0.25})_2O_7$ by balancing the ionic radii on the B-site.

Prefer zirconate/hafnate-based compositions over titanate-based compositions for superior amorphization resistance. The propensity for an $A_2B_2O_7$ pyrochlore to undergo irradiation-induced amorphization vs. an order–disorder transition to defect-fluorite is strongly tied to the B-site cation. Zr^{4+} and Hf^{4+} have higher ionic field strengths and favor the fluorite structure, making zirconate/hafnate pyrochlores more resistant to amorphization, as they can accommodate damage via a controlled structural transition. Xu *et al.* [264] showed that high-entropy $(La_{0.2}Ce_{0.2}Nd_{0.2}Sm_{0.2}Gd_{0.2})_2Zr_2O_7$ underwent a pyrochlore-to-fluorite transition under heavy–ion irradiation but remained crystalline. The review by Wang *et al.* [275] corroborates that zirconate pyrochlores generally possess better irradiation resistance. Conversely, studies on titanate-based high-entropy pyrochlores such as $(Yb_{0.2}Tm_{0.2}Lu_{0.2}Ho_{0.2}Er_{0.2})_2Ti_2O_7$ show amorphization at comparable doses to simple titanates, indicating the fundamental role of B-site chemistry [259,278].

The configurational entropy is maximized to enhance the chemical durability. High configurational entropy, achieved by incorporating multiple elements in near-equal proportions, creates a complex, distorted lattice with high lattice potential energy. This acts as a kinetic barrier, dramatically slowing the diffusion of constituent ions (including radioactive nuclides) through the lattice and into water, which is quantified by very low normalized elemental release rates (LR). Zhou *et al.* [274] demonstrated that high-entropy $(Eu_{1-x}Gd_x)_2(Ti_{0.2}Zr_{0.2}Hf_{0.2}Nb_{0.2}Ce_{0.2})_2O_7$ had LR values for Ce and Gd in the range of 10^{-6} to 10^{-8} $g{\cdot}m^{-2}{\cdot}d^{-1}$, vastly superior to doped simple pyrochlores. They attributed this to synergistic effects of compositional complexity and severe lattice distortion, which reduce oxygen vacancy concentration and increase migration barriers. Zhang *et al.* [262] reported LR values as low as 10^{-6} to 10^{-9} $g{\cdot}m^{-2}{\cdot}d^{-1}$ for $(Nd_2(Ti_{0.25}Zr_{0.25}Hf_{0.25}Sn_{0.25})_2O_7)$, confirming exceptional durability.

Advanced sintering techniques can be utilized to achieve high density with a fine, homogeneous microstructure. For waste forms, high density (> 95% theoretical) is nonnegotiable to minimize open porosity and leaching pathways. A fine, homogeneous grain size improves the mechanical strength and reduces the likelihood of localized corrosion or cracking. Conventional sintering often leads to excessive grain growth or incomplete densification in complex compositions. SPS is repeatedly used for densifying HEC waste forms. Ji *et al.* [276] used SPS to consolidate $(Gd_{0.2}Sm_{0.2}Dy_{0.2}Er_{0.2}Yb_{0.2})_2Ti_2O_7$ to 97.64% density with a hardness of 12.68 GPa. For oxides, reactive flash sintering (RFS) presents a breakthrough. Xu *et al.* [279] used a two-step RFS process for $(La_{0.2}Nd_{0.2}Sm_{0.2}Eu_{0.2}Gd_{0.2})_2Zr_2O_7$, achieving ~98% density with a grain size of ~684 nm, half that of one-step RFS, demonstrating precise control over densification and grain growth.

3.3.2.3 Other promising radiation-resistant HEC systems

High-entropy MAX phases such as $(TiVNbZrHf)_2SnC$ can show unique point defect properties, with lower antisite defect formation energies, potentially enhancing resistance to amorphization [270]. However, the design must be specific, as the amorphization resistance in $(Ti,M)_2AlC$ was found to decrease with increasing components, highlighting that elemental species are more critical than the number of components [280]. High-entropy transition metal diborides (e.g., $(Hf_{0.2}Nb_{0.2}Ta_{0.2}Ti_{0.2}Zr_{0.2})B_2$) and nitrides (e.g., (TiNbZrTa)N) show promising stability under irradiation, with nitride multilayers offering better resistance to elemental diffusion than their metallic counterparts [272,281].

3.3.3 The critical path ahead for radiation-tolerant HECs

The design strategy is inherently composition first, guided by principles of chemical complexity, targeted phase stability, and engineered defect behavior. For structural components, refractory high-entropy carbides and borides, designed for sluggish defect diffusion and helium management, are leading candidates. For waste immobilization, high-entropy pyrochlores engineered for atomic-scale incorporation and kinetic hindrance of leaching offer a transformative solution. The path forward requires a tightly coupled loop of computational prediction, advanced synthesis, and rigorous irradiation testing, as vividly documented in the provided research corpus, to transition these promising materials from the laboratory to the heart of next-generation nuclear energy systems.

Based strictly on previous works, future research should deepen the fundamental understanding of radiation damage mechanisms in HECs and advance their practical integration. First, the effects of lattice distortion, chemical short-range order, and electronic structure on defect evolution need to be decoupled. Pioneering work comparing ceramics and HEAs by Zhang *et al.* [282] on the role of electronic energy loss and inelastic thermal spikes provides a crucial starting point for similar studies in HECs, moving beyond simple displacement damage models. Second, the promising concept of disorder on both sublattices should be systematically explored, as evidenced by the synthesis of high-entropy carbonitrides $(TiZrNbHfTa)C_xN_y$ by Nikitin *et al.* [283] and the *ab initio* calculations by Li *et al.* [261], which revealed that introducing chemical disorder to the anion sublattice (forming carbonitrides) could significantly enhance defect recovery compared to cation-only disorder. Third, advanced manufacturing techniques are essential for component fabrication. Previous works highlight the success of field-assisted sintering techniques such as SPS and RFS for achieving high density and fine grains in complex ceramics [276,279]. Leveraging such methods, along with emerging additive manufacturing, is key to creating graded or composite HEC structures. Finally, to transition from promising laboratory materials to qualified reactor components, testing must advance beyond the ion irradiation surrogates used in almost all the present studies. Direct neutron irradiation experiments and corrosion tests in simulated reactor environments (e.g., molten salts for waste forms or coolants for structural materials) are indispensable next steps for validating in-service performance and long-term durability.

3.4 HECs for dielectric energy storage

3.4.1 Mechanisms of enhanced energy storage in HECs

Entropy-stabilized relaxor ferroelectric behavior. The core mechanism is the disruption of long-range ferroelectric order. The random distribution of multiple cations creates strong local compositional and charge heterogeneity, establishing random local electric and stress fields [284,285]. This leads to the formation of highly dynamic polar nanoregions (PNRs) instead of large, switchable ferroelectric domains. For instance, in high-entropy perovskite systems such as $(Ba_{0.2}Pb_{0.2}Sr_{0.2}RE_{0.2}K_{0.2})TiO_3$ (RE = La, Nd, and Sm), a global cubic structure coexists with localized PNRs, confirming a relaxor state characterized by a broad, frequency-dependent dielectric peak and slim polarization–electric (P–E) field hysteresis loops [286]. This results in significantly reduced remnant polarization (P_r) and low hysteresis loss, which is the direct source of high energy storage efficiency (η) [287].

Enhancement of dielectric breakdown strength (E_b). High entropy design concurrently improves the electric field a material can withstand, which is critical since recoverable energy density (W_{rec}) scales with E_b^2. This is achieved through multiple microstructural effects: (1) Grain refinement. The sluggish diffusion inherent to HECs inhibits grain growth during sintering (Fig. 8(a)) [287]. A consistent observation is that HECs exhibit much finer grains than their conventional counterparts. For example, the introduction of $Bi(Mg_{2/3}Nb_{1/3})O_3$ into $(Pb_{0.25}Ba_{0.25}Ca_{0.25}Sr_{0.25})TiO_3$ reduced the average grain size from 5.9 μm to 245 nm (Fig. 8(b)) [288]. Finer grains increase grain boundary density, which effectively scatters charge carriers and blocks the propagation of electrical breakdown trees [289]. (2) Increased electrical resistivity and band gap modification. The severe lattice distortion from mixed cations can modify the electronic structure. Studies on $BaTiO_3$-based HECs and Nb-doped $(Bi_{0.2}Na_{0.2}Ca_{0.2}Ba_{0.2}Sr_{0.2})TiO_3$ report widened band gaps and increased electrical resistivity, which suppress leakage current and improve E_b (Fig. 8(c)) [290,291]. (3) Nanoscale compositional heterogeneity. In some systems, HECs exhibit nanoscale segregation or chemical inhomogeneity. For example, in a $BaTiO_3$–$BiFeO_3$–$CaTiO_3$ high-entropy system, nanosegregations around grain boundaries were found to strongly scatter electron carriers, thereby enhancing the breakdown strength (Figs. 8(d) and 8(e)) [292].

Lattice distortion and delayed polarization saturation. The incorporation of cations with different ionic radii induces severe lattice distortion, which creates internal strain and modifies the energy landscape for dipole alignment. This can lead to delayed polarization saturation, meaning that a high maximum polarization (P_{max}) can be maintained under very high electric fields [293–295]. This effect is crucial for achieving a large polarization difference ($\Delta P = P_{max} - P_r$) at high E_b, directly contributing to high W_{rec}.

3.4.2 Design strategies for high-entropy dielectric ceramics

Crystallographic site engineering. The most common strategy involves populating the perovskite A-site with five or more cations. Examples include $(Bi_{0.2}Na_{0.2}Ba_{0.2}Sr_{0.2}Ca_{0.2})TiO_3$ [296] and $(Li_{0.2}Ca_{0.2}Sr_{0.2}Ba_{0.2}La_{0.2})TiO_3$ [287]. The choice of cations (monovalent Na^+/Li^+, divalent $Ba^{2+}/Sr^{2+}/Ca^{2+}$, trivalent La^{3+}) aims to maximize charge and size disorder to stabilize the relaxor state. Engineering entropy on the perovskite B-site focuses on tailoring octahedral bonding and relaxation. Examples are $Ba(Ti_{0.2}Zr_{0.2}Hf_{0.2}Sn_{0.2}Nb_{0.2})O_3$ and $Ba(Zr_{0.2}Sn_{0.2}Hf_{0.2}Nb_{0.2}Ti_{0.2})O_3$, which are often used as end-members to modify base ferroelectrics [291,297]. Advanced strategies incorporate high entropy on both sites for amplified disorder, as seen in proposed systems such as $(Bi_{0.2}Na_{0.2}Ba_{0.2}Sr_{0.2}Ca_{0.2})(Ti_{0.2}Zr_{0.2}Hf_{0.2}Sn_{0.2}Nb_{0.2})O_3$.

Composite and hybrid design strategies. (1) Blending with high-entropy end-members: A practical approach is to blend a conventional or medium-entropy ferroelectric matrix with a predesigned high-entropy perovskite. For instance, introducing

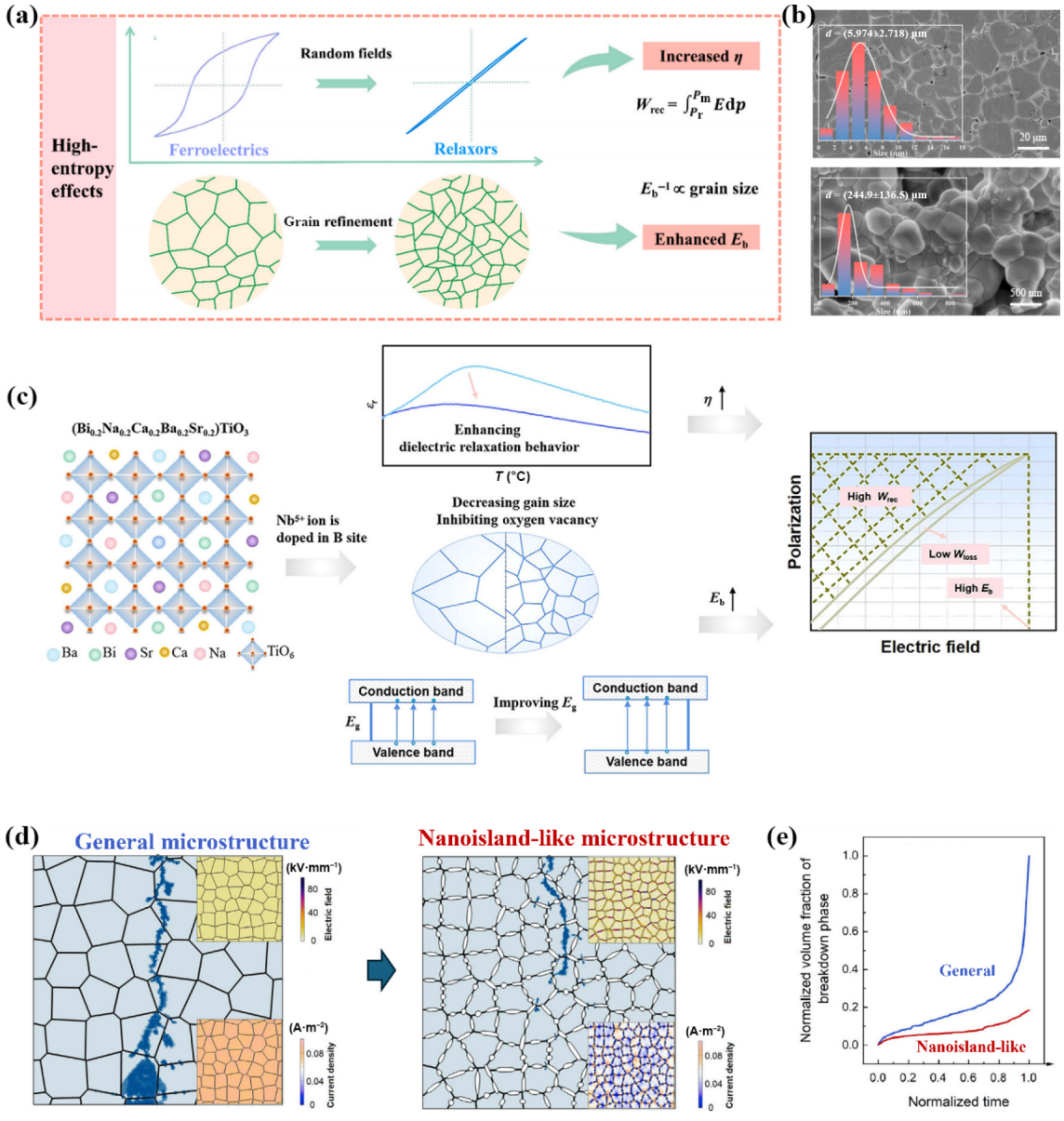

Fig. 8 Strategies for enhancing dielectric breakdown strength. (a) A high-entropy design that refines grain size, leading to improved E_b and W_{rec}. Reproduced with permission from Ref. [287], © Elsevier B.V. 2024. (b) Thermally etched surface SEM images of $(Pb_{0.25}Ba_{0.25}Ca_{0.25}Sr_{0.25})TiO_3$ (PBCST) and 0.95PBCST–0.05BMN (BMN = $Bi(Mg_{2/3}Nb_{1/3})O_3$). Reproduced with permission from Ref. [288], © Elsevier Ltd. and Techna Group S.r.l. 2023. (c) Nb doping induces lattice distortion and further disrupts ferroelectric order to enhance dielectric relaxation, inhibit grain growth, reduce oxygen vacancies, and promote band gap, thus leading to a high E_b. Reproduced with permission from Ref. [291], © The American Ceramic Society 2024. (d) Simulated electrical breakdown pathway within general and nanoisland-like microstructure. Insets show electric field distribution and current density at an applied electric field of 10 kV·mm^{-1}. (e) Evolution of breakdown phase volume fraction as a function of normalized time. where $Y = 0$ means initial state x, while $Y = 1$ means model was a complete breakdown Reproduced with permission from Ref. [292] for (d, e), © The Authors 2022.

$Ba(Zr_{0.2}Sn_{0.2}Hf_{0.2}Nb_{0.2}Ti_{0.2})O_3$ or $Sr(Zr_{0.2}Sn_{0.2}Hf_{0.2}Ti_{0.2}Nb_{0.2})O_3$ into $Bi_{0.5}Na_{0.5}TiO_3$ (BNT) or $BaTiO_3$ (BT) matrices effectively imports the benefits of high entropy (relaxor behavior, grain refinement) into a more manageable system [298,299]. (2) Defect and dopant engineering: Targeted doping is used to fine-tune properties. Donor doping (e.g., La^{3+}, Nb^{5+}) in HECs is reported to suppress oxygen vacancy formation, reduce leakage current, and improve E_b [291,300]. Sintering aids such as $MnCO_3$ or SiO_2 are employed to lower the sintering temperature and improve the densification of HECs, addressing processing challenges [301, 302].

Advanced processing and device integration. (1) Flash sintering: To overcome the high sintering temperatures and long cycles required due to sluggish diffusion, flash sintering was successfully applied to $(Na_{0.2}Bi_{0.2}Ba_{0.2}Sr_{0.2}Ca_{0.2})TiO_3$. This technique achieved densification in 60 s at a furnace temperature 400 °C lower than conventional sintering while also suppressing excessive grain growth [303]. (2) Multilayer ceramic capacitor (MLCC) fabrication: The ultimate translation of material performance into application. Studies have reported the successful fabrication of MLCCs using HEC dielectrics. For example, MLCCs based on a $BiFeO_3$-derived HEC composition achieved a W_{rec} of 12.1 J·cm^{-3} [304], and $BaTiO_3$-based high-entropy MLCCs demonstrated 17.2 J·cm^{-3} with 95.5% efficiency [305]. This involves tape-casting, electrode co-firing, and device-level optimization.

3.4.3 *Unresolved challenges in HEC capacitors*

Despite progress, there are several unresolved challenges:

(1) Processing complexity and compositional control. Synthesizing phase-pure HECs with homogeneous elemental distribution is difficult. The volatility of elements such as Na, K, and Bi during high-temperature sintering often leads to composition deviation and secondary phase formation [296,306]. The "sluggish diffusion" that benefits grain refinement also makes full densification challenging, requiring high temperatures or long sintering times. (2) Trade-off between energy density and efficiency. While high W_{rec} is frequently reported, achieving ultrahigh efficiency (η > 90%) simultaneously, especially at the highest energy densities, remains difficult. Many high-performing compositions show η in the 78%–87% range, indicating significant hysteresis or conductive losses under high field [294,307]. (3) Understanding long-term reliability. Data on performance degradation under combined electrical, thermal, and mechanical stress over extended periods or cycles are limited. One study mentions the risk of "thermal runaway" in capacitors, suggesting that failure mechanisms in HEC-based devices are not fully understood [308]. (4) Scalability and cost: The use of numerous, sometimes expensive, raw elements (e.g., Ta, Hf, Nb) and the need for controlled, often energy-intensive processing pose significant barriers to scalable and cost-effective manufacturing for widespread commercial application.

The development of advanced dielectric energy storage HECs may include the following directions: (1) AI-guided and computational design. A prominent trend is leveraging ML and phase-field simulations to navigate the vast HEC composition space. One study used a generative learning approach to screen over 10^{11} combinations, successfully identifying a high-performance $Bi(Mg_{0.5}Ti_{0.5})O_3$-based film with minimal experimentation [284]. Another proposed ML-assisted composition design for Pb-free relaxors [309]. This represents a paradigm shift from trial-and-error to rational, data-driven discovery. (2) Multifunctional HECs. Future materials will be designed for more than just storage. Research on Tm^{3+}/Yb^{3+} codoped systems demonstrates the integration of fluorescent temperature self-check capability with energy storage, conceptualizing smart capacitors for fault detection in high-voltage systems [308,310]. (3) Extreme environment stability. There is a strong drive to develop HECs for harsh environments. Studies on materials with stable performance from −50 to 260 °C [311] or under high pressure (up to 7 GPa) [312] indicate a focus on capacitors for aerospace, automotive, and deep-earth applications. (4) Performance under moderate electric fields. Alongside the pursuit of ultrahigh field performance, optimizing HECs for superior energy storage under moderate electric fields (200–400 kV·cm^{-1}) has been identified as important for the growing low-voltage electronics market [307,313].

3.5 HECs as electrodes for rechargeable batteries

The high-entropy strategy signifies a fundamental departure from conventional doping in functional material design. It involves the intentional creation of single-phase solid solutions where multiple principal cations coexist in significant proportions within a single crystallographic site of simple structures such as rock-salt, spinel, or layered oxides [314,315]. This compositional complexity is thermodynamically stabilized by high configurational entropy, which suppresses phase segregation [316]. For electrochemistry, this creates a unique state: a simple average crystal structure masking an atomic-scale landscape of severe chemical disorder, local strain, and diverse coordination environments. This intrinsic disorder is the engineered feature that grants unprecedented control over structural stability, redox activity, and charge transport to be used as electrodes for Na-ion and Li-ion batteries.

3.5.1 *Atomic-scale mechanisms: linking disorder to function*

Arresting structural degradation through lattice disorder. The random distribution of cations with differing ionic radii creates a statically strained lattice. This disordered strain field, thermodynamically stabilized by high entropy, imposes significant kinetic barriers to the collective atomic rearrangements responsible for failure. This effectively suppresses phase transitions (e.g., coherent O3 ↔ P3 transitions in layered oxides) by disrupting long-range cooperative slab gliding and inhibiting cation migration into alkali layers by kinetically trapping transition metals in sites with varied stabilization energies (Fig. 9(a)) and thus enhances the cycling performance (Fig. 9(b)) of high-entropy layered sodium oxide cathode materials [317,318].

Engineering electrochemical activity via local coordination. The diverse local coordination environments act as a "chemical toolkit" for precise redox tuning. The "cocktail effect", where the electronic structure of a redox-active metal is influenced by its nearest neighbors, allows for the modulation of cationic redox potentials and the activation of multielectron reactions (Fig. 9(c)) [319]. Simultaneously, high-entropy compositions can stabilize anionic (oxygen) redox by enhancing metal-oxygen covalency and localizing electron holes on oxygen, thereby inhibiting oxygen loss and voltage decay [320].

Enhancing charge transport through a disordered energy landscape. Atomic-scale disorder directly modifies pathways for ionic and electronic conduction. Severe local lattice distortion creates a broad distribution of site energies for mobile ions, which can overlap to form low-activation-energy percolation pathways for ionic diffusion (Fig. 9(d)) [321]. Furthermore, elemental intermixing can modify band structures to improve electronic conductivity, for instance, by inducing half-metallic character or narrowing band gaps [322].

3.5.2 *Mechanism-informed material design strategies*

3.5.2.1 Cathode design: stabilizing frameworks and tailoring redox

Cathodes, particularly for Na-ion and Li-ion batteries (SIBs and LIBs), require a delicate balance between high capacity and long-term structural integrity. High-entropy design directly addresses this by manipulating atomic-scale interactions.

Suppressing structural degradation via cationic disorder. The random distribution of cations with differing ionic radii creates a statically strained lattice. This disordered strain field kinetically hinders the collective atomic rearrangements responsible for detrimental phase transitions and cation migration. For instance, in layered oxide cathodes for SIBs, the harmful O3–P3 phase transition involving coherent slab gliding can be suppressed. This is exemplified by the work of Ding *et al.* [317], who demonstrated that in O3-type $NaNi_{0.3}Cu_{0.1}Fe_{0.2}Mn_{0.3}Ti_{0.1}O_2$, selecting compatible 3d-elements minimized cooperative planar strain within the transition metal layer, preventing the crack-inducing cation segregation observed in a Sn^{4+}-substituted analog and thereby ensuring robust cycling stability. This principle can be pushed to achieve near "zero-strain" behavior, as shown by Wang *et al.* [318] with $NaNi_{0.2}Fe_{0.2}Mn_{0.35}Cu_{0.05}Zn_{0.1}Sn_{0.1}O_2$, where the varied elemental functions (redox-active vs. structural pillars) enabled such effective internal buffering that the net volume change per cycle was negligible, leading to 87% capacity retention after 500 full-cell cycles.

Engineering reversible redox activity through local coordination. The diverse local environments in HECs act as a "chemical toolkit" for precise redox tuning. The electronic structure of a redox-active metal is influenced by its nearest

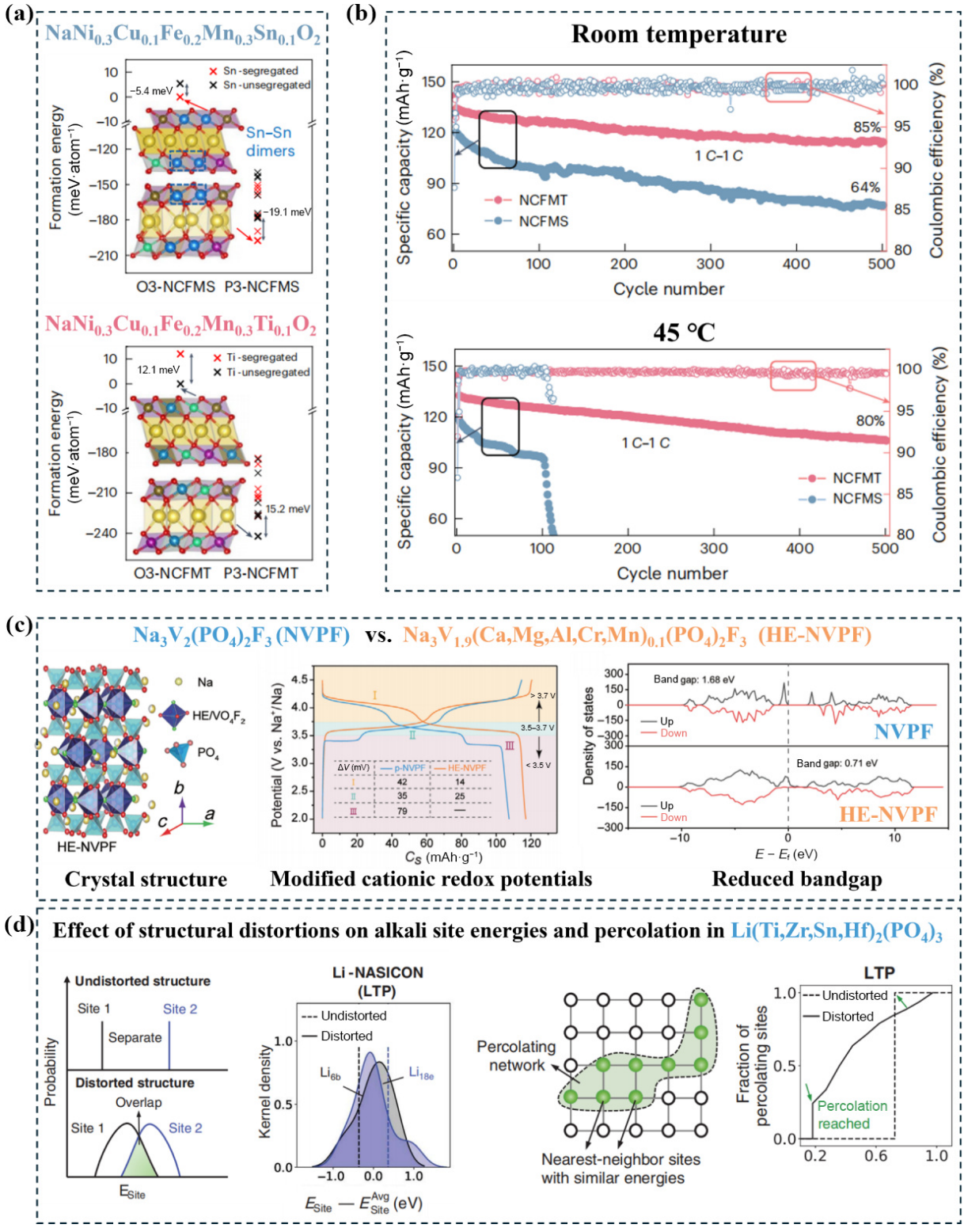

Fig. 9 Element engineering for improved rechargeable battery performance. (a) Calculated total energies for $NaNi_{0.3}Cu_{0.1}Fe_{0.2}Mn_{0.3}Sn_{0.1}O_2$ (O3/P3-NCFMS) and $NaNi_{0.3}Cu_{0.1}Fe_{0.2}Mn_{0.3}Ti_{0.1}O_2$ (O3/P3-NCFMT) with and without elemental segregation from density functional theory. (b) Room and high (45 °C) temperature cycling performance. Reproduced with permission from Ref. [317] for (a, b), © The Author(s) 2024, under exclusive license to Springer Nature Limited. (c) Crystal structure, modified cationic redox potentials, and reduced bandgap of $Na_3V_{1.9}(Ca,Mg,Al,Cr,Mn)_{0.1}(PO_4)_2F_3$ (HE-NVPF). Reproduced with permission from Ref. [319], © Wiley-VCH GmbH 2022. (d) Local lattice distortion-induced broad distribution of site energies for mobile ions. Reproduced with permission from Ref. [321], © The American Association for the Advancement of Science 2022.

neighbors, which can shift potentials and activate multielectron reactions. Gu *et al.* [319] leveraged this by applying multication substitution at the V-site in $Na_3V_2(PO_4)_2F_3$, which altered the local crystal field to raise the average operating voltage by 0.1 V while simultaneously enhancing the electronic conductivity, thereby boosting the energy density. Furthermore, high-entropy compositions can stabilize anionic (oxygen) redox by enhancing metal–oxygen covalency and localizing charge. Wang *et al.* [320]

engineered a layered cathode with strong Cu–O and Ti–O bonds emerging from the specific HEC composition, which enhanced electron localization on oxygen anions during charging, inhibited oxygen evolution, and enabled highly reversible anionic redox with minimal voltage decay (0.4 mV·cycle^{-1}).

Enhancing charge transport via a disordered energy landscape. Atomic-scale disorder directly modifies pathways for ionic conduction. Severe local lattice distortion creates a broad distribution of site energies for mobile ions, which can overlap to form percolation pathways with a lower effective activation energy. Zeng *et al.* [321] demonstrated this principle in solid electrolytes, showing that high-entropy compositions in Li-NASICON and garnet structures increased ionic conductivity by orders of magnitude due to a "flattened" energy landscape. This concept is also active in cathodes; for example, Lun *et al.* [322] found that in disordered rock-salt (DRX) cathodes, systematically increasing the number of transition metal species reduced short-range order and enhanced Li^+ percolation, directly boosting rate capability.

3.5.2.2 Anode design: mitigating conversion and alloying strain

Anodes based on conversion or alloying reactions offer high capacities but suffer from drastic volume changes. High-entropy chemistry provides a unique solution by combining multielectron redox with intrinsic structural resilience.

Buffering volume change in conversion oxides. Spinel or rock-salt HEO anodes utilize multiple redox-active cations (e.g., Fe, Co, Ni, Mn) for high capacity. Crucially, the entropy-stabilized matrix provides exceptional durability against the pulverizing stress of conversion reactions. This is vividly demonstrated by the work of Sun *et al.* [323] on spinel $(Cr_{0.2}Mn_{0.2}Fe_{0.2}Co_{0.2}Ni_{0.2})_3O_4$ (S-HEO), which delivered a high specific capacity of 560 mAh·g^{-1} and, remarkably, 100% capacity retention after 5000 cycles, a feat attributed to the synergic stabilization effect of the five constituent species. The reaction mechanism itself can be modified; Ma *et al.* [324] showed that introducing Li_2O into $(FeMgNiCrMn)_3O_4$ induced oxygen vacancies, leading to an enhanced Li^+ intercalation process prior to conversion, resulting in a high reversible capacity of 850.7 mAh·g^{-1} after 200 cycles at 2 A·g^{-1}.

Utilizing synergistic frameworks and alloys: Beyond simple oxides, high-entropy perovskite fluorides (HEPFs) and alloys (HEAs) offer alternative pathways. HEPFs such as $KMgMnFeCoNiF_3$, synthesized by Wang *et al.* [325], leverage a 3D open framework and synergistic multimetal redox to achieve high-rate capability. For alloying anodes, HEA composites such as the $Co_{0.2}Sb_{0.2}Fe_{0.2}Mn_{0.2}Ni_{0.2}$ carbon nanofiber composites reported by Zheng *et al.* [326] utilized elemental synergy to accommodate volumetric strain, enabling an ultrahigh capacity of 1400 mAh·g^{-1} after 800 cycles for LIBs.

3.5.2.3 Solid-state electrolyte design: Optimizing ion conduction pathways

Stabilizing conductive phases and engineering transport. By populating a single crystallographic site with multiple cations, a high-entropy design can stabilize high-conductivity phases (e.g., cubic garnet) at room temperature and engineer the ion migration landscape. Han *et al.* [327] synthesized $Li_{6.2}La_3(Zr_{0.2}Hf_{0.2}Ti_{0.2}Nb_{0.2}Ta_{0.2})_2O_{12}$, which exhibited not only excellent ionic conductivity but also superior air stability—a critical practical advantage—retaining its performance after two months of air exposure. Furthermore, Umair *et al.* [328] designed a medium-entropy garnet, $Li_6La_3Zr_{0.5}Ti_{0.5}Ta_{0.5}Nb_{0.5}O_{12}$, achieving an ultrahigh ionic conductivity of 1.52×10^{-3} S·cm^{-1} and a high critical current density of 2.5 mA cm^{-2}, showcasing the potential for high-power solid-state batteries.

3.5.3 Unfinished work on HECs for battery applications

The high-entropy strategy represents a fundamental and powerful shift in battery material design. Intentionally engineering atomic-scale cation disorder provides direct control over the microscopic mechanisms that govern macroscopic performance: kinetically arresting degradation pathways, chemically tuning redox activity, and physically optimizing charge transport landscapes. This mechanistic rationale has successfully guided the design of superior cathodes, anodes, and solid-state electrolytes, as evidenced by a growing body of literature. The future of this paradigm hinges on a concerted, interdisciplinary effort to master the synthesis of these complex materials, deepen fundamental understanding through coupled experimental and computational science, and rigorously validate their performance in integrated, practical battery systems. Success in these areas will solidify the role of high-entropy ceramics as key enablers of next-generation, high-performance, and sustainable energy storage.

Synthesis, processing, and scalability. The reproducible synthesis of phase-pure HECs with homogeneous elemental distribution at scale remains nontrivial. Traditional high-temperature solid-state routes risk element volatilization (e.g., F, Li) [329], while scalable solution-based methods require precise control. The cost and supply concerns associated with using multiple, sometimes critical raw materials necessitate a focus on earth-abundant element combinations [318,330]. Future efforts must prioritize the development of low-temperature, energy-efficient synthetic routes (e.g., advanced sol–gel, combustion) and establish robust processing protocols for electrode fabrication using these complex powders.

Fundamental understanding and predictive design. While qualitative mechanisms are recognized, quantitatively deciphering the role of each element in complex redox and transport processes remains a grand challenge. The "cocktail effect" is often invoked but poorly predicted. Characterizing the local atomic structure, short-range order, and dynamic ion migration in these disordered systems requires advanced techniques [331,332]. The path forward lies in a tightly coupled loop of advanced *in situ*/*operando* characterization (using synchrotron/neutron total scattering, X-ray absorption spectroscopy (XAS), and high-resolution STEM) and multiscale computational modeling (from DFT and molecular dynamics to machine learning potentials). This integrated approach is essential to build predictive composition–structure–property maps and enable truly rational design, as called for in several reviews [333,334].

Electrochemical and interfacial mechanism clarification. Deconvoluting which elements participate in redox at specific voltages, especially when coupled with anionic redox, is complex. The hypothesis that lattice distortion flattens the ion migration energy landscape, while supported by models and some data [321], needs more direct and widespread experimental validation across different material families. Furthermore, the stability of HEC electrodes against various electrolytes and the nature of the solid–electrolyte interphase (SEI) formed on HEO anodes are scarcely investigated but critical for longevity [335]. Systematic studies combining electrochemical techniques (galvanostatic intermittent titration technique (GITT) and electrochemical impedance spectroscopy (EIS)) with element-specific spectroscopy and computational analysis are required to unravel these complex mechanisms.

Application-oriented validation and integration. A significant gap exists between promising half-cell data and validated full-cell performance. Demonstrating long-term cycling, rate capability, and safety in practical full cells with realistic parameters (high

active material loading, limited Li/Na excess, lean electrolyte) is paramount for assessing commercial viability [318,336]. Research must aggressively transition to full-cell engineering and evaluation under realistic conditions. Concurrently, extending the high-entropy strategy to interface engineering—perhaps creating entropy-stabilized interphases or composite electrodes—presents a promising frontier to solve interfacial challenges [337].

3.6 HECs for efficient catalyst

3.6.1 *Catalytic mechanism of HECs*

In a conventional catalyst, one or two metals primarily govern the active sites. In HECs, the cationic sublattice is a mosaic of multiple elements, each with distinct electronic configurations, electronegativities, and redox potentials [74,338]. This creates a continuum of local electronic environments rather than discrete, uniform sites. The superior performance of HECs in thermal, photo, and electrocatalytic reactions stems from two intertwined mechanistic pillars: the synergistic cooperation of multiple cationic species and the prolific presence of catalytically active defects.

Multiactive site synergy. (1) Orchestrated reaction pathways. Different cations can preferentially catalyze different steps of a complex reaction. For instance, in photocatalytic CO_2 reduction to CH_4, elements with d^{10} configurations (e.g., Zn, Ga, In) have been identified as crucial for the challenging 8-electron methanation pathway, while d^0 elements (Ti^{4+}, Zr^{4+}, Nb^{5+}, and Ta^{5+}) often facilitate charge separation and light absorption [339]. The mixed atomic-scale electronic configuration can even eliminate the need for noble metal cocatalysts by inherently providing both electron donor and acceptor sites within the same lattice [339]. (2) Optimized adsorption energies. The combined interaction of elements yields properties unpredictable from the means of constituents. In oxygen evolution reaction (OER) catalysts such as $(AlCrCoNiFe_2)O$ or $(Fe_{0.2}Ni_{0.2}Co_{0.2}Mn_{0.2}Zn_{0.2})_3O_4$, diverse 3d transition metals (Fe, Co, Ni, and Mn) collaboratively adjust the binding strength of OH, O, and OOH intermediates, leading to lower overpotentials [340,341]. The presence of spectator or stabilizing elements such as Al, Cr, or Zn enhances structural integrity without sacrificing, and sometimes even enhancing, the collective activity of the active ensemble [340]. (3) Entropy-stabilized active sites. The high configurational entropy stabilizes the single-phase structure even under harsh reaction conditions. This prevents phase segregation that would deactivate conventional multimetal catalysts. For example, a high-entropy perovskite air electrode $Ba_{0.95}K_{0.05}Co_{0.2}Zn_{0.2}Ga_{0.2}Zr_{0.2}Y_{0.2}O_{3-\delta}$ (BKCX) maintained its structure and performance over hundreds of hours of reversible operation in a protonic ceramic cell, a feat difficult for conventional perovskites prone to cation segregation [342].

Defect engineering: oxygen vacancies and beyond. (1) Enhanced oxygen mobility and storage. Defects, particularly oxygen vacancies (V_O), are not merely byproducts but are intrinsic, often abundant, and highly functional features in HECs, especially HEOs. The lattice distortion in HEOs lowers the energy barrier for oxygen ion migration. Combined with the presence of redox-active cations, this creates a highly mobile lattice oxygen network. Materials such as $(CeHfZrSnEr)O_x$, synthesized via ultrasound, exhibit high oxygen vacancy concentrations, which are pivotal for oxidation reactions [343]. In CO oxidation over Ce-containing fluorite HEOs, the synergy between redox pairs (e.g., Ce^{3+}/Ce^{4+}, Mn^{2+}/Mn^{3+}) and facile V_O formation/annihilation provides a continuous Mars-van Krevelen-type reaction pathway [344]. (2) Promotion of adsorption and activation. V_O sites are often strong adsorption centers for molecules such as H_2O, CO_2, and O_2. In photocatalytic and photoelectrochemical processes, they serve as traps for photogenerated electrons, reducing charge carrier recombination. For instance, Eu-doped $(La_{0.2}Nd_{0.2}Sm_{0.2}Gd_{0.2}Y_{0.2})_2Zr_2O_7$ showed enhanced photocatalytic activity, attributed in part to defect-modulated band structures and improved charge separation [345]. (3) Stabilizing clusters. Defect-rich HEO surfaces can anchor and stabilize precious metal nanoparticles or single atoms, preventing sintering. Pd nanoclusters supported on nanoporous $CeHfZrSnErO_x$ remained highly dispersed and active for CO oxidation even after treatment at 900 °C, outperforming Pd/CeO_2 [343]. The high-entropy support provides a spectrum of binding sites, effectively "pinning" the metal clusters. Similarly, a Pt-(MgCoNiCuZn)O high-entropy single-atom catalyst demonstrated remarkable long-term stability for CO_2 conversion [346].

3.6.2 *Design strategies for high-entropy ceramic catalysts*

The development of high-performance HEC catalysts follows a multifaceted design philosophy, encompassing composition selection, synthesis innovation, and morphology control.

Entropy-driven composition design. (1) Targeted element selection. The choice of elements is dictated by the target reaction. For the OER, a combination of established active 3d metals (Fe, Co, Ni, and Mn) with stabilizers (Al, Cr, and Zn) is common [340,341]. For CO_2 photoreduction, mixing d^0 and d^{10} elements is a strategic approach to balance light absorption, charge separation, and product selectivity (Fig. 10(a)) [339]. For thermal oxidation, incorporating redox-active couples (Ce, Mn, Cu, and Co) alongside stabilizers (Zr, Al, Y, and La) is key [344]. (2) Entropy maximization and phase stability. The primary goal is to achieve a single-phase solid solution. This often requires calculating the entropy of mixing and ensuring a favorable enthalpy contribution. The use of elements with similar ionic radii and compatible crystal field stabilization energies promotes single-phase formation, as seen in rock salt, fluorite, perovskite, and spinel HEOs [338,347]. (3) Beyond oxides. The paradigm extends to other anion lattices. High-entropy nitrides (e.g., (TiHfNbTaMo)N) and carbides offer metallic conductivity beneficial for electrocatalysis [348]. High- and medium-entropy fluorides (e.g., rutile-type $(Co,Cu,Mg,Ni,Zn,Mn,Fe)F_2$) and borides ($(TiVCrMo)B_2$) open new avenues for anion-dependent activity, such as in nitrate reduction to ammonia [349].

Innovative synthesis for nanostructuring and porosity. Bulk HECs often suffer from a low surface area. Advanced synthesis aims to create nanostructured, high-surface-area morphologies. Sol–gel, coprecipitation, and solution combustion synthesis (SCS) allow molecular-level mixing and yield nanopowders. For instance, a facile sol–gel method produced nanostructured Ce-containing HEOs with surface areas up to 138 $m^2 \cdot g^{-1}$, crucial for exposing active sites [344]. Solution combustion synthesis has also been effectively used to prepare Ce-free high-entropy fluorite oxides with tunable oxygen vacancy concentrations [350]. To create porous architectures, methods such as dealloying eutectic alloys can yield core–shell nanostructures (e.g., high-entropy intermetallic oxide) [348]. Templating approaches are advancing toward complex geometries; for example, direct vat-photopolymerization 3D printing using Pickering emulsions has been demonstrated to fabricate hierarchically porous SiC architectures loaded with Co/Ni-based catalysts in a single step, showcasing a powerful route for creating structured HEC supports [351]. Flame aerosol synthesis is a transformative, scalable one-step route to produce high-entropy oxide nanoceramics, even with up to 22 distinct cations, featuring excellent thermal stability for efficient CO_2 hydrogenation

(Fig. 10(b)) [346]. Pulsed laser fragmentation in liquids can downsize micropowders to nanoparticles, drastically increasing the surface area and activity for photocatalysis [352]. (4) Mechanochemical synthesis. Ball milling offers a solvent-free, scalable route for synthesizing HEOs and HEFs, as demonstrated for rutile-type high-entropy fluorides [349].

Postsynthesis activation and modification. (1) Defect engineering. Treatments under reducing atmospheres, doping with lower-valence cations, or laser processing can intentionally introduce more oxygen vacancies. F-doping in perovskite HEOs (e.g., $BaCo_{0.2}Zn_{0.2}Ga_{0.2}Zr_{0.2}Y_{0.2}O_{2.9-\delta}F_{0.1}$) was used to modulate electron pairs and metal–oxygen bonds, enhancing proton conductivity and catalytic activity in fuel cells (Fig. 10(c)) [342]. (2) Hybridization. Compositing HECs with conductive supports improves electron transfer in electrocatalysis. A novel composite of graphene and (AlCrCuFeNi)O high-entropy ceramic was developed as a cathode, which effectively removed 99% of methyl orange within 90 min in an electro-Fenton process, demonstrating superior catalytic activity and stability [353].

3.6.3 *The unfinished agenda for HECs in catalysis*

High-entropy ceramics, particularly oxides and carbonitrides, have firmly established a new paradigm in catalytic materials science. Their activity stems from a powerful confluence of entropy-stabilized diversity and engineered imperfection: The synergistic interplay of multiple cationic active sites fine-tunes reaction pathways [339,340], while a high density of defects such as oxygen vacancies enhances adsorption, charge transfer, and ionic mobility [343,344]. Design strategies have evolved from simple entropy maximization [338,347] to sophisticated nanoarchitecting [346,348] and postsynthetic tuning [342]. However, the journey from a fascinating material class to a technological mainstay requires overcoming challenges in fundamental understanding, scalable synthesis of earth-abundant compositions, and device integration [351,355,356]. As research moves deeper into the complex interplay within these "multivariate" materials and broader into new catalytic applications, high-entropy ceramics are poised to catalyze not only chemical transformations but also a fundamental shift in how we design and conceive functional materials for energy and sustainability.

The "black box" nature of multicomponent synergy makes it difficult to pinpoint the exact role of each element or predict optimal compositions. The complex local structures and dynamic surface reconstruction under operating conditions are poorly understood. Leveraging *in situ*/*operando* characterization tech

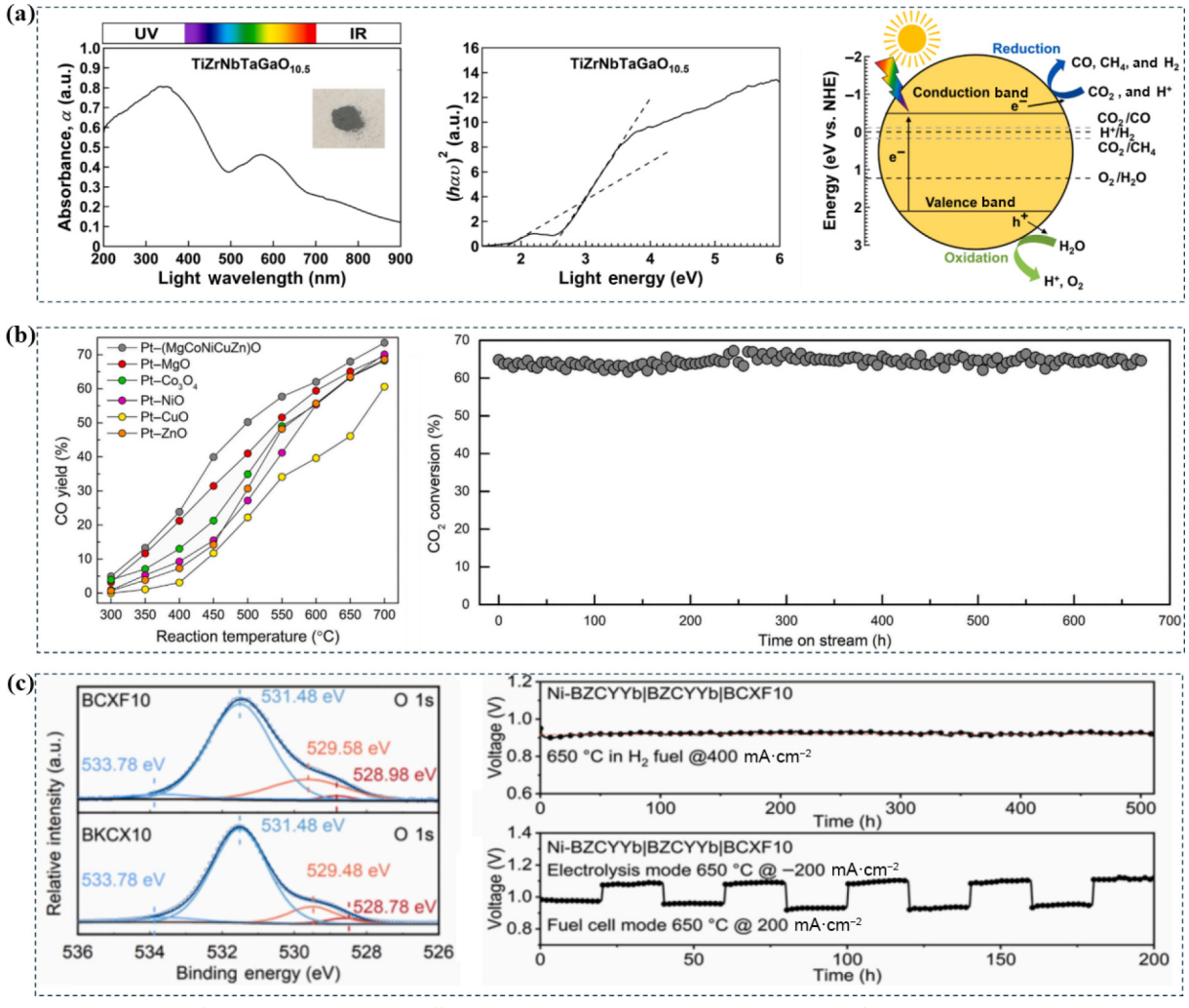

Fig. 10 Enhanced catalysis performance in HECs through different design strategies. (a) Mixing d^0 and d^{10} elements for balancing light absorption, charge separation, and product selectivity in CO_2 photoreduction. Reproduced with permission from Ref. [339], © Acta Materialia Inc. 2024. (b) High entropy design for excellent thermal stability for efficient CO_2 hydrogenation. Reproduced with permission from Ref. [346], © Elsevier Inc. 2024. (c) F-doping to modulate electron pairs and metal–oxygen bonds for enhancing proton conductivity and catalytic activity in fuel cells. Reproduced with permission from Ref. [342], © Elsevier B.V. 2025.

niques (XAS, XRD, STEM, ambient-pressure XPS) coupled with high-throughput experimentation and advanced computational modeling (machine learning, *ab initio* molecular dynamics on large supercells) is essential. This will move the field from Edisonian discovery to rational, predictive design. Studies using *in situ* XAS to identify Co, Mn, and Ni as dynamic active sites in (AlCoCrFeMnNi)O for seawater splitting represent a step in this direction [354].

Many promising synthesis routes (e.g., flame spray pyrolysis, laser processing) are energy-intensive or not yet scalable. The use of rare or expensive elements (e.g., Hf, Ta, noble metals) in some compositions raises cost concerns for large-scale applications such as water splitting or environmental remediation. The development of simpler, low-energy, and scalable solid-state or solution-based methods is crucial. Research should focus on HECs composed entirely of earth-abundant elements without sacrificing performance. Scalable methods such as solution combustion synthesis offer promising pathways [350].

While HECs are touted for exceptional thermal stability, their long-term durability under complex real-world conditions—such as in acidic/alkaline electrolytes, the presence of poisoning species (e.g., Cl^- in seawater), or cyclic redox stresses—is not fully established. Metal leaching, especially from less stable cations, remains a concern. Extensive durability testing under application-specific conditions is needed. Designing HECs with a "self-healing" capability or with a protective surface layer could be explored. The demonstrated 1000 h stability of an (AlCoCrFeMnNi)O catalyst in seawater OER is an encouraging benchmark [354].

Research heavily emphasizes OER, CO_2 reduction, CO oxidation, and organic pollutant degradation [339,340,344,348]. There is vast potential in unexplored territories: selective hydrogenation, ammonia synthesis or decomposition, methane activation, photocatalytic organic synthesis, and biocatalysis. The unique surface of HECs could break scaling relations that limit conventional catalysts.

Most research addresses powder catalysts, which pose practical issues for device integration, recyclability, and pressure drop in flow systems. The future lies in engineering HECs into macroscopic functional forms: wash-coated monoliths, 3D-printed structures, free-standing electrodes, and membranes. Significant progress is evident in the development of applied forms, such as high-entropy perovskite oxide wash coated onto porous alumina ceramic (PAC) monoliths for peroxymonosulfate activation, which combines high activity with easy recyclability [355]. Similarly, macroporous high-entropy spinel oxide monoliths fabricated via a sol–gel method have shown remarkable OER performance and stability, highlighting the potential of monolithic HEC catalysts [356]. The advancement of 3D printing techniques for structured catalyst supports further enables this transition from powder to practical devices [351].

4 Quantitative efforts: Challenges and progress from concepts to models

The transition of HECs from a novel curiosity to a legitimate engineering material class hinges on the development of quantitative, predictive design frameworks. As illustrated in Section 3, moving beyond Edisonian trial-and-error, researchers are actively building strategies that integrate thermodynamics, advanced characterization, kinetics, and data science to navigate the immense compositional landscape. This section details the progress and ongoing challenges in these quantitative endeavors.

4.1 Thermodynamics and phase stability prediction

The foundational question for any prospective HEC composition is deceptively simple: Will it form a single-phase solid solution, or will it decompose into a mixture of simpler compounds? Answering this requires navigating a complex energy landscape shaped by enthalpy and entropy. The Gibbs free energy equation, $\Delta G_{mix} = \Delta H_{mix} - T\Delta S_{mix}$, is the cornerstone, where a negative ΔG signifies stability. The "high-entropy" hypothesis posits that a large, positive ΔS_{conf} can overcome an unfavorable (positive) enthalpy of mixing (ΔH_{mix}) at sufficiently high temperatures, leading to entropy stabilization [188]. However, the real picture is far more nuanced, and quantitative tools are evolving to capture this complexity.

Early work adapted the Hume–Rothery rules from metallic solid solutions to ceramic systems. The criteria-favorable atomic size difference (δ_r), similar crystal structure, compatible electronegativity, and matching valency provided a useful, qualitative starting filter. For instance, the success of the quintessential $(Ti_{0.2}Zr_{0.2}Hf_{0.2}Nb_{0.2}Ta_{0.2})C$ system can be rationalized by the compatible ionic radii and shared rock-salt structure [190–192]. However, the synthesis of carbides incorporating elements such as Mo or W, whose stable carbides are not rock salt, exposed the limits of these rules, pointing to a stabilizing effect of high configurational entropy [191,199,357].

This is where density functional theory (DFT) has become indispensable. DFT allows for *ab initio* calculation of the enthalpy of mixing (ΔH_{mix}). Studies reveal that for many stable HEC systems, ΔH_{mix} is slightly positive but small [191,192]. The stabilizing force is the large ΔS_{conf}, which scales with the number of components. At high temperatures, the $-T\Delta S$ term dominates, driving negative ΔG_{mix}. This rationale underpinned the synthesis of $(V_{0.2}Nb_{0.2}Ta_{0.2}Mo_{0.2}W_{0.2})C$, where DFT-derived "entropy descriptors" successfully predicted formability [191]. Beyond stability, DFT enables property prediction. For example, first-principles investigations of lightweight $(Nb_{0.25}Ti_{0.25}Zr_{0.25}V_{0.25})C$ predicted an excellent combination of low density, high hardness and fracture toughness [192].

DFT also reveals complexities such as site preferences, which reduce achievable configurational entropy from the ideal mixing value. In spinel HEOs such as $(Al,Cr,Fe,Mn,Ni)_3O_4$, DFT shows that Al^{3+} prefers tetrahedral sites, explaining property variations and challenging the assumption of perfect randomness [358,359].

The CALPHAD methodology extends thermodynamic modeling from 0 K to application temperatures. It integrates data from experiments and DFT to model Gibbs free energies across complex multicomponent spaces. Its application in HECs, while growing, is hampered by a stark lack of robust thermodynamic data for ternary and higher-order systems. Most successful applications remain in high-entropy alloys. Ceramics are often used to guide sintering profiles by estimating solidus temperatures from simpler subsystems. Insightful CALPHAD studies have elucidated a critical nuance: For many HECs, the enthalpy of mixing is at least as important as configurational entropy. True thermodynamic stability at room temperature for most compositions likely requires a negative ΔH_{mix} to offset the reduced $T\Delta S$ term, implying that many synthesized HECs are metastable, kinetically trapped phases.

A major advance in quantitative design is the recognition of carbon content as a primary control variable. Carbon vacancies are intrinsic point defects that drastically influence thermodynamics and kinetics [197–199,202]. Research on systems such as $(Ti_{0.2}Zr_{0.2}Nb_{0.2}Ta_{0.2}Mo_{0.2})C_x$ has mapped precise "carbon windows" (e.g., x = 0.70–0.85) for single-phase formation [198].

Deviations lead to secondary phases. This nonstoichiometry can be strategically employed. For the notoriously difficult-to-form (Zr,Hf,Ta,Ti)C single phase, reducing the C/TM ratio promoted solid solution formation at lower temperatures by increasing entropy and reducing bond strength [197].

The primary limitation is the pervasive role of kinetics. Synthesis techniques such as SPS are far from equilibrium, often producing metastable single phases that equilibrium thermodynamics might not predict. The "formability" discussed is thus often a kinetic outcome. Furthermore, current models heavily prioritize the cation sublattice. A comprehensive framework must integrate the complex interplay between cation disorder, anion vacancy concentration, and potential anion sublattice interactions. Nonideal interactions lead to short-range ordering, as detected by neutron PDF in rare-earth RE_3TaO_7, which can significantly reduce ΔS_{conf} [360]. Charge-coupled substitutions (e.g., aliovalent doping) can be entropy-stabilizing if charge compensation creates point defects, expanding the design space but complicating prediction [361].

Therefore, the current quantitative strategy is hierarchical. (1) Use size/valence descriptors for primary screening. For example, research on pyrochlores demonstrates a size disorder (δ) threshold of approximately 5.2% as a boundary for single-phase formation [234]. (2) DFT was applied to selected candidates to assess ΔH_{mix}, site disorder, and electronic structure. (3) Acknowledge that kinetics will often deliver metastable, single-phase materials even if equilibrium thermodynamics predicts minor secondary phases. The goal is not the perfect prediction of equilibrium states but the reliable prediction of synthesizable and quenchable single-phase HECs.

4.2 Correlating structural distortion and properties

The concept of "severe lattice distortion" is hypothesized to be the root cause of enhanced mechanical properties and suppressed thermal transport. Moving from a compelling hypothesis to quantified, predictive relationships has been a central challenge. The strategy has evolved from asserting distortion based on composition to directly measuring it and empirically correlating it with macroscopic properties.

Advanced characterization techniques bring the abstract idea of lattice distortion into tangible focus. Atomic-resolution STEM coupled with EDS/EELS provides direct visual proof of random, homogeneous cation distribution at the atomic scale, as seen in high-entropy perovskite oxides [52] and single-crystal perovskite films of $Ba(Zr_{0.2}Sn_{0.2}Ti_{0.2}Hf_{0.2}Nb_{0.2})O_3$ [362]. It can also directly image lattice strain and dislocation networks. Synchrotron X-ray/neutron diffraction and PDF analysis are where quantification begins. High-resolution diffraction refines average lattice parameters and atomic displacement parameters (ADPs), which quantitatively measure static disorder. The real power lies in total scattering and PDF analysis. The PDF, $G(r)$, describes the probability of finding two atoms separated by a distance r. In HECs, PDF peaks are broadened at higher r, directly quantifying static lattice distortion. PDF has revealed short-range ordering within long-range disordered structures, as in $(Y_{0.2}Yb_{0.2}Er_{0.2})_3TaO_7$, providing a microstructural mechanism for ultralow thermal conductivity [360]. Extended X-ray absorption fine structure (EXAFS) offers element-specific local structural information, confirming random distribution and providing quantitative measures of local bond length variations.

While a universal formula remains elusive, strong empirical trends have solidified the causal link. For the hardness and strength, the enhancement of hardness in HECs over the rule-of-mixtures average is one of the most replicated results. Micropillar compression tests on (Hf–Ta–Zr–Nb)C single crystals revealed a yield strength significantly higher than that of binary monocrystals [363]. The strengthening is directly attributed to intense local strain fields that act as potent barriers to dislocation motion—a classic solid solution strengthening mechanism amplified in a multicomponent matrix. Vickers hardness values for HECs such as high-entropy silicides $(Mo_{0.2}Nb_{0.2}Ta_{0.2}Ti_{0.2}W_{0.2})Si_2$ (16.7 GPa) far exceed their binary counterparts [77].

Thermal conductivity (κ) shows the most dramatic and quantifiable correlation. High-entropy borides and carbides exhibit thermal conductivities 5–10 times lower than their binary counterparts [364–366]. This is a direct consequence of phonon scattering by mass disorder, strain field disorder, and point defect scattering. Researchers have identified robust descriptors. A seminal study on pyrochlores established that the size disorder parameter (δ_{size}) correlates well with reduced κ. Furthermore, work on single-crystal entropy-stabilized oxides (ESOs) showed that local ionic charge disorder is exceptionally effective in reducing κ to near the amorphous limit [234].

For K_{IC}, the correlations are more complex. While distortion can be embrittle, some HECs leverage transformation toughening. The multicomponent oxide $Zr_{1-4x}Y_xYb_xTa_xNb_xO_2$ exhibits a high K_{IC} of ~4.59 MPa·m$^{1/2}$ due to stress-induced phase transformation [367].

The field has successfully moved from assuming distortion to measuring it. PDF and EXAFS provide quantitative metrics of local strain. The correlation between increased compositional complexity (and its proxy, increased measured distortion) and improved hardness/strength and reduced thermal conductivity is well established as a dominant trend. A significant hurdle is isolating the effect of lattice distortion from other variables, such as grain size or porosity. Therefore, research has focused on comparing dense, single-phase HECs with binaries or studying property evolution as a function of a controlled variable such as vacancy concentration. The next frontier is to move from trend-based to model-based prediction, integrating quantitative distortion parameters into multiscale models to predictively bridge atomic-scale disorder to macroscale properties.

4.3 Studies on kinetic effects

While thermodynamics determines what is stable, kinetics dictates what forms and how it evolves over time, especially under extreme conditions. The sluggish diffusion effect, widely discussed in high-entropy alloys, is equally pivotal in ceramics. The evidence is largely phenomenological but overwhelmingly consistent, pointing to a fundamental barrier to atomic migration within the distorted lattice.

The most compelling case comes from the observed behavior during oxidation, ablation, and microstructural evolution. HECs consistently outperform constituent binaries. For example, (Zr,Ti,Hf,Nb,Ta)C exhibits a parabolic oxidation rate constant two orders of magnitude lower than ZrC [258]. During oxyacetylene ablation, HEC coatings form complex, gradient oxide scales that persist for minutes, whereas simpler coatings fail in seconds. This implies that the diffusion of species necessary for scale evolution is dramatically slowed. A key insight is "synergistic oxidation": In a true solid solution, the rapid preferential oxidation of the most reactive component is kinetically hindered by the need to break its chemical bonds with others, forcing a slower, cooperative process. Direct comparisons show dramatic suppression. For instance, high-entropy $(La,Ce,Nd,Sm,Eu)_2Zr_2O_7$ showed minimal grain growth after annealing at 1500°C compared to conventional La_2ZrO_7 [368].

The very existence of many single-phase HECs is kinetic. Sluggish diffusion prevents nucleation/growth of equilibrium phases upon cooling, allowing kinetic trapping. This also confers superior resistance to densification during service, a critical advantage for thermal barrier coatings. The high sintering temperatures (> 2000 °C) required point to slow diffusion. Conversely, this can be exploited; adding Cr to (Ti,Zr,Nb,Ta,Mo)C enabled full densification at 1600 °C but resulted in an ultrafine grain size, suggesting nuanced kinetic effects on different diffusion pathways [212,213].

The atomic-scale mechanism stems from the disordered lattice creating a "rough" energy landscape for diffusing species. A diffusing atom encounters a sequence of local environments with varying bond strengths, sizes, and electrostatic potentials, resulting in a wide distribution of migration energy barriers. The overall rate is governed by the highest barriers. Different host cations may have opposing chemical affinities for a diffusing species, creating local potential wells that trap defects. Severe static strain directly increases the energy required for an atom to squeeze through a "bottleneck" during a hop. Molecular dynamics simulations are beginning to quantify these increased barriers. The most significant bottleneck is the absence of direct diffusion coefficient data. There are rarely published measurements of cation or anion tracer diffusion coefficients in HECs. These fundamental data are essential for modeling creep, long-term stability, and oxidation rates. Acquiring it is experimentally daunting. Future progress hinges on innovative experimental techniques coupled with computational efforts using kinetic Monte Carlo or molecular dynamics with machine-learned potentials to simulate diffusion barriers. Until this gap is filled, the understanding of kinetics in HECs will remain primarily phenomenological, although powerfully explanatory and strategically valuable for designing materials for high-temperature stability.

4.4 Machine learning-aided design

The vast compositional space of HECs is intractable for purely intuition- or simulation-led exploration. Machine learning emerges as a transformative tool to mine existing knowledge, identify patterns, and accelerate discovery [369–372]. Its application is in the pioneering stage, characterized by promising proof-of-concept studies that starkly reveal the field's data-driven growing pains.

Supervised learning models are trained on experimental data. For example, artificial neural networks have been used with high-throughput data to predict oxidation recession rates of diboride–SiC composites, rapidly identifying novel compositions [229]. Models are also built to predict hardness and thermal conductivity based on compositional descriptors such as atomic radius, mass, and their variances (δ_r and δ_m) [239,373–376]. Treated as a classification problem (single-phase vs. multiphase), ML models use features from elemental properties and thermodynamic parameters to learn complex boundaries, effectively creating a data-driven refinement of Hume–Rothery rules [59,377–381]. This revolutionary application starts with a target property profile to find optimal compositions. One study defined desired anti-ablation oxide scale characteristics and used theoretical guidance to design the HEC coating $(Hf_{0.36}Zr_{0.24}Ti_{0.1}Sc_{0.1}Y_{0.1}La_{0.1})C_{1-\delta}$, which showed superior ablation resistance [382].

The single greatest impediment is the lack of large, consistent, and high-fidelity datasets. The number of thoroughly characterized HEC compositions is minuscule compared to mature fields. Data are scattered, with key features (e.g., processing details) often missing. Measurements from different labs introduce noise. Publication bias toward successful syntheses cripples a model's ability to learn true boundaries of stability and performance. Choosing input features is critical. Beyond elemental properties, researchers incorporate features from DFT (mixing enthalpy) and phase diagram characteristics. Explainable AI (XAI) efforts, such as Shapley Additive exPlanations (SHAP) values, are crucial to extract physical insights. The future lies in creating a virtuous cycle:

Community-wide initiatives for standardized, open-access databases are essential, including detailed processing paths and "negative" results. Integrating physical principles with data-driven learning. This includes using computational features, incorporating processing parameters, and leveraging transfer learning from larger, related datasets (e.g., general oxide properties) before fine-tuning on HEC data. Then, machine learning was integrated with robotic high-throughput experimentation to accelerate the discovery of HEC. An ML model suggests promising compositions; the robotic platform synthesizes and tests them; results feedback to improve the model, exponentially accelerating exploration. ML can develop surrogate models for expensive DFT calculations or infer properties for mesoscale models, creating a pipeline from atomic composition to component-level performance.

The successful execution of this virtuous cycle, however, relies not on a single computational tool but on the judicious orchestration of a diverse methodological toolkit. Table 2 places machine learning within this broader landscape, contrasting its capabilities and limitations with those of DFT, molecular dynamics, CALPHAD, and other quantitative approaches. A clear appreciation of each method's domain of applicability is essential for constructing the integrated workflows that will propel HECs from discovery to design. The future of quantitative HEC design lies in a synergistic feedback loop: human-defined rules and physics-based models guide initial exploration → ML analyzes data to find nonintuitive patterns and suggest optima → human experts validate and interpret → the expanded database fuels more accurate ML models (Fig. 11). This approach will ultimately unlock the systematic design of HECs for next-generation technologies.

5 Controversies and deliberation

The rapid ascent of HECs from a novel concept to a major research frontier has been propelled by remarkable empirical successes. However, beneath the surface of enthusiastic reporting lies a bedrock of fundamental assumptions, inherent trade-offs, and unanswered questions that warrant critical scrutiny. Before dissecting these controversies, it is instructive to first consolidate the prevailing conceptual framework that has guided the field thus far. Table 3 succinctly summarizes the thermodynamic and kinetic origins of the widely invoked "four core effects" along with their primary impacts on crystal structure, microstructure, and resultant properties. This tabulated overview could serve as a reference for the deliberate re-evaluation that follows.

5.1 Re-evaluating the role of entropy

The term "high-entropy" privileges ΔS_{conf} as the defining design principle. While crucial for stabilizing single-phase solid solutions against phase separation, its relationship to functional properties is neither linear nor universally positive. A critical re-evaluation reveals boundary conditions and potential detrimental effects.

Defining true entropy stabilization vs. high-entropy compositions. A core controversy lies in distinguishing ESOs from high-entropy oxides (HEOs) or CCCs. True entropy

stabilization, as first shown in (Mg,Co,Ni,Cu,Zn)O [4], requires a reversible solid-state transformation between a multiphase and single-phase state, proving that entropy dominates the thermodynamic landscape. However, many materials labeled as HECs have not demonstrated this reversibility. As highlighted in the database, critical reviews argue that stability may be

Table 2 Comparison of computational methods for high-entropy ceramics

Method	Basic principle	Predictable quantity	Advantage	Limitation	Applicable scenario	Ref.
DFT	Solve Kohn–Sham equations	Formation enthalpy, electronic structure, elastic constants, defect energies	Atomic-scale accuracy	Computationally expensive	Stability prescreening, mechanism studies	[191,192,261]
Molecular dynamics	Newton's equations + potential functions	Diffusion coefficients, thermal conductivity, and phase transition processes	Simulates kinetics	Potential accuracy dependent	High-temperature behavior, defect evolution	[188,270]
CALPHAD	Extrapolation of thermodynamic databases	Phase diagrams, phase fractions, thermodynamic driving forces	Engineering temperature range	Lack of multicomponent data	Sintering temperature prediction, phase composition	[185,186]
Machine learning	Data-driven model training	Phase formation, hardness, thermal conductivity	High-throughput screening	Data and feature dependent	Composition space exploration, property prediction	[59,376,377]
Entropy descriptors	Statistics based on atomic properties	Single-phase formability	Fast, physically intuitive	Empirical, limited universality	Rapid prescreening	[14,191,393]
Multiscale modeling	Coupling DFT + MD + phase field	Atomistic to microstructure	Cross-scale prediction	Complex, many parameters	Full-process property prediction	[227,381]

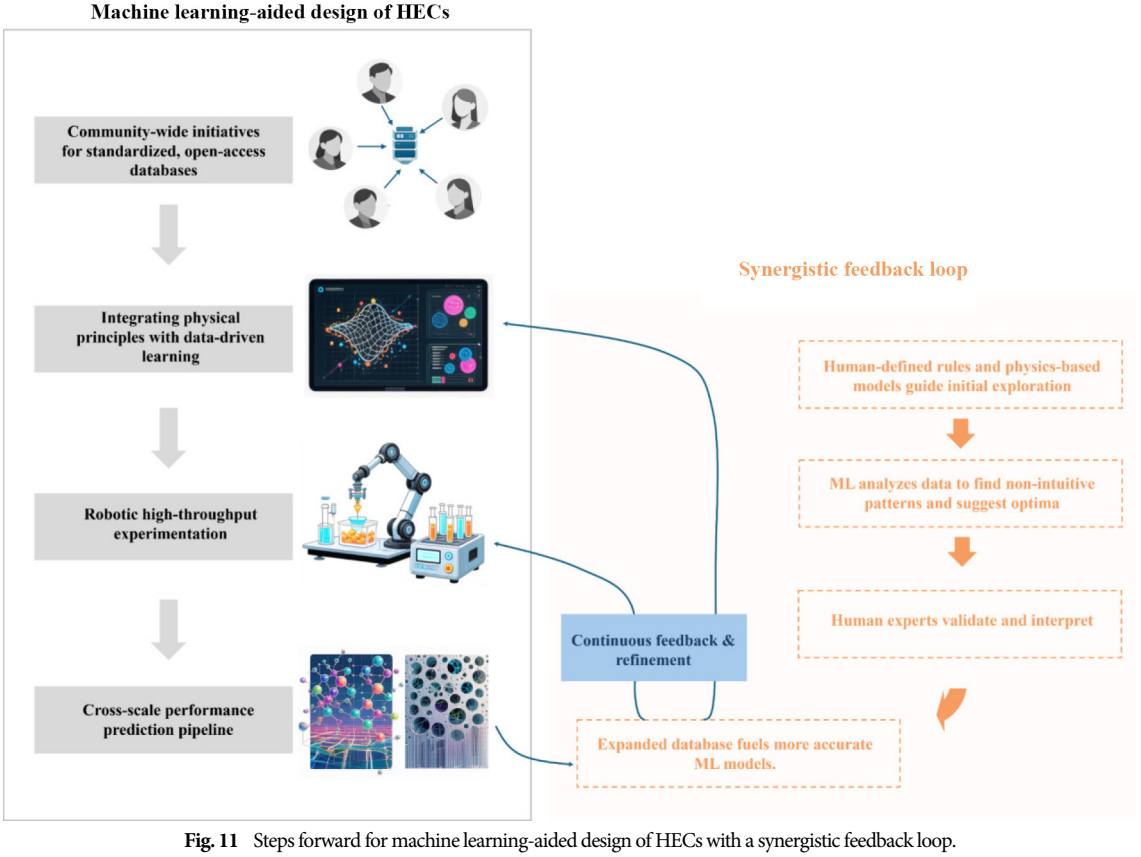

Fig. 11 Steps forward for machine learning-aided design of HECs with a synergistic feedback loop.

Table 3 Mechanisms of the four core effects and their correlations with properties

Core effect	Thermodynamic/ kinetic origin	Impact on crystal structure	Impact on microstructure	Dominant property	Synergistic effect	Ref.
High-entropy effect	$\Delta G = \Delta H - T\Delta S < 0$	Stabilizes single-phase solid solution	Suppresses phase separation	High-temperature phase stability	Enables other effects	[4,188,232]
Severe lattice distortion	Atomic radius mismatch → local strain	Broadened bond length/ angle distribution	Hinders dislocation motion	↑ Hardness, ↓ Thermal conductivity	Enhances solid solution strengthening	[52,157,160]
Sluggish diffusion	Rugged energy landscape → ↑ migration barriers	No direct impact	↓ Grain growth, ↑ Oxidation resistance	↓ Creep, ↑ Phase stability	Maintains fine–grain strengthening	[188,258,368]
Cocktail effect	Multielement synergy → nonadditive behavior	Electronic structure modulation	Local chemical ordering	Functional properties (catalysis, dielectrics)	Optimizes overall performance	[9,319,340]

enthalpically driven or kinetically trapped, with configurational entropy playing a secondary role [7,9,13,24,92,188]. The conflation of "high-entropy" with "entropy-stabilized" is a significant point of contention, necessitating more rigorous thermodynamic characterization.

Performance saturation and "dilution" effect. Maximizing configurational entropy is not always functionally beneficial, leading to a "cocktail effect" vs. "dilution effect" debate. While some HEOs exhibit a colossal dielectric constant (CDC), this is often attributed to extrinsic effects such as Maxwell–Wagner polarization at internal interfaces [236,383,384]. Introducing more cations can homogenize the microstructure, reduce these interfaces, and thus dilute the dielectric response. This exemplifies how the drive for maximum entropy can oppose the optimization of properties relying on specific microstructural features. In catalytic HEOs, adding too many cations can reduce the surface concentration of the most active element, potentially lowering activity unless a unique synergistic active site is created [345,352]. Intriguingly, some optimal oxidation and ablation resistances have been reported for medium-entropy or nonequimolar designs [184,193,195,196,385]. For UHTCs, excessive disorder might hinder the formation of a specific, protective oxide scale or dilute the concentration of a key element (e.g., Hf for refractory oxide formation) below a critical threshold.

Kinetic overriding of thermodynamics. Synthesis techniques such as SPS or RFS are highly nonequilibrium. Many reported "single-phase" HECs may be metastable, kinetically trapped states. Their formation is less about achieving a global entropy maximum and more about rapid processing, bypassing thermodynamic equilibrium. The question becomes: Are we stabilizing a phase or simply freezing a disordered precursor? Furthermore, at lower service temperatures, the thermodynamic drive for decomposition may persist, making long-term microstructural stability under stress an unproven assumption for many systems. In essence, entropy is a powerful tool for phase stabilization but a blunt instrument for property optimization. The field is maturing toward targeted engineering of "just enough" disorder to achieve a specific outcome.

5.2 High entropy vs. medium entropy

The arbitrary threshold of five principal elements for "high-entropy" is being pragmatically challenged. A key deliberation is whether medium-entropy ceramics (MECs), with 3 or 4 principal cations, offer a better balance between performance, processability, and cost. As illustrated above, evidence suggests that MECs can match or exceed HECs in key properties [184,193,195,196,385]. The study on size disorder as a descriptor explicitly noted that medium-entropy ceramics can outperform their high-entropy counterparts in achieving low thermal conductivity [108,386–388]. The largest incremental gain often comes from moving to a 3- or 4-component system, adding more elements may provide only marginal improvement.

The synergistic oxidation of a (Hf,Zr,Ti)C MEC powder is superior to a physical mixture of the individual carbides, proving that the solid-solution effect is potent at the medium-entropy level [184,389]. Optimal ablation resistance is sometimes found in nonequimolar 3-component systems, not in 5-component equimolar HECs [196]. Studies on medium-entropy perovskites for SOFC cathodes have shown excellent performance and suppressed cation segregation, demonstrating that high configurational entropy is not a prerequisite for all advanced functionalities [390–392].

Achieving a homogeneous single-phase solid solution becomes statistically and kinetically more challenging with more components. MECs are consistently easier to synthesize at lower temperatures with greater reproducibility. Sourcing and blending 5 or 6 high-purity transition metal powders is exponentially more expensive and complex than handling 3 or 4. This is critical for industrial scalability. The compositional space of 3–4 element systems is vastly smaller and more tractable for computational screening and empirical optimization.

The data suggest an entropy threshold for a given property. For stabilizing a rock–salt structured carbide, there might be 3–4 components [393,394]. For minimizing thermal conductivity, it might be 4–5 [157,234]. Adding components beyond the threshold yields diminishing returns or negative effects while drastically increasing cost and complexity. This shifts the debate from "how high can we go?" to "what is the minimum complexity required?" For many applications where performance, reliability, and cost are all critical, MECs within the broader framework of CCCs may represent the most rational engineering solution.

5.3 "Single-phase" vs. "multi-phase"

The early HEC paradigm celebrated the single-phase solid solution as the ideal state. Single-phase HECs offer homogeneous properties, simplified modeling, and often exhibit the lowest thermal conductivity due to maximum phonon scattering from lattice distortion. Their oxidation can lead to a uniform, well-adhered complex oxide scale, which is critical for environmental barrier coatings to prevent preferential attack along phase boundaries. However, a deliberate analysis reveals that consciously engineered multiphase or dual-phase microstructures can offer superior performance for specific challenges, presenting a fundamental strategic trade-off.

The primary trade-off is toughness. Monolithic single-phase ceramics are intrinsically brittle. While solid solution strengthening increases hardness, it does not provide reliable toughening mechanisms. Achieving a true, dense single phase often requires extreme sintering conditions. Deliberately introducing secondary phases creates microstructural complexity that can be harnessed. A dual-phase structure, often a mixture of pyrochlore and fluorite in rare-earth zirconates, is not a synthesis failure but a design choice [395–399]. The interface can activate toughening mechanisms such as crack deflection. Materials with ferroelastic domains or transformable tetragonal phases (e.g., certain Zr–Y–Yb–Ta–Nb–O oxides) exhibit significantly higher fracture toughness [400,401]. Incorporating a ductile metal phase or engineered interfaces in composites provides crack bridging and energy dissipation.

Multiphase designs allow for local chemistry optimization. In HEC–SiC composites, SiC provides SiO_2 for glassy phase sealing upon oxidation, while HEC provides the refractory oxide skeleton during oxidation, a synergistic, multimaterial response [35,180,181,205–207]. Adding SiC to a boride HEC can improve densification and boost both hardness and fracture toughness [402]. The introduction of secondary phases, especially those with different oxidation products, can create weak interfaces or galvanic corrosion cells, potentially disrupting the formation of a continuous, protective oxide scale. The superior oxidation resistance of single-phase HECs over some multiphase counterparts highlights this compromise [184,403].

The debate is about design philosophy. The single-phase approach seeks perfection in disorder and homogeneity. The multiphase approach embraces heterogeneity as a tool to manage specific failure modes. The future lies in architectured composites where HEC matrices are combined with tailored secondary phases.

5.4 Unresolved key scientific questions

Despite rapid progress, fundamental gaps in understanding hinder predictive design. Addressing these issues is critical for transitioning from phenomenological discovery to foundational science.

Direct atomic-scale evidence for local ordering vs. true randomness. While average techniques suggest randomness, the assumption of a perfectly random solid solution is likely an oversimplification. Is there SRO or clustering? Techniques such as neutron/X-ray total scattering with PDF analysis have revealed SRO in systems such as rare-earth niobates. However, systematic mapping of the nature, extent, and influence of SRO across different HEC families is needed. This local chemical environment directly determines diffusion pathways, defect behavior, and electronic properties.

Quantitative decoupling of the "core effects" and direct measurement of sluggish diffusion. The four proposed core effects (high-entropy, lattice distortion, sluggish diffusion, cocktail) are intertwined. How can we quantitatively isolate the contribution of each? Furthermore, the "sluggish diffusion effect" is widely invoked but lacks direct experimental measurements of cation/anion diffusion coefficients in HECs. What are the activation energies? Until these data are available, models for creep, aging, and oxidation growth remain speculative.

Structural evolution kinetics under extreme nonoxidizing environments. Research is heavily focused on oxidation/ablation. What happens under extreme irradiation (fusion/fission environments) or ultrahigh vacuum/high temperature conditions? How do complex defect interactions in a disordered lattice affect swelling, amorphization resistance, and creep? Preliminary works suggest promise, but mechanisms are unexplored.

True nature of dynamic interface evolution during environmental attack. During ablation/oxidation, a dynamic interdiffusion zone exists between the scale and substrate. What is its precise evolving structure and chemistry? How do the competing kinetics of oxide formation, cation out-diffusion, and oxygen in-diffusion couple with thermodynamic drives in this gradient region? *In-situ* studies at extreme temperatures are needed to move beyond postmortem analysis.

Predictive models for multiproperty optimization and the limits of entropy. We lack integrated models that can simultaneously predict phase stability, thermodynamic properties, kinetic coefficients, and functional properties from composition. Furthermore, in ionic/covalent ceramics with multiple sublattices, what is the theoretical and practical limit of configurational entropy? The discovery of ultrahigh-entropy phases with more than twenty cations pushes this boundary but raises questions about the actual degree of disorder achieved.

Addressing these questions requires a shift from exploratory synthesis to hypothesis-driven, fundamental science. It calls for collaboration between synthetic chemists, characterization experts, and theorists developing next-generation multiscale models. Confronting these "original sins" is the necessary path for the field's maturation into a disciplined engineering science.

6 From lab to application: Bottlenecks in processing and characterization

The journey of HECs from scientific discovery to real-world deployment is a formidable materials challenge. While the core tenets of entropy engineering promise transformative properties, their practical realization is entangled with profound hurdles in synthesis, manufacturing, and characterization. This transition is not merely a matter of scaling up but requires a paradigm shift in how we process, shape, and fundamentally understand these compositionally complex materials. The following analysis dissects these critical bottlenecks, contrasting theoretical potential with the stark realities of laboratory data and process limitations.

6.1 Performance mapping: unveiling promise amidst data scatter

A critical survey of the literature reveals several technological arenas where HECs exhibit compelling advantages, although not yet fully realized. It is essential to preface this discussion with a crucial caveat: The reported advantages signify emergent trends and potential, not established industrial benchmarks. Performance metrics often exhibit significant dispersion, reflecting the sensitivity of HECs to specific compositions, processing nuances, and measurement protocols. This inherent variability itself constitutes a primary challenge in translating laboratory-scale promise into reliable application.

Ultra-high temperature structural materials. HEC carbides and borides stand poised to redefine materials for extreme environments, where temperatures exceed 2000 °C coupled with oxidative and ablative fluxes. Their multi-cation design engineers the formation of intricate, often protective oxide scales that outperform those of conventional UHTCs. A prime example is the ablation-resistant $(Hf_{0.2}Zr_{0.2}Ta_{0.2}Nb_{0.2}Ti_{0.2})C$–SiC composite, which demonstrated remarkably low recession rates under an oxyacetylene flame (5 $MW{\cdot}m^{-2}$) [404]. Furthermore, entropy-driven phase stability offers tantalizing prospects for next-generation nuclear materials, where resistance to radiation-induced swelling and amorphization is paramount, as noted in prospective reviews [405].

New-generation thermal barrier coating materials. Here, entropy engineering acts as a master key to simultaneously unlock low thermal conductivity and exceptional environmental durability. High-entropy rare-earth zirconates, such as $(La_{0.2}Nd_{0.2}Sm_{0.2}Eu_{0.2}Gd_{0.2})_2Zr_2O_7$, achieve "glass-like" thermal conductivity (< 2 $W{\cdot}m^{-1}{\cdot}K^{-1}$) via intense phonon scattering from mass and strain field fluctuations while also exhibiting superior thermal-cycle life compared to traditional coatings [406]. Crucially, this compositional complexity confers enhanced resistance to corrosive molten silicate deposits (CMAS), a key failure mode for turbine coatings. High-entropy rare-earth monosilicates leverage multicomponent synergy to form dense, protective reaction layers, drastically slowing infiltration [407].

High-performance dielectric energy storage materials. This domain represents one of the most spectacular successes of the high-entropy strategy. By injecting configurational disorder into perovskite ferroelectrics, researchers disrupt long-range polar order, fostering a landscape of PNRs. This leads to slim hysteresis loops, delayed polarization saturation, and dramatically enhanced dielectric breakdown strength. The result is a breakthrough in lead-free energy storage, with systems such as $(Bi_{0.2}Na_{0.2}Ba_{0.2}Sr_{0.2}Ca_{0.2})TiO_3$-based ceramics achieving W_{rec} exceeding 8 $J{\cdot}cm^{-3}$ alongside efficiencies (η) > 90% [408]. Machine-learning-guided design has pushed this frontier even further, yielding compositions with $W_{rec} \approx 17.2$ $J{\cdot}cm^{-3}$ [409].

Frontier applications. The versatility of HECs extends into specialized niches. In catalysis, high-entropy oxides and oxynitrides offer a rich tapestry of tunable active sites and electronic structures. For instance, a $TiZrNbHfTaO_6N_3$ oxynitride demonstrated superior photocatalytic CO_2 reduction, attributed to optimized charge-carrier dynamics [114]. For electromagnetic wave absorption, the engineered lattice distortion in diborides and

carbides introduces defect-mediated loss mechanisms, enabling high-performance, thermally stable absorbers [410].

6.2 Powder synthesis and densification: navigating the homogeneity-grain growth tightrope

The choice of synthesis route for high-entropy ceramic powders profoundly impacts the starting point. Solid-state reactions, while simple and scalable, often struggle with chemical inhomogeneity, requiring repetitive high-temperature treatments that risk coarsening and impurity retention [411]. Carbothermal/borothermal reduction yields fine powders for non-oxides but is a delicate dance of atmosphere and temperature; incomplete reduction leaves residual carbon or oxides that sabotage subsequent sintering [412]. Solution-based methods (e.g., sol–gel) excel at molecular-level mixing, enabling low-temperature synthesis of highly active powders, exemplified by nano-structured HEO catalysts with high surface area [344]. However, precursor complexity and scalability remain barriers. Ultrafast high-temperature synthesis emerges as a disruptive alternative, using Joule heating to achieve synthesis in seconds, potentially freezing in homogeneous non-equilibrium states [413].

A fundamental challenge in sintering high-entropy ceramics lies in balancing the essential process of densification with the ongoing battle against excessive grain growth. SPS reigns supreme for densification, leveraging rapid heating to kinetically suppress grain growth. However, this very high speed creates its own set of problems. The intrinsic "sluggish diffusion" of HECs can hinder full densification, while thermal/current gradients in the SPS die can produce inhomogeneous samples. For example, a reactive-SPSed $(Ti_{0.2}Hf_{0.2}Nb_{0.2}Ta_{0.2}W_{0.2})C$ exhibited a radial gradient of residual graphite, directly correlating with localized grain size variations [414]. The high temperatures required for density can still trigger rapid grain growth. In $(Ti_{0.2}Hf_{0.2}Zr_{0.2}Nb_{0.2}Ta_{0.2})B_2$, a mere 50 °C increase in sintering temperature caused the average grain size to skyrocket from ~6.7 to 41.2 μm [415].

The community is actively developing strategies to decouple densification from coarsening. (1) Grain boundary pinning. Introducing secondary phases such as SiC whiskers or sintering aids (e.g., Cr_3C_2) to physically hinder boundary migration [416]. (2) Liquid-phase assistance. Using metallic binders (e.g., Co) [417] or low melting temperature phases such as $CrSi_2$ [418] to form transient liquids, enabling full density at temperatures hundreds of degrees lower. (3) Novel sintering modalities: Techniques such as ultrafast high-temperature sintering achieve densification in minutes, drastically shrinking the window for grain growth [419]. The core quest is to identify a precise time-temperature-pressure-composition nexus that concurrently delivers full density, phase purity, and a fine-grained microstructure, a formidable optimization challenge for multi-cation systems.

6.3 Advanced manufacturing and macroscopic preparation: The chasm between powder and part

Perhaps the most glaring bottleneck is the near-total absence of viable routes to transform HEC powders into complex-shaped, macroscopic components. The literature landscape is dominated by simple pellets and discs, highlighting a critical gap between material synthesis and component fabrication.

While AM promises geometric freedom, its application to monolithic HECs remains in its infancy. Most reported work involves laser cladding of high-entropy alloy (HEA) matrices reinforced with ceramic particles (e.g., TiC, WC) [420]. These are metallic systems, not monolithic HECs. A pioneering study demonstrated the fabrication of fully dense, nano-architected HEC lattices using two-photon polymerization coupled with advanced sintering [421]. This breakthrough, however, is confined to microscale architectures and is far from a scalable component manufacturing route.

The AM of bulk HECs faces a trifecta of hurdles: (1) the lack of suitable feedstock powders (spherical, flowable) or photocurable slurries for multi-cation systems, (2) extreme processability issues due to high melting points, cracking susceptibility, and uncontrolled phase evolution during rapid thermal cycles, and (3) the herculean task of sintering intricate green bodies to full density without distortion. Given the difficulties in printing large, complex parts, joining emerges as a critical intermediary step. Techniques such as active brazing using tailored high-entropy fillers show promise for assembling smaller HEC pieces or bonding HECs to metals [422]. The stark reality is that advanced manufacturing pathways for net-shaped HEC components are virtually non-existent, representing a monumental barrier that must be overcome to move beyond test coupons and into functional engineering systems.

6.4 Characterization technique challenges: Seeing the disordered forest and the atomic trees

The very attributes that make HECs promising, their chemical disorder and complex local environments, also make them extraordinarily difficult to characterize. Our understanding is gated by the limitations of our analytical tools, particularly at the atomic scale and under operating conditions.

The foundational hypothesis of random cationic mixing is notoriously difficult to verify. In principle, ideal for 3D nanoscale compositional mapping, atom probe tomography (APT) has a vanishingly low success rate for brittle, multi-component ceramics. Challenges in fabricating viable tips and the complex field-evaporation behavior of multiple ionic species render reliable quantitative data rare, a gap implicitly acknowledged across the literature [143]. While aberration-corrected STEM with EDS is a workhorse (Fig. 12(a)) [52], it provides 2D projections. Quantitative mapping of five or more heavy elements at atomic-column resolution is plagued by signal overlap and beam sensitivity. Techniques such as geometric phase analysis (GPA) offer direct visualization of lattice strain fields [423] but do not directly reveal chemical ordering.

The most compelling property claims for HECs relate to their performance at extreme temperatures, yet we largely observe them through post-mortem analysis. There is a severe scarcity of *in-situ* data on phase stability, grain growth kinetics, oxidation mechanisms, and mechanical behavior at temperatures above 1500 °C. How does the protective oxide scale dynamically form and evolve? What are the real-time creep mechanisms? These questions remain unanswered. Isolated studies point the way forward, such as operando synchrotron X-ray microscopy to track battery electrode morphology [424] or *in-situ* high-temperature XRD to observe entropy-stabilization reversals [425]. However, conducting such experiments in controlled, ultra-high-temperature environments remains a formidable technical challenge. For *in situ* STEM, observing microstructural evolution (grain growth, precipitate formation, dislocation dynamics) or phase transitions in real time has been established (Fig. 12(b)) [58]; however, investigating the evolution at temperatures above 1200 °C is technically demanding. It requires special heating holders, and the risk of sample reaction, contamination, or drift increases dramatically. This characterization bottleneck forces reliance on extrapolation and computation, introducing significant uncertainty in predicting the long-term, in-service performance of HECs.

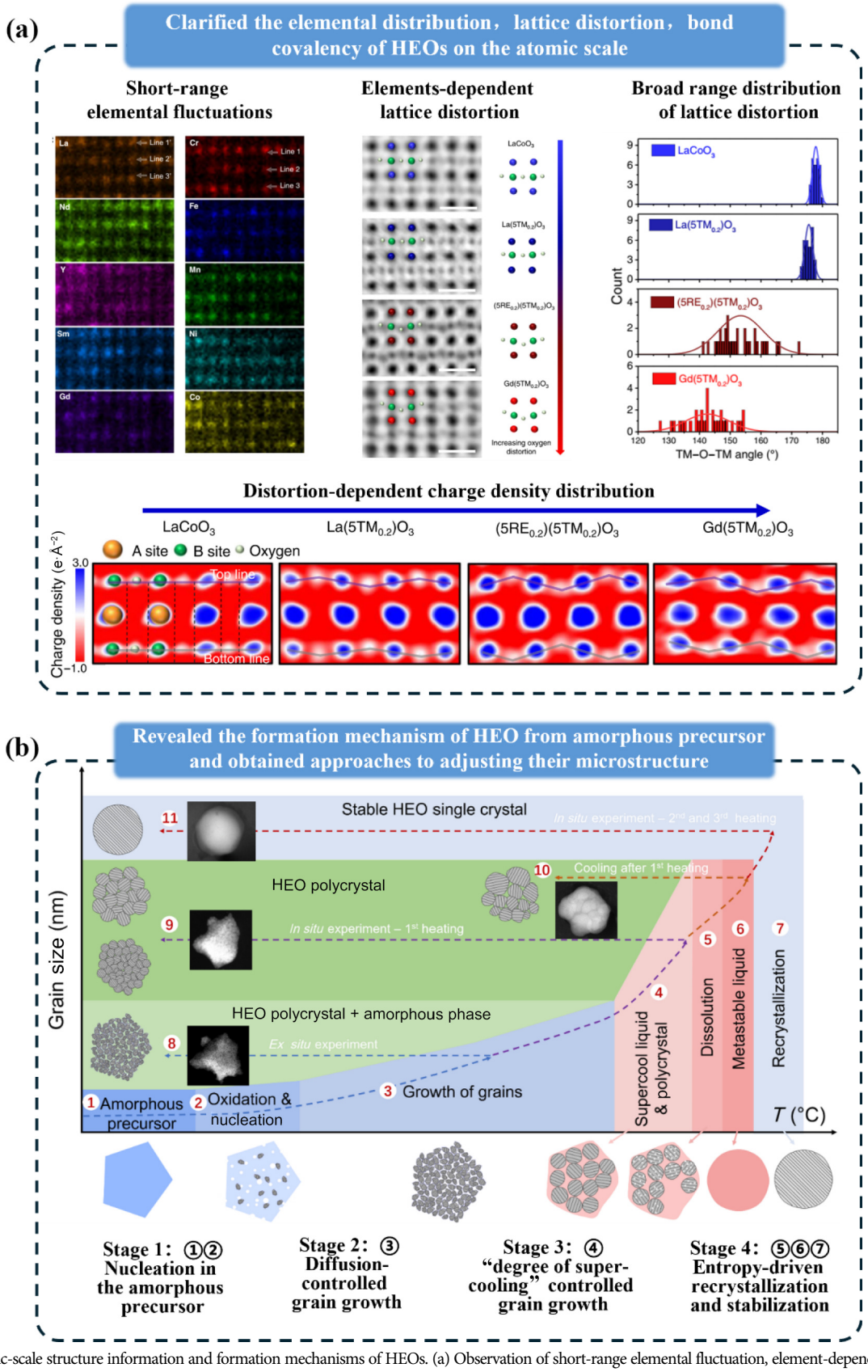

Fig. 12 Atomic-scale structure information and formation mechanisms of HEOs. (a) Observation of short-range elemental fluctuation, element-dependent and broad distribution of lattice distortion, and distortion-dependent charge density distribution, and thus bond covalency. Reproduced with permission from Ref. [52], © The Author(s) 2022. (b) *In situ* STEM observation of 4-stage formation mechanisms of HEO and microstructure tuning principles Reproduced with permission from Ref. [58], © American Chemical Society 2022.

The narrative of HEC is thus one of spectacular potential shadowed by profound practical challenges. We have mapped islands of exceptional performance in a sea of processing and characterization complexity. The path forward requires more than

incremental improvements; it demands a concerted, interdisciplinary synthesis. This synthesis must couple computational-guided design with innovative powder synthesis, master the delicate kinetics of densification, invent entirely new approaches to component-scale manufacturing, and pioneer characterization tools capable of probing atomic disorder in real-time under extreme conditions. Only through such an integrated campaign can we bridge the formidable chasm separating the tantalizing promise of the laboratory from the rigorous demands of real-world application.

7 Summary and outlook: A roadmap toward ordered development

Based on the comprehensive analysis of the present literature, here is a summary and outlook for the field of HECs, charting a roadmap (Fig. 13) from foundational discovery toward ordered development. The exploration of HECs has evolved from initial demonstrations of entropy-stabilized phases to a vibrant, multidisciplinary field grappling with profound complexity. The journey began by venturing into the "uncharted centers of phase diagrams" [1,2], embracing compositional chaos to discover new materials. After nearly a decade of intensive research, signs of "order" are emerging from this initial "chaos"—established paradigms, deepened mechanistic understanding, and identified application vectors are now providing a framework for systematic advancement. The future roadmap must focus on consolidating these gains, building robust infrastructure for the community, and strategically transitioning from laboratory curiosity to technological demonstration.

7.1 Core conclusions: Summarizing the signs of "order" emerging from the "chaos" in HECs

The initial phase of HEC research was characterized by exploratory synthesis across oxide, carbide, boride, nitride, silicide, and silicate systems. From this, several key paradigms and mechanistic understandings have crystallized, bringing order to the field.

Paradigm of "four core effects" and beyond. The conceptual framework for HECs was effectively unified with that of HEAs through the articulation and subsequent clarification of the "four core effects": high-entropy, severe lattice distortion, sluggish diffusion, and the cocktail effect [230]. This framework provides a universal language to explain phenomena such as reduced thermal conductivity (due to phonon scattering from lattice distortion and mass fluctuation), enhanced hardness (solid-solution strengthening from distortion), and improved phase stability at high temperatures (sluggish diffusion). Research has further refined this, showing that configurational entropy alone is not always the sole stabilizer; enthalpy and synergy play critical roles, and the pursuit should be for "compositionally complex ceramics" that include medium-entropy and nonequimolar designs [7,9,13,15].

Paradigms for phase formation and stability. Empirical rules have been established to predict single-phase formation in different crystal systems, bringing order to composition selection. For high-entropy diborides with hexagonal AlB_2 structures, revised Hume–Rothery size-difference factors are used [72,120,185]. For rock-salt carbide solid solutions, lattice parameter mismatch of the constituent monocarbides is a key predictive factor [71,363]. For perovskite oxides, Goldschmidt's

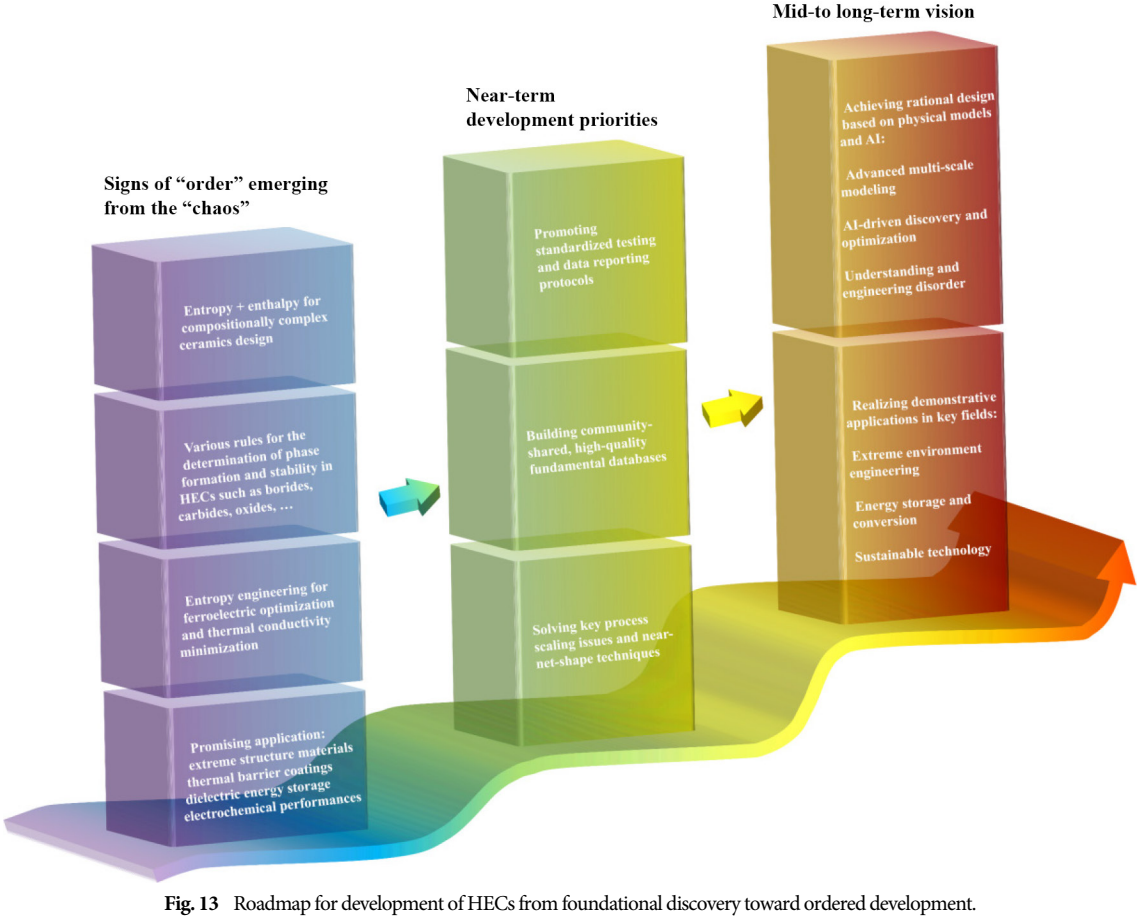

Fig. 13 Roadmap for development of HECs from foundational discovery toward ordered development.

tolerance factor, rather than just cation-size difference, influences the formation and temperature stability of single cubic phases [78]. The concept of "entropy stabilization" has been rigorously debated, with understanding evolving to recognize that while high configurational entropy can stabilize solid solutions against segregation, many HECs are stable due to favorable enthalpy or are metastable but kinetically trapped by sluggish diffusion [232].

Paradigm of property tailoring via entropy engineering. A powerful paradigm has emerged: configurational entropy is a tunable design parameter. In ferroelectrics, increasing entropy systematically enhances relaxor behavior, reduces polar domain size, delays polarization saturation, and dramatically improves energy storage density and efficiency [103,165,411]. In thermal barrier materials, high entropy in pyrochlores and fluorites is a reliable strategy to minimize thermal conductivity (via size disorder) and suppress grain growth, directly linking the "sluggish diffusion" effect to a critical application performance metric [15,30,31,38,79].

Order emerged in promising application directions. (1) Structural materials for extreme temperature and environments. High-entropy carbides and diborides show enhanced mechanical properties and unique stability under extreme conditions (irradiation, high stress at high temperatures), carving a niche in extreme environmental applications. (2) Thermal barrier coatings. High-entropy rare-earth zirconates consistently demonstrate the "trifecta" of low thermal conductivity, good phase stability, and slow grain growth, making them direct, performance-advantaged replacements for current YSZ-based systems. (3) Dielectric energy storage. Lead-free HEC relaxors have broken long-standing trade-offs, achieving both ultrahigh energy density and efficiency, positioning them as top candidates for next-generation pulsed power capacitors. (4) Electrochemical energy storage, energy conversion, and catalysis materials. High-entropy perovskite and spinel oxides exhibit superior activity and durability as electrodes for fuel cells and electrolyzers, leveraging the cocktail effect and tailored surface chemistry.

7.2 Near-term development priorities

Promoting standardized testing and data reporting protocols. The literature reveals a significant dispersion in reported properties. For example, hardness values for similar HEC compositions vary based on the indentation load method, and thermal conductivity measurements can be influenced by porosity and grain boundary density. Priority action might be focused on establishing and adopting community guidelines for standardized characterization protocols. This should include standardized indentation loads and methods for hardness, specified geometries and atmospheres for thermal conductivity measurement, and unified testing procedures for dielectric breakdown strength and energy storage efficiency.

Building community-shared, high-quality fundamental databases. Rational design is hampered by a lack of systematic, high–fidelity data. While pioneering studies use first-principles calculations and machine learning, they are limited by available experimental data for training and validation. Open-access databases for HECs are desired for creation, such as (a) Synthesis databases: documenting compositions, precursor materials, synthesis routes, sintering conditions, and resulting phase information. (b) Property database: housing standardized mechanical, thermal, electrical, and functional property data linked to specific microstructural descriptors (density, grain size). (c) Stability database: compiling data on high-temperature phase stability, oxidation behavior, and corrosion resistance.

Solving key process scaling issues. Nearly all reported HEC bulks are small laboratory-scale samples from SPS. Scaling up powder synthesis (beyond 100 g batches) and consolidating larger, more complex shapes are critical bottlenecks. Dedicated research into scalable powder synthesis techniques, such as industrial-scale carbothermal reduction or novel solution-based methods, is needed. Furthermore, the field must move beyond the SPS and HP for shaping. Near-term research should focus on adapting near-net-shape techniques such as slip casting, gel casting, or additive manufacturing specifically for HEC slurries or feedstocks, followed by pressure-less sintering.

7.3 Mid- to long-term vision

Achieving rational design based on physical models and AI. The future lies in closing the loop between prediction, synthesis, and characterization. (1) Advanced multiscale modeling: *Ab initio* calculations (such as those used for carbides) are integrated to predict phase stability and electronic structure, with CALPHAD for thermodynamic modeling and machine learning potentials for molecular dynamics simulations of properties and kinetics [426,427]. The goal is a virtual "materials genome" for HECs. (2) AI-driven discovery and optimization. Machine learning, such as that for discovering carbides [59], will evolve from a screening tool to an active design partner. AI models will propose novel nonequimolar, medium-entropy, or high-entropy compositions tailored for specific property portfolios (e.g., maximize fracture toughness while maintaining oxidation resistance up to 3000 °C), significantly accelerating the exploration of the vast compositional space. (3) Understanding and engineering disorder. The pinnacle of rational design will be moving beyond the assumption of random mixing. Advanced characterization and modeling must converge to understand, quantify, and ultimately design desired levels of short-range order or specific local atomic environments to target exceptional properties, turning disorder from a statistical fact into a precision tool.

Realizing demonstration applications in key fields. The mid-to-long-term success of HECs will be measured by their adoption in engineered systems. The focus should be on moving from coating demonstrators to integrated components. (1) Extreme environment engineering. The incorporation of HEC thermal barrier coatings on next-generation gas turbine blades enables higher operating temperatures and efficiency in aviation or power generation. The qualification of HEC leading edges or nozzle components in hypersonic vehicle test flights, validating their performance under combined thermal, mechanical, and oxidative stress. (2) Energy storage and conversion. Deployment of HEC-based multilayer ceramic capacitors in electric vehicle power electronics or grid inverters, demonstrating superior power density and reliability. The installation of protonic ceramic fuel cells or electrolyzers with HEC air electrodes in pilot-scale systems showcases efficiency and longevity gains. (3) Sustainable technology. Utilizing HEC catalysts in industrial CO_2 conversion or hydrogen production processes, leveraging their stability and tunable activity.

In conclusion, the field of HEC stands at a pivotal point. The initial chaos of exploration has yielded identifiable patterns, validated theories, and promising application targets. The path forward requires a concerted shift in mindset: from solely discovering new compositions to underlying the basic theory fundamentals and building the communal infrastructure (standards, databases) and scalable processes necessary for maturation. By prioritizing reproducibility, data sharing, and rational design, the community can systematically navigate the

vast compositional complexity, transforming HECs from a fascinating scientific phenomenon into a cornerstone family of materials for 21st-century technology.

Acknowledgements

Lei Su appreciates the financial support from the Characteristic Development Guidance Funds for the Central Universities, the Top Young Talents Program of Xi'an Jiaotong University, and the Fundamental Research Funds for the Central Universities. Lei Su and Hongjie Wang are thankful for the financial support from the Basic Research Plan of Natural Science in Shaanxi Province (Nos. 2024JC-YBMS-323 and 2024JC-YBMS-264) and the Research Program of Shaanxi Laboratory of Advanced Materials (Nos. 2025XCLSXSYS-RZ-07 and 2024ZY-JCYJ-04-03).

Availability of data and materials

The data that support the findings of this study are available from the corresponding author upon reasonable request.

Competing interests

The authors have no competing interests to declare that are relevant to the content of this article. The author Lei Su is the Editorial Committee member of this journal. The author Yanchun Zhou is the Editor-in-Chief of this journal.

References

[1] Oses C, Toher C, Curtarolo S. High-entropy ceramics. *Nat Rev Mater* 2020, **5**: 295–309.

[2] Xiang HM, Xing Y, Dai FZ, *et al.* High-entropy ceramics: Present status, challenges, and a look forward. *J Adv Ceram* 2021, **10**: 385–441.

[3] Ren JN, Kumkale VY, Hou H, *et al.* A review of high-entropy materials with their unique applications. *Adv Compos Hybrid Mater* 2025, **8**: 195.

[4] Rost CM, Sachet E, Borman T, *et al.* Entropy-stabilized oxides. *Nat Commun* 2015, **6**: 8485.

[5] Du G, Li CH, Li JM, *et al.* Research progress on high entropy oxide ceramics: Principles, preparation, and properties. *J Mater Res Technol* 2025, **35**: 265–288.

[6] Musicó BL, Gilbert D, Ward TZ, *et al.* The emergent field of high entropy oxides: Design, prospects, challenges, and opportunities for tailoring material properties. *APL Mater* 2020, **8**: 040912.

[7] Wright AJ, Luo J. A step forward from high-entropy ceramics to compositionally complex ceramics: A new perspective. *J Mater Sci* 2020, **55**: 9812–9827.

[8] Gao MC, Miracle DB, Maurice D, *et al.* High-entropy functional materials. *J Mater Res* 2018, **33**: 3138–3155.

[9] Sarkar A, Breitung B, Hahn H. High entropy oxides: The role of entropy, enthalpy and synergy. *Scripta Mater* 2020, **187**: 43–48.

[10] Feng XC, Guo FW, Luo LR, *et al.* Engineering design of feedstock powder and relevant thermal-mechanical performance of thermal/environmental barrier coatings. *J Adv Ceram* 2025, **14**: 9221033.

[11] Li JC, Su YF, Chen SN, *et al.* High-entropy diboride: A novel high-temperature self-lubricating ceramic with enhanced mechanical and tribological properties. *J Adv Ceram* 2025, **14**: 9221085.

[12] Akrami S, Edalati P, Fuji M, *et al.* High-entropy ceramics: Review of principles, production and applications. *Mater Sci Eng R Rep* 2021, **146**: 100644.

[13] Brahlek M, Gazda M, Keppens V, *et al.* What is in a name: Defining "high entropy" oxides. *APL Mater* 2022, **10**: 110902.

[14] Divilov S, Eckert H, Hicks D, *et al.* Disordered enthalpy–entropy descriptor for high-entropy ceramics discovery. *Nature* 2024, **625**: 66–73.

[15] Wright AJ, Wang QY, Huang CY, *et al.* From high-entropy ceramics to compositionally-complex ceramics: A case study of fluorite oxides. *J Eur Ceram Soc* 2020, **40**: 2120–2129.

[16] Fu H, Jiang Y, Zhang MZ, *et al.* High-entropy rare earth materials: Synthesis, application and outlook. *Chem Soc Rev* 2024, **53**: 2211–2247.

[17] Liu YF, Hou JD, Cheng CF, *et al.* The effect of non-equimolar doping on the preparation and electrical conductivity of Sr(Ti,Zr,Zn,Sn,Hf)$O_{3-\sigma}$ high entropy perovskite oxide. *Ceram Int* 2023, **49**: 21546–21554.

[18] Meng H, Tang ZY, Bai H, *et al.* Accelerating the discovery of high-entropy hexaborides by data-driven prediction: From equimolar to non-equimolar. *J Am Ceram Soc* 2024, **107**: 6456–6464.

[19] Yan SX, Luo SH, Yang L, *et al.* Novel P2-type layered medium-entropy ceramics oxide as cathode material for sodium-ion batteries. *J Adv Ceram* 2022, **11**: 158–171.

[20] Liu YP, Tuo P, Dai FZ, *et al.* A highly deficient medium-entropy perovskite ceramic for electromagnetic interference shielding under harsh environment. *Adv Mater* 2024, **36**: 2400059

[21] Wang JX, Ren YX, Zhu XK, *et al.* Novel medium-entropy $Ca_3(Co_{0.25}Zn_{0.25}Mg_{0.25}Cu_{0.25})_2SiV_2O_{12}$ microwave dielectric ceramics with high $Q\times f$ and near-zero τ_f. *J Adv Ceram* 2025, **14**: 9221110.

[22] Wang WJ, Cheng CF, Qiao JW, *et al.* Fabrication and mechanical properties of multi-principal cation (Mg,Ti,Cr,Zr,Al,Si) mullite ceramic. *Ceram Int* 2024, **50**: 25738–25748.

[23] Yildiz AB, Hu YX, Babu RP, *et al.* Design, synthesis, structure, and stability of novel multi-principal element (Ti,Zr,Hf,W)C ceramic with a miscibility gap. *J Eur Ceram Soc* 2022, **42**: 4429–4435.

[24] Li YF, Ouyang ZY, Ding YY, *et al.* Tuning anionic components to control the phase stability and mechanical properties of high-entropy carbonitrides. *Mater Design* 2025, **252**: 113775.

[25] Wang HY, Bi JQ, Yang Y, *et al.* Preparation, characterization and performance of high-entropy carbonitride ceramics. *Ceram Int* 2024, **50**: 3034–3040.

[26] Wang YC, Csanádi T, Zhang HF, *et al.* Synthesis, microstructure, and mechanical properties of novel high entropy carbonitrides. *Acta Mater* 2022, **231**: 117887.

[27] Guan JY, Liu YC, Li DX, *et al.* The new complex high-entropy metal boron carbonitride: Microstructure and mechanical properties. *J Am Ceram Soc* 2022, **105**: 6417–6426.

[28] Hedman D, Feltrin AC, Miyamoto Y, *et al.* *Ab initio* aided design of novel quaternary, quinary and senary high-entropy borocarbides. *J Mater Sci* 2022, **57**: 422–443.

[29] Tomassetti CR, Kafle GP, Marcial ET, *et al.* Prospect of high-temperature superconductivity in layered metal borocarbides. *J Mater Chem C* 2024, **12**: 4870–4884.

[30] Zhang YH, Xie M, Wang ZG, *et al.* Marked reduction in the thermal conductivity of $(La_{0.2}Gd_{0.2}Y_{0.2}Yb_{0.2}Er_{0.2})_2Zr_2O_7$ high-entropy ceramics by substituting Zr^{4+} with Ti^{4+}. *Ceram Int* 2022, **48**: 9602–9609.

[31] Wang J, Jin QQ, Song JB, *et al.* Revealing the low thermal conductivity of high-entropy rare-earth tantalates via multi-scale defect analysis. *J Adv Ceram* 2023, **12**: 2087–2100.

[32] Yan XH, Zhu BH, Zhang Y, *et al.* Phase formation and unusual interstitial solid-solution strengthening behavior of (CoCrFeMnNi)N_x high-entropy ceramic films. *Surf Coat Tech* 2024, **477**: 130392.

[33] Ma YM, Liu XS, Dong WQ, *et al.* Interstitial carbide synergistically strengthening high-entropy alloy $CoCrFeNiV_{0.5}C$. *Mat Sci Eng A* 2020, **792**: 139802.

[34] Ward TZ, Wilkerson RP, Musicó BL, *et al.* High entropy ceramics for applications in extreme environments. *J Phys Mater* 2024, **7**: 021001.

[35] Lu K, Liu JX, Wei XF, *et al.* Microstructures and mechanical properties of high-entropy $(Ti_{0.2}Zr_{0.2}Hf_{0.2}Nb_{0.2}Ta_{0.2})C$ ceramics with the addition of SiC secondary phase. *J Eur Ceram Soc* 2020, **40**: 1839–1847.

[36] Zhang W, Chen L, Shi Z, *et al.* From single high-entropy phase to multi-phase transition: Microstructural evolution of multi-

component carbide (ZrHfVNbMoW)C realized by adjusting Hf content and temperature. *J Eur Ceram Soc* 2024, **44**: 1385–1395.
[37] Luo SC, Guo WM, Plucknett K, *et al.* Fine-grained dual-phase high-entropy ceramics derived from boro/carbothermal reduction. *J Eur Ceram Soc* 2021, **41**: 3189–3195.
[38] Xu L, Su L, Wang HJ, *et al.* Phase evolution and thermophysical properties of high-entropy $RE_2(Y_{0.2}Yb_{0.2}Nb_{0.2}Ta_{0.2}Ce_{0.2})_2O_7$ oxides. *J Am Ceram Soc* 2022, **105**: 5490–5500.
[39] Sun JL, Zhao J, Chen Y, *et al.* Toughening in low-dimensional nanomaterials high-entropy ceramic nanocomposite. *Compos Part B Eng* 2022, **231**: 109586.
[40] Li YT, Jiang X, Wang XT, *et al.* Integration of hardness and toughness in $(CuNiTiNbCr)N_x$ high entropy films through nitrogen-induced nanocomposite structure. *Scripta Mater* 2024, **238**: 115763.
[41] Zheng YQ, Wu XF, Liu L, *et al.* Functionally gradient Al_2O_3 ceramics with tailored high-entropy carbide hardening phase and ZrO_2 toughening phase. *J Am Ceram Soc* 2026, **109**: 70372.
[42] Zhang W, Liao JJ, Yang ZB, *et al.* Improved corrosion resistance of reactive gas pulse sputtered (TiTaNbZrNi)N high entropy alloy coatings with a hybrid architecture of multilayered and compositionally graded structures. *J Nucl Mater* 2021, **543**: 152558.
[43] Xue Y, Zhang HX, Zhao XQ, *et al.* Enhanced thermal shock resistance of gradient high-entropy $(La_{0.2}Nd_{0.2}Sm_{0.2}Eu_{0.2}Gd_{0.2})_2Ce_2O_7$/YSZ thermal barrier coatings. *Ceram Int* 2024, **50**: 18024–18034.
[44] Chen H, Xiang HM, Dai FZ, *et al.* High porosity and low thermal conductivity high entropy $(Zr_{0.2}Hf_{0.2}Ti_{0.2}Nb_{0.2}Ta_{0.2})C$. *J Mater Sci Technol* 2019, **35**: 1700–1705.
[45] Wen ZH, Tang ZY, Liu YW, *et al.* Ultrastrong and high thermal insulating porous high-entropy ceramics up to 2000 nC. *Adv Mater* 2024, **36**: 2311870.
[46] Chen H, Xiang HM, Dai FZ, *et al.* Porous high entropy $(Zr_{0.2}Hf_{0.2}Ti_{0.2}Nb_{0.2}Ta_{0.2})B_2$: A novel strategy towards making ultrahigh temperature ceramics thermal insulating. *J Mater Sci Technol* 2019, **35**: 2404–2408.
[47] Chen GJ, Li CW, Li H, *et al.* Porous $(Ce_{0.2}Zr_{0.2}Ti_{0.2}Sn_{0.2}Ca_{0.2})O_{2-\delta}$ high-entropy ceramics with both high strength and low thermal conductivity. *J Eur Ceram Soc* 2021, **41**: 309–314.
[48] Zhang XL, Zhang WB, Yin Y, *et al.* Sol–gel method preparation and high-rate energy storage of high-entropy ceramic (FeCoCrMnNi)C porous powder. *Ceram Int* 2023, **49**: 29327–29338.
[49] Zhang RZ, Reece MJ. Review of high entropy ceramics: Design, synthesis, structure and properties. *J Mater Chem A* 2019, **7**: 22148–22162.
[50] Wang Y, Xu JR, Chen BS, *et al.* Distinct lattice distortion role in high entropy diboride ceramics. *Mater Today* 2026, **92**: 115–125.
[51] Barber JP, Deary WJ, Titus AN, *et al.* Disorder by design: Unveiling local structure and functional insights in high entropy oxides. *Mater Horiz* 2025, **12**: 10453–10477.
[52] Su L, Huyan HX, Sarkar A, *et al.* Direct observation of elemental fluctuation and oxygen octahedral distortion-dependent charge distribution in high entropy oxides. *Nat Commun* 2022, **13**: 2358.
[53] Ding N, Jiang HH, Xu CR, *et al.* Lattice distortion and the influence on mechanical and thermodynamic properties of high entropy (HfZrTaNbTi)X (X = C, N, NC) by *ab initio* investigation. *Ceram Int* 2022, **48**: 35353–35364.
[54] Li LY, Zhang M, Jiang M, *et al.* High entropy ceramics for electromagnetic functional materials. *Adv Funct Mater* 2025, **35**: 2416673.
[55] Kotsonis GN, Almishal SSI, Marques dos Santos Vieira F, *et al.* High-entropy oxides: Harnessing crystalline disorder for emergent functionality. *J Am Ceram Soc* 2023, **106**: 5587–5611.
[56] Zhang L, Jia JR, Yan JH. Challenges and strategies for synthesizing high performance micro and nanoscale high entropy oxide materials. *Small* 2024, **20**: 2309586.
[57] Wang X, Liu Q, Wang X. High-entropy materials: From bulk to sub-nano. *Adv Funct Mater* 2025, **35**: 2504275.
[58] Su L, Chen X, Xu L, *et al.* Visualizing the formation of high-entropy fluorite oxides from an amorphous precursor at atomic resolution. *ACS Nano* 2022, **16**: 21397–21406.
[59] Kaufmann K, Maryanovsky D, Mellor WM, *et al.* Discovery of high-entropy ceramics via machine learning. *Npj Comput Mater* 2020, **6**: 42.
[60] Hu FF, Wu Z, Cao WS, *et al.* Multiscale lattice and bonding dynamics in high-entropy ferroelectrics. *Phys Rev B* 2025, **112**: 174114.
[61] Liang ZH, Yang YY, Tao ZP, *et al.* High-entropy materials for electrocatalytic oxygen reduction reaction. *J Mater Chem A* 2025, **13**: 25195–25212.
[62] Liu J, Yang QQ, Zou J, *et al.* Strong high-entropy diboride ceramics with oxide impurities at 1800 °C. *Sci China Mater* 2023, **66**: 2061–2070.
[63] Chen ZY, Lin CC, Zheng W, *et al.* Influence of average radii of RE^{3+} ions on phase structures and thermal expansion coefficients of high-entropy pyrosilicates. *J Adv Ceram* 2023, **12**: 1090–1104.
[64] Jang H, Lee W, Kim HJ, *et al.* Active learning-guided accelerated discovery of ultra-efficient high-entropy thermoelectrics. *Adv Mater* 2026, **38**: 15054.
[65] Spiridigliozzi L, Ferone C, Cioffi R, *et al.* A simple and effective predictor to design novel fluorite-structured high entropy oxides (HEOs). *Acta Mater* 2021, **202**: 181–189.
[66] Bérardan D, Franger S, Meena AK, *et al.* Room temperature lithium superionic conductivity in high entropy oxides. *J Mater Chem A* 2016, **4**: 9536–9541.
[67] Gild J, Samiee M, Braun JL, *et al.* High-entropy fluorite oxides. *J Eur Ceram Soc* 2018, **38**: 3578–3584.
[68] Anand G, Wynn A P, Handley C M, *et al.* Phase stability and distortion in high-entropy oxides. *Acta Mater* 2018, **146**: 119–125.
[69] Zhou JY, Zhang JY, Zhang F, *et al.* High-entropy carbide: A novel class of multicomponent ceramics. *Ceram Int* 2018, **44**: 22014–22018.
[70] Yan XL, Constantin L, Lu YF, *et al.* $(Hf_{0.2}Zr_{0.2}Ta_{0.2}Nb_{0.2}Ti_{0.2})C$ high-entropy ceramics with low thermal conductivity. *J Am Ceram Soc* 2018, **101**: 4486–4491.
[71] Castle E, Csanádi T, Grasso S, *et al.* Processing and properties of high-entropy ultra-high temperature carbides. *Sci Rep-UK* 2018, **8**: 8609.
[72] Gild J, Zhang YY, Harrington T, *et al.* High-entropy metal diborides: A new class of high-entropy materials and a new type of ultrahigh temperature ceramics. *Sci Rep-UK* 2016, **6**: 37946.
[73] Mayrhofer PH, Kirnbauer A, Ertelthaler P, *et al.* High-entropy ceramic thin films: A case study on transition metal diborides. *Scripta Mater* 2018, **149**: 93–97.
[74] Jin T, Sang XH, Unocic RR, *et al.* Mechanochemical-assisted synthesis of high-entropy metal nitride via a soft urea strategy. *Adv Mater* 2018, **30**: 1707512.
[75] Shen WJ, Tsai MH, Yeh JW. Machining performance of sputter-deposited $(Al_{0.34}Cr_{0.22}Nb_{0.11}Si_{0.11}Ti_{0.22})_{50}N_{50}$ high-entropy nitride coatings. *Coatings* 2015, **5**: 312–325.
[76] Qin Y, Liu JX, Li F, *et al.* A high entropy silicide by reactive spark plasma sintering. *J Adv Ceram* 2019, **8**: 148–152.
[77] Gild J, Braun J, Kaufmann K, *et al.* A high-entropy silicide: $(Mo_{0.2}Nb_{0.2}Ta_{0.2}Ti_{0.2}W_{0.2})Si_2$. *J Materiomics* 2019, **5**: 337–343.
[78] Jiang SC, Hu T, Gild J, *et al.* A new class of high-entropy perovskite oxides. *Scripta Mater* 2018, **142**: 116–120.
[79] Xu L, Wang HJ, Su L, *et al.* A new class of high-entropy fluorite oxides with tunable expansion coefficients, low thermal conductivity and exceptional sintering resistance. *J Eur Ceram Soc* 2021, **41**: 6670–6676.
[80] Biesuz M, Spiridigliozzi L, Dell'Agli G, *et al.* Synthesis and sintering of (Mg,Co,Ni,Cu,Zn)O entropy-stabilized oxides obtained by wet chemical methods. *J Mater Sci* 2018, **53**: 8074–8085.
[81] Hong WC, Chen F, Shen Q, *et al.* Microstructural evolution and mechanical properties of (Mg,Co,Ni,Cu,Zn)O high-entropy ceramics. *J Am Ceram Soc* 2019, **102**: 2228–2237.

[82] Rák Z, Maria JP, Brenner DW. Evidence for Jahn–Teller compression in the (Mg,Co,Ni,Cu,Zn)O entropy-stabilized oxide: A DFT study. *Mater Lett* 2018, **217**: 300–303.
[83] Grzesik Z, Smoła G, Stygar M, *et al.* Defect structure and transport properties in (Co,Cu,Mg,Ni,Zn)O high entropy oxide. *J Eur Ceram Soc* 2019, **39**: 4292–4298.
[84] Zhao ZF, Xiang HM, Dai FZ, *et al.* $(La_{0.2}Ce_{0.2}Nd_{0.2}Sm_{0.2}Eu_{0.2})_2Zr_2O_7$: A novel high-entropy ceramic with low thermal conductivity and sluggish grain growth rate. *J Mater Sci Technol* 2019, **35**: 2647–2651.
[85] Zhao ZF, Chen H, Xiang HM, *et al.* High entropy defective fluorite structured rare-earth niobates and tantalates for thermal barrier applications. *J Adv Ceram* 2020, **9**: 303–311.
[86] Wang KL, Zhu JP, Wang HL, *et al.* Air plasma-sprayed high-entropy $(Y_{0.2}Yb_{0.2}Lu_{0.2}Eu_{0.2}Er_{0.2})_3Al_5O_{12}$ coating with high thermal protection performance. *J Adv Ceram* 2022, **11**: 1571–1582.
[87] Li ML, Zhao XT, Shao G, *et al.* Oscillatory pressure sintering of high entropy $(Zr_{0.2}Ta_{0.2}Nb_{0.2}Hf_{0.2}Mo_{0.2})B_2$ ceramic. *Ceram Int* 2021, **47**: 8707–8710.
[88] Li JC, Zhou YC, Su YF, *et al.* Synthesis and mechanical and elevated temperature tribological properties of a novel high-entropy $(TiVNbMoW)C_{4.375}$ with carbon stoichiometry deviation. *J Adv Ceram* 2023, **12**: 242–257.
[89] Qin MD, Yan QZ, Liu Y, *et al.* A new class of high-entropy M_3B_4 borides. *J Adv Ceram* 2021, **10**: 166–172.
[90] Luo XW, Luo LR, Zhao XF, *et al.* Single-phase rare-earth high-entropy zirconates with superior thermal and mechanical properties. *J Eur Ceram Soc* 2022, **42**: 2391–2399.
[91] Zhou NX, Jiang SC, Huang T, *et al.* Single-phase high-entropy intermetallic compounds (HEICs): Bridging high-entropy alloys and ceramics. *Sci Bull* 2019, **64**: 856–864.
[92] Qin MD, Vega H, Zhang DW, *et al.* 21-Component compositionally complex ceramics: Discovery of ultrahigh-entropy weberite and fergusonite phases and a pyrochlore-weberite transition. *J Adv Ceram* 2022, **11**: 641–655.
[93] Wen ZH, Tang ZY, Meng H, *et al.* A promising new class of high-entropy ceramics: High-entropy oxycarbides with good oxidation resistance. *Corros Sci* 2022, **207**: 110574.
[94] Wen TQ, Liu HH, Ye BL, *et al.* High-entropy alumino-silicides: A novel class of high-entropy ceramics. *Sci China Mater* 2020, **63**: 300–306.
[95] Chen H, Xiang HM, Dai FZ, *et al.* High entropy $(Yb_{0.25}Y_{0.25}Lu_{0.25}Er_{0.25})_2SiO_5$ with strong anisotropy in thermal expansion. *J Mater Sci Technol* 2020, **36**: 134–139.
[96] Zhang WM, Zhao B, Xiang HM, *et al.* One-step synthesis and electromagnetic absorption properties of high entropy rare earth hexaborides (HE REB_6) and high entropy rare earth hexaborides/borates (HE REB_6/HE $REBO_3$) composite powders. *J Adv Ceram* 2021, **10**: 62–77.
[97] Lu MX, Fang Y, Xu XY, *et al.* Non-equimolar bismuth-layered $[Ca_xSr_{(1-x)/3}Ba_{(1-x)/3}Pb_{(1-x)/3}]Bi_4Ti_4O_{15}$ $Bi_4Ti_4O_{15}$ high-entropy ceramics with high curie temperature. *J Materiomics* 2025, **11**: 100945.
[98] Zhukova I, Tatarková M, Kombamuthu V, *et al.* Theoretical prediction, synthesis and mechanical properties of nonequimolar (Ta–Hf–Zr–Nb–Ti)B_2 entropy-stabilized borides. *J Eur Ceram Soc* 2025, **46**: 117903.
[99] Fan D, Xu YX, Ding Y, *et al.* Study on oxidation behavior and mechanism of non-equimolar $(Zr,Ti,Ta,W)B_2$ with improved oxidation resistance. *J Eur Ceram Soc* 2026, **46**: 117977.
[100] Liu XY, Zhang P, Han Y, *et al.* Tailoring thermal and mechanical properties of rare earth niobates by coupling entropy and composite engineering. *J Eur Ceram Soc* 2023, **43**: 1141–1146.
[101] Wang ZP, Yu ZW, Zhang LK, *et al.* Tailoring structural, mechanical, and electronic properties of $(Ti_{0.25}Ta_{0.25}Zr_{0.25}Nb_{0.25-x}La)C$ high-entropy carbide ceramics via rare-earth La incorporation: A comprehensive first-principles study. *Ceram Int* 2025, **51**: 33721–33730.
[102] Mo YL, Guan XH, Wang SB, *et al.* Oriented catalysis through chaos: High-entropy spinels in heterogeneous reactions. *Chem Sci* 2025, **16**: 1652–1676.
[103] Yang Z, Xiang XL, Yang J, *et al.* High-entropy oxides as energy materials: From complexity to rational design. *Mater Futures* 2024, **3**: 042103.
[104] Kante MV, Weber ML, Ni S, *et al.* A high-entropy oxide as high-activity electrocatalyst for water oxidation. *ACS Nano* 2023, **17**: 5329–5339.
[105] Borghesi C, Fabiani C, Bondi R, *et al.* Tailoring high-entropy oxides as emerging radiative materials for daytime passive cooling. *Chem Mater* 2023, **35**: 10384–10393.
[106] Chauhan A, Bernardo E, Galusek D. Tailoring optical properties of $(Ce,Pr)O_{2-\delta}$-$(La,Sm,Y)_2O_3$ high entropy oxides by substituting Pr with Gd or Dy for multi-wavelength emission applications. *Open Ceram* 2025, **21**: 100730.
[107] Ning YT, Pu YP, Wu CH, *et al.* Achieving high energy storage performance below 200 kV/cm in $BaTiO_3$-based medium-entropy ceramics. *Ceram Int* 2023, **49**: 20326–20333.
[108] Wei MY, Xu J, Zhu JT, *et al.* Influence of size disorder parameter on the thermophysical properties of rare-earth-zirconate medium-entropy ceramics. *J Am Ceram Soc* 2023, **106**: 2037–2048.
[109] Yang QQ, Wang XG, Bao WC, *et al.* Influence of equiatomic Zr/(Ti, Nb) substitution on microstructure and ultra-high strength of (Ti,Zr,Nb)C medium-entropy ceramics at 1900 °C. *J Adv Ceram* 2022, **11**: 1457–1465.
[110] Demirskyi D, Nishimura T, Yoshimi K, *et al.* High-strength, medium entropy Zr–Ta–Nb diboride ceramics. *Scripta Mater* 2023, **225**: 115170.
[111] Hossain MD, Borman T, Kumar A, *et al.* Carbon stoichiometry and mechanical properties of high entropy carbides. *Acta Mater* 2021, **215**: 117051.
[112] Wen YB, Liu YF. Processing and microstructure of a fluorite high-entropy oxide $(Zr_{0.2}Ce_{0.2}Hf_{0.2}Y_{0.2}Al_{0.2})O_{2-\delta}$. *Ceram Int* 2022, **48**: 2546–2554.
[113] Wright AJ, Huang CY, Walock MJ, *et al.* Sand corrosion, thermal expansion, and ablation of medium- and high-entropy compositionally complex fluorite oxides. *J Am Ceram Soc* 2021, **104**: 448–462.
[114] Akrami S, Edalati P, Shundo Y, *et al.* Significant CO_2 photoreduction on a high-entropy oxynitride. *Chem Eng J* 2022, **449**: 137800.
[115] Edalati P, Shen XF, Watanabe M, *et al.* High-entropy oxynitride as a low-bandgap and stable photocatalyst for hydrogen production. *J Mater Chem A* 2021, **9**: 15076–15086.
[116] Dippo OF, Mesgarzadeh N, Harrington TJ, *et al.* Bulk high-entropy nitrides and carbonitrides. *Sci Rep-UK* 2020, **10**: 21288.
[117] Yang Y, Bi JQ, Qiao LJ, *et al.* Effect of grain size on mechanical properties and tribological behavior of size-tunable high entropy diboride ceramics obtained by two-step SPS sintering. *J Adv Ceram* 2024, **13**: 1835–1843.
[118] Xie H, Qin MD, Hong M, *et al.* Rapid liquid phase-assisted ultrahigh-temperature sintering of high-entropy ceramic composites. *Sci Adv* 2022, **8**: 8241.
[119] Gild J, Kaufmann K, Vecchio K, *et al.* Reactive flash spark plasma sintering of high-entropy ultrahigh temperature ceramics. *Scripta Mater* 2019, **170**: 106–110.
[120] Qin MD, Gild J, Wang HR, *et al.* Dissolving and stabilizing soft WB_2 and MoB_2 phases into high-entropy borides via boron-metals reactive sintering to attain higher hardness. *J Eur Ceram Soc* 2020, **40**: 4348–4353.
[121] Chen H, Mi B, Wang J, *et al.* Research progress of high-entropy ceramic films via arc ion plating. *Coatings* 2026, **16**: 82
[122] Li YT, Chen XM, Zeng XK, *et al.* Hard yet tough and self-lubricating $(CuNiTiNbCr)C_x$ high-entropy nanocomposite films: Effects of carbon content on structure and properties. *J Mater Sci Technol* 2024, **173**: 20–30.

[123] Ren K, Wang QK, Shao G, *et al.* Multicomponent high-entropy zirconates with comprehensive properties for advanced thermal barrier coating. *Scripta Mater* 2020, **178**: 382–386.
[124] Lv JS, Li W, Li T, *et al.* Ablation behavior of high-entropy boride $(Hf–Zr–Ta–Ti)B_2$ coating fabricated via supersonic atmospheric plasma spraying for carbon/carbon composites. *Compos Part B Eng* 2024, **270**: 111137.
[125] Khan NA, Akhavan B, Zhou CF, *et al.* High entropy nitride (HEN) thin films of $AlCoCrCu_{0.5}FeNi$ deposited by reactive magnetron sputtering. *Surf Coat Tech* 2020, **402**: 126327.
[126] Arshad M, Amer M, Hayat Q, *et al.* High-entropy coatings (HEC) for high-temperature applications: Materials, processing, and properties. *Coatings* 2022, **12**: 691.
[127] Zoita NC, Dinu M, Parau AC, *et al.* The characteristics of light $(TiCrAl_{0.5}NbCu)C_xN_y$ high-entropy coatings deposited using a HiPIMS/DCMS technique. *Crystals* 2023, **13**: 1565.
[128] Yang JX, Dai BH, Chiang CY, *et al.* Rapid fabrication of high-entropy ceramic nanomaterials for catalytic reactions. *ACS Nano* 2021, **15**: 12324–12333.
[129] Han YJ, Yu RW, Liu HH, *et al.* Synthesis of the superfine high-entropy zirconate nanopowders by polymerized complex method. *J Adv Ceram* 2022, **11**: 136–144.
[130] Phakatkar AH, Saray MT, Rasul MG, *et al.* Ultrafast synthesis of high entropy oxide nanoparticles by flame spray pyrolysis. *Langmuir* 2021, **37**: 9059–9068.
[131] Ma MD, Hu XF, Meng H, *et al.* High-entropy metal carbide nanowires. *Cell Rep Phys Sci* 2022, **3**: 100839.
[132] Zhao JH, Zhang YL, Chen H, *et al.* Single-source precursor derived high-entropy metal–carbide nanowires: Microstructure and growth evolution. *J Adv Ceram* 2023, **12**: 2041–2052.
[133] Su JY, Cao ZZ, Jiang ZP, *et al.* High entropy oxide nanofiber by electrospun method and its application for lithium battery anode material. *Int J Appl Ceram Tec* 2022, **19**: 2004–2015.
[134] Chen HX, Li S, Huang SX, *et al.* High-entropy structure design in layered transition metal dichalcogenides. *Acta Mater* 2022, **222**: 117438.
[135] Nemani SK, Zhang BW, Wyatt BC, *et al.* High-entropy 2D carbide MXenes: $TiVNbMoC_3$ and $TiVCrMoC_3$. *ACS Nano* 2021, **15**: 12815–12825.
[136] Zhou J, Tao QZ, Ahmed B, *et al.* High-entropy laminate metal carbide (MAX phase) and its two-dimensional derivative MXene. *Chem Mater* 2022, **34**: 2098–2106.
[137] Solomon JM, Shamblin J, Lang M, *et al.* Chemical ordering in substituted fluorite oxides: A computational investigation of $Ho_2Zr_2O_7$ and $RE_2Th_2O_7$ (RE = Ho, Y, Gd, Nd, La). *Sci Rep-UK* 2016, **6**: 38772.
[138] Boston R, Schmidt WL, Lewin GD, *et al.* Protocols for the fabrication, characterization, and optimization of n-type thermoelectric ceramic oxides. *Chem Mater* 2017, **29**: 265–280.
[139] Decterov SA. Thermodynamic database for multicomponent oxide systems. *Chim Tech Acta* 2018, **5**: 16–48.
[140] Aamlid SS, Mugiraneza S, González-Rivas MU, *et al.* Short-range order and local distortions in entropy stabilized oxides. *Chem Mater* 2024, **36**: 9636–9645.
[141] Jiang B, Bridges CA, Unocic RR, *et al.* Probing the local site disorder and distortion in pyrochlore high-entropy oxides. *J Am Chem Soc* 2021, **143**: 4193–4204.
[142] Szymanski NJ, Lun ZY, Liu J, *et al.* Modeling short-range order in disordered rocksalt cathodes by pair distribution function analysis. *Chem Mater* 2023, **35**: 4922–4934.
[143] Ferrari A, Körmann F, Asta M, *et al.* Simulating short-range order in compositionally complex materials. *Nat Comput Sci* 2023, **3**: 221–229.
[144] Aamlid SS, Oudah M, Rottler J, *et al.* Understanding the role of entropy in high entropy oxides. *J Am Chem Soc* 2023, **145**: 5991–6006.
[145] Gaboardi M, Monteverde F, Saraga F, *et al.* Local structure in high-entropy transition metal diborides. *Acta Mater* 2022, **239**: 118294.
[146] Mandal S, Sharma J, Chakraborty T, *et al.* Structural, magnetic and X-ray absorption spectroscopy studies of new Cr-based low, medium and high-entropy spinel oxides. *J Alloys Compd* 2025, **1010**: 177993.
[147] Wu J, Ma XS, Zhou DH, *et al.* High-entropy high-temperature high-piezoelectricity ceramics. *Adv Mater* 2025, **37**: 2419134.
[148] Liao JH, Chen H, Xie YS, *et al.* Modeling short-range order in high-entropy cation-disordered rocksalt-type cathodes. *Adv Energy Mater* 2025, **15**: 2501857.
[149] Mansley ZR, Millares MF, Kazanjian O, *et al.* Understanding the role of short-range order in high-entropy layered oxides for energy storage. *Nano Lett* 2025, **25**: 11594–11600.
[150] Zinouyeva M, Fracchia M, Maranini G, *et al.* X-ray analysis of $Mg_{0.2}Co_{0.2}Ni_{0.2}Cu_{0.2}Zn_{0.2}O$: Disentangling elemental contributions in a prototypical high-entropy oxide. *J Mater Chem A* 2026, **14**: 1221–1233.
[151] Gaur A, Sharma J, Kaur G, *et al.* Jahn-teller effect: Impact of distortion on oxygen electrocatalysis. *Adv Funct Mater*, 2026, **36**: 16674
[152] Berardan D, Meena AK, Franger S, *et al.* Controlled Jahn–Teller distortion in (MgCoNiCuZn)O-based high entropy oxides. *J Alloys Compd* 2017, **704**: 693–700.
[153] Tomboc GM, Zhang XD, Choi S, *et al.* Stabilization, characterization, and electrochemical applications of high-entropy oxides: Critical assessment of crystal phase–properties relationship. *Adv Funct Mater* 2022, **32**: 2205142.
[154] Lu WY, Xu JR, Huang SS, *et al.* The coupling of carbon non-stoichiometry and short-range order in governing mechanical properties of high-entropy ceramics. *npj Comput Mater* 2025, **11**: 64.
[155] Liew SL, Ni XP, Wei FX, *et al.* High-entropy fluorite oxides: Atomic stabiliser effects on thermal–mechanical properties. *J Eur Ceram Soc* 2022, **42**: 6608–6613.
[156] Monteverde F, Saraga F, Gaboardi M. Compositional disorder and sintering of entropy stabilized $(Hf,Nb,Ta,Ti,Zr)B_2$ solid solution powders. *J Eur Ceram Soc* 2020, **40**: 3807–3814.
[157] Braun JL, Rost CM, Lim M, *et al.* Charge-induced disorder controls the thermal conductivity of entropy-stabilized oxides. *Adv Mater* 2018, **30**: 1805004.
[158] Cheng BY, Lou HB, Sarkar A, *et al.* Pressure-induced tuning of lattice distortion in a high-entropy oxide. *Commun Chem* 2019, **2**: 114.
[159] Zhao SJ. Lattice distortion in high-entropy carbide ceramics from first-principles calculations. *J Am Ceram Soc* 2021, **104**: 1874–1886.
[160] Zhang H D, Zhang J, Chen L, *et al.* Progressive entropy engineering in AlTiHfNbTaZrN: Achieving superior thermomechanical properties through lattice distortion and thermodynamic kinetic factors. *Eur Ceram Soc* 2025, **45**: 117558
[161] Jia YG, Chen SJ, Shao X, *et al.* Synergetic effect of lattice distortion and oxygen vacancies on high-rate lithium-ion storage in high-entropy perovskite oxides. *J Adv Ceram* 2023, **12**: 1214–1227.
[162] Zhu SS, Zhu JP, Ye SB, *et al.* High-entropy rare earth titanates with low thermal conductivity designed by lattice distortion. *J Am Ceram Soc* 2023, **106**: 6279–6291.
[163] Liu YW, Fu YM, Gu FC, *et al.* Lattice-distortion-driven reduced lattice thermal conductivity in high-entropy ceramics. *Adv Sci* 2025, **12**: 2501157.
[164] Wen YB, Liu YF. Quantitative analysis of atomic-scale local lattice distortions in high-entropy fluorite oxide $(Zr_{0.2}Ce_{0.2}Hf_{0.2}Y_{0.2}Al_{0.2})O_{2-\delta}$. *Ceram Int* 2023, **49**: 26141–26146.
[165] Yang WT, Han Z, Zheng GP. The influences of lattice distortion on the antiferroelectric transition and relaxation of oxygen vacancies in high-entropy perovskites $(Bi_{0.2}Na_{0.2}Ba_{0.2}K_{0.2}X_{0.2})TiO_3$ with X = Ca, Sr or La. *Scripta Mater* 2021, **203**: 114096.
[166] Li ZX, Yang HC, Zhong CW, *et al.* Tuning lattice distortion and

defect chemistry via medium-entropy strategy in $Sr_{0.5}Ba_xCa_{0.5-x}MoO_4$ microwave dielectric ceramics. *Acta Mater* 2026, **303**: 121740.
[167] Zhang YN, Zhu JP, Zou H, *et al.* Effect of lattice distortion on thermal conduction behavior in a novel high-entropy rare-earth tantalates. *J Alloys Compd* 2024, **976**: 172942.
[168] Lin Y, Bu W, He P, *et al.* Entropy enhancing toughness of diborides: First-principles insights and experimental validation. *J Adv Ceram*, 2026, **15**: 9221266.
[169] Yang Y, Bi JQ, Sun KN, *et al.* The effect of chemical element on hardness in high-entropy transition metal diboride ceramics. *J Eur Ceram Soc* 2023, **43**: 5774–5781.
[170] Shojaie-bahaabad , Bozorg M, Najafizadeh M, *et al.* Ultra high temperature ceramic coatings in thermal protection systems (TPS). *Ceram Int* 2024, **50**: 9937–9951.
[171] Li XX, Fu QG, Wen ZH, *et al.* Research progress on ultra-high temperature ceramic structural materials for extreme environments. *J Inorg Mater* 2025, **40**: 1045–1078.
[172] Li JC, Zhang YL, Zhao YX, *et al.* A novel $(Hf_{1/3}Zr_{1/3}Ti_{1/3})C$ medium-entropy carbide coating with excellent long-life ablation resistance applied above 2100 °C. *Compos Part B Eng* 2023, **251**: 110467.
[173] Ni N, Ding Q, Shi YC, *et al.* Ablation behavior of high-entropy carbides ceramics $(Hf_{0.2}Zr_{0.2}Ta_{0.2}Nb_{0.2}Ti_{0.2})C$ upon exposition to an oxyacetylene torch at 2000 °C. *J Eur Ceram Soc* 2023, **43**: 2306–2319.
[174] Yang YL, Wang SQ, Zou YC, *et al.* High-temperature oxidation-resistant composite coatings for extreme environments: Material systems, design strategies, preparation technologies, performance characterizations, and research challenges. *J Compos Sci* 2026, **10**: 51.
[175] Ye ZM, Zeng Y, Xiong X, *et al.* The synergistic role of hierarchical preferential oxidation in the enhanced ablation performance of multi-phase multicomponent ultra-high temperature ceramics. *J Eur Ceram Soc* 2023, **43**: 6718–6731.
[176] Li JC, Zhao JH, Li T, *et al.* Microstructure evolution and phase interface characterization in anti-ablation $(Hf_{1/4}Zr_{1/4}Ta_{1/4}Ti_{1/4})C$-coated C/C composites. *Compos Part B Eng* 2024, **281**: 111569.
[177] Chen ZZ, Wang HX, Li CR, *et al.* Oxyacetylene ablation of $(Hf_{0.2}Ti_{0.2}Zr_{0.2}Ta_{0.2}Nb_{0.2})C$ at 1350–2050 °C. *J Eur Ceram Soc* 2023, **43**: 2700–2707.
[178] Ouyang HB, Chen ZH, Li CY, *et al.* C/C–(HfZrTi)C composites prepared by a novel precursor infiltration and pyrolysis method: A silicon-free strategy to improve the ablation resistance at ultra-high temperatures. *J Alloys Compd* 2025, **1036**: 181690.
[179] Liu Y, Guo WM, Liu Y, *et al.* Enhanced ablation resistance of pressureless liquid-phase sintered SiC ceramics via $(Hf_{0.2}Zr_{0.2}Ta_{0.2}Nb_{0.2}Ti_{0.2})B_2$ addition. *Ceram Int* 2025, **51**: 31097–31103.
[180] Luo X, Zhang XX, Yang X, *et al.* Effect of SiC addition on the ablation behavior of (Zr–Hf–Ti–Ta)C coatings. *Ceram Int* 2025, **51**: 54342–54357.
[181] Lu L, Wen QB, Hu JR, *et al.* Single-source-precursor synthesis and air-plasma ablation behavior of (Ti,Zr,Hf)C/SiC ceramic nanocomposites at 2200 °C. *J Adv Ceram* 2024, **13**: 1043–1059.
[182] Wang YC, Zhang BH, Zhang CY, *et al.* Ablation behaviour of (Hf–Ta–Zr–Nb)C high entropy carbide ceramic at temperatures above 2100 °C. *J Mater Sci Technol* 2022, **113**: 40–47.
[183] Chen SY, Chen ZK, Song WL, *et al.* High-temperature ablation behavior and failure mechanism of $(Hf_{0.25}Zr_{0.25}Ti_{0.25}Ta_{0.25})C$ high-entropy carbide in wide temperature range. *J Eur Ceram Soc* 2024, **44**: 6815–6826.
[184] Li JC, Lu FY, Li T, *et al.* Superior synergistic oxidation resistance of medium-entropy carbide ceramic powders rather than multi-phase carbide ceramic powders. *J Adv Ceram* 2024, **13**: 1223–1233.
[185] Backman L, Gild J, Luo J, *et al.* Part I: Theoretical predictions of preferential oxidation in refractory high entropy materials. *Acta Mater* 2020, **197**: 20–27.
[186] Backman L, Gild J, Luo J, *et al.* Part II: Experimental verification of computationally predicted preferential oxidation of refractory high entropy ultra-high temperature ceramics. *Acta Mater* 2020, **197**: 81–90.
[187] Backman L, Opila EJ. Thermodynamic assessment of the group IV, V and VI oxides for the design of oxidation resistant multi-principal component materials. *J Eur Ceram Soc* 2019, **39**: 1796–1802.
[188] Tang XC, Thompson GB, Ma KK, *et al.* The role of entropy and enthalpy in high entropy carbides. *Comp Mater Sci* 2022, **210**: 111474.
[189] Tan YQ, Chen C, Li SG, *et al.* Oxidation behaviours of high-entropy transition metal carbides in 1200 °C water vapor. *J Alloys Compd* 2020, **816**: 152523.
[190] Feng XK, Wang XC, Wu LF, *et al.* The effects of refractory elements on the properties of quaternary high entropy carbides—A first-principles and experiment study. *Comp Mater Sci* 2024, **245**: 113324.
[191] Harrington TJ, Gild J, Sarker P, *et al.* Phase stability and mechanical properties of novel high entropy transition metal carbides. *Acta Mater* 2019, **166**: 271–280.
[192] Ouyang ZY, Wang ZL, Wu Y, *et al.* A first-principles investigation of light weight high mechanical performance high-entropy carbides: The research of bottom-up compositional designing. *J Phys Chem Solids* 2024, **192**: 112069.
[193] Xu YX, Yu L, Zhao T, *et al.* Composition design of oxidation resistant non-equimolar high-entropy ceramic materials: An example of $(Zr–Hf–Ta–Ti)B_2$ ultra-high temperature ceramics. *J Adv Ceram* 2024, **13**: 2087–2100.
[194] Zhang XX, Luo X, Liu ZG, *et al.* Effect of (Ti,Zr,Hf)C medium-entropy and (Ti,Zr,Hf,Ta)C high-entropy modification on microstructure and ablative properties of C/C–SiC composites. *Mater Charact* 2025, **223**: 114952.
[195] Liu GA, Fang C, Li ML, *et al.* Breaking conventional understanding: Superior oxidation resistance of a novel Ta and Mo containing high-entropy transition metal diboride. *J Mater Sci Technol* 2026, **252**: 313–327.
[196] Song X, Yan H, Cui TY, *et al.* Ablation behavior of medium entropy carbide ceramics with different molar ratios of (Hf,Zr,Ti)C in oxyacetylene flame. *Ceram Int* 2025, **51**: 5987–5997.
[197] Song JT, Chen GQ, Xiang HM, *et al.* Regulating the formation ability and mechanical properties of high-entropy transition metal carbides by carbon stoichiometry. *J Mater Sci Technol* 2022, **121**: 181–189.
[198] Luo SC, Guo WM, Fang ZL, *et al.* Effect of carbon content on the microstructure and mechanical properties of high-entropy $(Ti_{0.2}Zr_{0.2}Nb_{0.2}Ta_{0.2}Mo_{0.2})C_x$ ceramics. *J Eur Ceram Soc* 2022, **42**: 336–343.
[199] Li JC, Fan HZ, Zhang QQ, *et al.* Carbon vacancies enhanced oxidation resistance of high-entropy carbides $(Ti_{0.2}V_{0.2}Nb_{0.2}Mo_{0.2}W_{0.2})C$. *Ceram Int* 2024, **50**: 9926–9930.
[200] Anwar F, Tarraste M, Berger LM, *et al.* Effect of carbon content on the microstructure and phases of $(Ti,V,Nb,Cr,Mo)C_x$ high-entropy carbide. *Proc Est Acad Sci* 2025, **74**: 132–136.
[201] Valášek D, Pouchlý V, Salamon D. Turning of high entropy alloy into high entropy carbides by modifying carbon content during reactive sintering. *Ceram Int* 2024, **50**: 15367–15372.
[202] Liu JX, Guo LW, Wu Y, *et al.* Lattice rigidity in high-entropy carbide ceramics with carbon vacancies. *J Am Ceram Soc* 2023, **106**: 5612–5619.
[203] Tan YQ, Liao W, Teng Z, *et al.* Synthesis, mechanical, and thermophysical properties of high-entropy $(Zr,Ti,Nb,Ta,Hf)C_{0.8}$ ceramic. *J Am Ceram Soc* 2023, **106**: 4382–4389.
[204] Ďaková L, Hrubovčáková M, Tatarko P, *et al.* Enhanced ablation/oxidation resistance of high-entropy carbides: The role of SiC whiskers. *Int J Appl Ceram Tec* 2025, **22**: 70059.
[205] Guo WJ, Hu J, Ye YC, *et al.* Ablation behavior of (TiZrHfNbTa)C high-entropy ceramics with the addition of SiC secondary under an oxyacetylene flame. *Ceram Int* 2022, **48**: 12790–12799.

[206] Shen TZ, Li CY, Ouyang HB, *et al.* High-entropy ($Ta_{0.2}Nb_{0.2}Ti_{0.2}Hf_{0.2}Zr_{0.2}$)C–SiC ceramics: Achieving superior ablation resistance through SiC particle size optimization. *J Eur Ceram Soc* 2026, **46**: 117800.

[207] Wang YC, Yu D, Yin J, *et al.* Ablation behavior of (Hf–Ta–Zr–Nb–Ti)C high-entropy carbide and (Hf–Ta–Zr–Nb–Ti)C–*x*SiC composites. *J Am Ceram Soc* 2022, **105**: 6395–6406.

[208] Hassan R, Fahrenholtz WG, Balani K, *et al.* SiC addition to a dual phase high entropy ultra-high temperature ceramic. *Ceram Int* 2024, **50**: 55650–55657.

[209] Ren H, Chen RR, Liu T, *et al.* Unraveling the oxidation mechanism of Y-doped AlCoCrFeNi high-entropy alloy at 1100 °C. *Appl Surf Sci* 2024, **652**: 159316.

[210] Xu WJ, Jia BS, Jiang XY, *et al.* Enhanced oxidation resistance of Y-doped high-entropy carbide films via oxidation formation of amorphous and high-entropy oxide layers. *ACS Appl Mater Inter* 2025, **17**: 65877–65888.

[211] Zhao X, Bai YH, Yang Y, *et al.* Ablation-resistant Y_2O_3-modified ($Hf_{0.2}Ta_{0.2}Zr_{0.2}Ti_{0.2}Nb_{0.2}$)C high entropy ceramics in oxyacetylene flame above 2100 °C. *J Eur Ceram Soc* 2025, **45**: 117723.

[212] Wang YC, Csanádi T, Fogarassy Z, *et al.* The role of Cr addition on the processing and mechanical properties of high entropy carbides. *J Eur Ceram Soc* 2022, **42**: 5273–5279.

[213] Wang PC, Liu WH, Xu ZQ, *et al.* Unraveling the oxidation behavior and mechanism of (TiZrTaNbCr)C high-entropy ceramic by introducing Cr_3C_2. *J Eur Ceram Soc* 2024, **44**: 2687–2694.

[214] Wen ZH, Liu YW, Yang J, *et al.* Exceptional oxidation resistance of high-entropy carbides up to 3600 °C. *Adv Mater* 2025, **37**: 2507254.

[215] Gong WL, Yang YM, Li ZW, *et al.* Effects of W contents on the oxidation resistance of (Zr,Hf,Nb,Ta,W)C high-entropy carbides at 800–1200 °C. *J Eur Ceram Soc* 2025, **45**: 117367.

[216] Peng Z, Sun W, Xiong X, *et al.* Novel refractory high-entropy ceramics: Transition metal carbonitrides with superior ablation resistance. *Corros Sci* 2021, **184**: 109359.

[217] Ouyang ZY, Li YF, Jin N, *et al.* Regulating nitrogen fraction, phasic composition and mechanical properties in ($Ti_{0.2}V_{0.2}Nb_{0.2}Ta_{0.2}W_{0.2}$)($C_xN_y$) high-entropy ceramic via carbon stoichiometry. *J Eur Ceram Soc* 2024, **44**: 5190–5202.

[218] Hassan R, Fahrenholtz WG, Hilmas GE, *et al.* Synergistic hardening in a dual phase high-entropy (Hf,Nb,Ta,Ti,Zr)C–(Hf,Nb,Ta,Ti,Zr)B_2 ultra-high temperature ceramic. *J Am Ceram Soc* 2025, **108**: 20203.

[219] Feng L, Fahrenholtz WG, Hilmas GE, *et al.* Boro/carbothermal reduction co-synthesis of dual-phase high-entropy boride-carbide ceramics. *J Eur Ceram Soc* 2023, **43**: 2708–2712.

[220] Guo WJ, Hu J, Fang W, *et al.* A novel strategy for rapid fabrication of continuous carbon fiber reinforced (TiZrHfNbTa)C high-entropy ceramic composites: High-entropy alloy *in-situ* reactive melt infiltration. *J Eur Ceram Soc* 2023, **43**: 2295–2305.

[221] Cai FY, Ni DW, Chen BW, *et al.* Efficient fabrication and properties of 2D C_f/($Ti_{0.2}Zr_{0.2}Hf_{0.2}Nb_{0.2}Ta_{0.2}$)C–SiC high-entropy ceramic matrix composites via slurry infiltration lamination combined with precursor infiltration and pyrolysis. *J Eur Ceram Soc* 2023, **43**: 7403–7410.

[222] Miao HM, Xie CY, Wang YF, *et al.* Fabrication and properties of 3-dimensional 5-directional C_f/($Zr_{0.2}Hf_{0.2}Ta_{0.2}Nb_{0.2}Ti_{0.2}$)C–SiC high-entropy ceramic matrix composites by precursor infiltration and pyrolysis process. *Ceram Int* 2025, **51**: 15055–15066.

[223] He ZW, Wang MZ, Hao XL, *et al.* Novel cemented carbide produced with $TiN_{0.3}$ and high-entropy alloys. *Rare Metals* 2017, **36**: 494–500.

[224] Pötschke J, Dahal M, Vornberger A, *et al.* Production and properties of high entropy carbide based hardmetals. *Metals* 2021, **11**: 271.

[225] Anwer Z, Cabezas L, Jiménez-Piqué E, *et al.* Facile synthesis of high entropy carbide-nickel based cermets by *in-situ* carbo-thermal reduction of transition metal oxides. *Acta Mater* 2024, **272**: 119924.

[226] Nisar A, Zhang C, Boesl B, *et al.* A perspective on challenges and opportunities in developing high entropy-ultra high temperature ceramics. *Ceram Int* 2020, **46**: 25845–25853.

[227] Gao XQ, Chen L, Liu RK, *et al.* Multiscale structure–mechanical property relationship and data-driven design of ultra-high temperature ceramics: A review. *Extreme Mech Lett* 2025, **79**: 102392.

[228] Zhu TL, Wang Z. Advances in processing and ablation properties of carbon fiber reinforced ultra-high temperature ceramic composites. *Rev Adv Mater Sci* 2024, **63**: 20240029.

[229] Yan YG, Liao YL, Wang K. Accelerated discovery of oxidation-resistant ultra-high temperature ceramics via data driven methodology. *Corros Sci* 2023, **223**: 111457.

[230] Hsu WL, Tsai CW, Yeh AC, *et al.* Clarifying the four core effects of high-entropy materials. *Nat Rev Chem* 2024, **8**: 471–485.

[231] Toher C, Oses C, Esters M, *et al.* High-entropy ceramics: Propelling applications through disorder. *MRS Bull* 2022, **47**: 194–202.

[232] McCormack SJ, Navrotsky A. Thermodynamics of high entropy oxides. *Acta Mater* 2021, **202**: 1–21.

[233] Zhang P, Lou ZH, Qin MJ, *et al.* High-entropy ($Ca_{0.2}Sr_{0.2}Ba_{0.2}La_{0.2}Pb_{0.2}$)$TiO_3$ perovskite ceramics with A-site short-range disorder for thermoelectric applications. *J Mater Sci Technol* 2022, **97**: 182–189.

[234] Wright AJ, Wang QY, Ko ST, *et al.* Size disorder as a descriptor for predicting reduced thermal conductivity in medium- and high-entropy pyrochlore oxides. *Scripta Mater* 2020, **181**: 76–81.

[235] Song D, Song T, Paik U, *et al.* Glass-like thermal conductivity in mass-disordered high-entropy $(Y,Yb)_2(Ti,Zr,Hf)_2O_7$ for thermal barrier material. *Mater Design* 2021, **210**: 110059.

[236] Bérardan D, Franger S, Dragoe D, *et al.* Colossal dielectric constant in high entropy oxides. *Phys Status Solidi-R* 2016, **10**: 328–333.

[237] Tao ZW, Zheng PF, Dong GH, *et al.* The mechanical behaviors in oxides: Beyond brittleness. *Adv Mater* 2026, **38**: 15834.

[238] Liew SL, Zhou J, Wei FX, *et al.* Design and synthesis of single phase $Hf_{0.25}Zr_{0.25}Ce_{0.25}Y_{0.125}Si_{0.125}O_{2-\delta}$ high-entropy ceramics. *J Alloys Compd* 2022, **904**: 164097.

[239] Liu DB, Shi BL, Geng LY, *et al.* High-entropy rare-earth zirconate ceramics with low thermal conductivity for advanced thermal-barrier coatings. *J Adv Ceram* 2022, **11**: 961–973.

[240] Hutterer P, Lepple M. Influence of composition on structural evolution of high-entropy zirconates—cationic radius ratio and atomic size difference. *J Am Ceram Soc* 2023, **106**: 1547–1560.

[241] Yan RX, Liang WP, Miao Q, *et al.* Mechanical, thermal and CMAS resistance properties of high-entropy $(Gd_{0.2}Y_{0.2}Er_{0.2}Tm_{0.2}Yb_{0.2})_2Zr_2O_7$ ceramics. *Ceram Int* 2023, **49**: 20729–20741.

[242] Banerjee R, Chatterjee S, Ranjan M, *et al.* High-entropy perovskites: An emergent class of oxide thermoelectrics with ultralow thermal conductivity. *ACS Sustain Chem Eng* 2020, **8**: 17022–17032.

[243] Gao C, Zhu JP, Ye SB, *et al.* Novel high-entropy perovskite titanate: A potential thermal protective material with improved thermophysical properties. *J Eur Ceram Soc* 2025, **45**: 116878.

[244] Zhang P, Gong LY, Lou ZH, *et al.* Reduced lattice thermal conductivity of perovskite-type high-entropy ($Ca_{0.25}Sr_{0.25}Ba_{0.25}RE_{0.25}$)$TiO_3$ ceramics by phonon engineering for thermoelectric applications. *J Alloys Compd* 2022, **898**: 162858.

[245] Chen H, Zhao B, Zhao ZF, *et al.* Achieving strong microwave absorption capability and wide absorption bandwidth through a combination of high entropy rare earth silicide carbides/rare earth oxides. *J Mater Sci Technol* 2020, **47**: 216–222.

[246] Xu L, Su L, Wang HJ, *et al.* High-entropy $Sm_2B_2O_7$ (B = Ti, Zr, Sn, Hf, Y, Yb, Nb, and Ta) oxides with highly disordered B-site cations for ultralow thermal conductivity. *J Mater Sci Technol* 2022, **119**: 182–189.

[247] Xu L, Su L, Wang HJ, *et al.* Tuning stoichiometry of high-entropy oxides for tailorable thermal expansion coefficients and low thermal conductivity. *J Am Ceram Soc* 2022, **105**: 1548–1557.

[248] Xue Y, Zhao XQ, An YL, *et al.* High-entropy ($La_{0.2}Nd_{0.2}Sm_{0.2}Eu_{0.2}Gd_{0.2}$)$_2Ce_2O_7$: A potential thermal barrier material with

improved thermo-physical properties. *J Adv Ceram* 2022, **11**: 615–628.
[249] Lv K, Wei P, Zhuang L, *et al.* Ten-cation high-entropy rare-earth monosilicate: A potential thermal/environmental barrier coating material. *Int J Appl Ceram Tec* 2026, **23**: 70152.
[250] Sun YN, Xiang HM, Dai FZ, *et al.* Preparation and properties of CMAS resistant bixbyite structured high-entropy oxides RE_2O_3 (RE = Sm, Eu, Er, Lu, Y, and Yb): Promising environmental barrier coating materials for Al_{2O_3f}/Al_2O_3 composites. *J Adv Ceram* 2021, **10**: 596–613.
[251] Yeh JW, Lin SJ. Breakthrough applications of high-entropy materials. *J Mater Res* 2018, **33**: 3129–3137.
[252] Zhang Y, Ren K, Wang WY, *et al.* Discovering the ultralow thermal conductive $A_2B_2O_7$-type high-entropy oxides through the hybrid knowledge-assisted data-driven machine learning. *J Mater Sci Technol* 2024, **168**: 131–142.
[253] Han LL, Zhu SY, Rao ZY, *et al.* Multifunctional high-entropy materials. *Nat Rev Mater* 2024, **9**: 846–865.
[254] Liu DB, Wang YG, Zhou FF, *et al.* A novel high-entropy $(Sm_{0.2}Eu_{0.2}Tb_{0.2}Dy_{0.2}Lu_{0.2})_2Zr_2O_7$ ceramic aerogel with ultralow thermal conductivity. *Ceram Int* 2021, **47**: 29960–29968.
[255] Zhang DB, Yu Y, Feng XL, *et al.* Thermal barrier coatings with high-entropy oxide as a top coat. *Ceram Int* 2022, **48**: 1349–1359.
[256] Fu MS, Ma X, Zhao KN, *et al.* High-entropy materials for energy-related applications. *iScience* 2021, **24**: 102177.
[257] Wang C, Sun GT, He CY, *et al.* Entropy-driven multiphase engineering enables superior broadband infrared emissivity in high-entropy oxides. *Adv Mater* 2026, **38**: 08636.
[258] Xin XT, Bao WC, Wang XG, *et al.* Reduced He ion irradiation damage in ZrC-based high-entropy ceramics. *J Adv Ceram* 2023, **12**: 916–929.
[259] Kinsler-Fedon C, Nuckols L, Nelson CT, *et al.* Effects of Au^{2+} irradiation induced damage in a high-entropy pyrochlore oxide single crystal. *Scripta Mater* 2022, **220**: 114916.
[260] Wu JX, Zhang M, Li ZQ, *et al.* High-entropy $(Sm_{0.2}Eu_{0.2}Gd_{0.2}Dy_{0.2}Er_{0.2})_2Hf_2O_7$ ceramic with superb resistance to radiation-induced amorphization. *J Mater Sci Technol* 2023, **155**: 1–9.
[261] Li YL, Zhao SJ, Wu ZG. Uncovering the effects of chemical disorder on the irradiation resistance of high-entropy carbide ceramics. *Acta Mater* 2024, **277**: 120187.
[262] Zhang K, Duan XL, Jiang MH, *et al.* Design and synthesis of high-entropy $A_2B_2O_7$-type pyrochlore ceramics for the immobilization of molten salt radwastes. *Ceram Int* 2024, **50**: 52640–52648.
[263] Wang ZZ, Zhu CZ, Wang H, *et al.* Preparation and irradiation stability of $A_2B_2O_7$ pyrochlore high-entropy ceramic for immobilization of high-level nuclear waste. *J Nucl Mater* 2023, **574**: 154212.
[264] Xu L, Niu M, Wang HJ, *et al.* Response of structure and mechanical properties of high entropy pyrochlore to heavy ion irradiation. *J Eur Ceram Soc* 2022, **42**: 6624–6632.
[265] Tunes MA, Fritze S, Osinger B, *et al.* From high-entropy alloys to high-entropy ceramics: The radiation-resistant highly concentrated refractory carbide (CrNbTaTiW)C. *Acta Mater* 2023, **250**: 118856.
[266] Wang F, Yan XL, Wang TY, *et al.* Irradiation damage in $(Zr_{0.25}Ta_{0.25}Nb_{0.25}Ti_{0.25})C$ high-entropy carbide ceramics. *Acta Mater* 2020, **195**: 739–749.
[267] Zhang GW, Daghbouj N, AlMotasem AT, *et al.* Exploring radiation damage in $(Hf_{0.2}Zr_{0.2}Ta_{0.2}Ti_{0.2}Nb_{0.2})C$ high-entropy carbide ceramic: Integrating experimental and atomistic investigations. *Int J Refract Met H* 2024, **123**: 106755.
[268] Zhang JT, Xu S, Wen CM, *et al.* A study on He ion irradiation damage in $(Ti_{0.25}Zr_{0.25}Nb_{0.25}Ta_{0.25})C$ high-entropy carbide ceramics from room temperature to 700 °C. *J Eur Ceram Soc* 2025, **45**: 116855.
[269] Khanolkar A, Datye A, Zhang Y, *et al.* Effects of irradiation damage on the hardness and elastic properties of quaternary and high entropy transition metal diborides. *J Appl Phys* 2024, **136**: 105106.
[270] Xiao H, Zhao S, Liu QY, *et al.* Point defect properties in high entropy MAX phases from first-principles calculations. *Acta Mater* 2023, **248**: 118783.
[271] Zhu YB, Chai JL, Wang ZG, *et al.* Microstructural damage evolution of $(WTiVNbTa)C_5$ high-entropy carbide ceramics induced by self-ions irradiation. *J Eur Ceram Soc* 2022, **42**: 2567–2576.
[272] Wang J, Shu R, Chai JL, *et al.* Xe-ion-irradiation-induced structural transitions and elemental diffusion in high-entropy alloy and nitride thin-film multilayers. *Mater Design* 2022, **219**: 110749.
[273] Liu ZL, Wei C, De YY, *et al.* Phase structure of high-entropy pyrochlore oxides: From powder synthesis to ceramic sintering. *J Eur Ceram Soc* 2023, **43**: 7613–7622.
[274] Zhou L, Li F, Liu JX, *et al.* High-entropy $A_2B_2O_7$-type oxide ceramics: A potential immobilising matrix for high-level radioactive waste. *J Hazard Mater* 2021, **415**: 125596.
[275] Wang YH, Jing C, Ding ZY, *et al.* The structure, property, and ion irradiation effects of pyrochlores: A comprehensive review. *Crystals* 2023, **13**: 143.
[276] Ji XY, Lei PH, Chen JH, *et al.* Synthesis and irradiation behavior of $(Gd_{0.2}Sm_{0.2}Dy_{0.2}Er_{0.2}Yb_{0.2})_2Ti_2O_7$ high-entropy pyrochlore waste forms consolidated by spark plasma sintering. *Vacuum* 2025, **232**: 113893.
[277] Ma ZZ, Wang YH, Rui TH, *et al.* Synthesis, microstructures, and aqueous chemical durability of high-entropy pyrochlore ceramic $Eu_2B_2O_7$ (B Ti, Zr, Sn, Hf, Nb, and Ce) for nuclear waste immobilization. *J Eur Ceram Soc* 2026, **46**: 117844.
[278] Weber WJ, Kinsler-Fedon C, Keppens V, *et al.* Temperature dependence of irradiation-induced amorphization in a high-entropy titanate pyrochlore. *MRS Commun* 2024, **14**: 1364–1370.
[279] Xu C, He JM, Chen ZX, *et al.* Two-step reactive flash sintering of high entropy pyrochlore: Densification, grain growth, and microstructural homogeneity. *J Am Ceram Soc* 2024, **107**: 797–802.
[280] Xiao H, Zhao S, Zhang J, *et al.* Distinct amorphization resistance in high-entropy MAX-phases $(Ti,M)_2AlC$ (M = Nb, Ta, V, Zr) under *in situ* irradiation. *Npj Comput Mater* 2024, **10**: 196.
[281] Zhang Y, Khanolkar AR, Bawane KK, *et al.* Physical properties and their influence on irradiation damage in metal diborides and in high-entropy materials. *Jom* 2024, **76**: 2602–2618.
[282] Zhang YW, Silva C, Lach TG, *et al.* Role of electronic energy loss on defect production and interface stability: Comparison between ceramic materials and high-entropy alloys. *Curr Opin Solid St M* 2022, **26**: 101001.
[283] Nikitin DS, Shanenkov II, Nassyrbayev AR, *et al.* Synthesis of high-entropy Ti–Zr–Nb–Hf–Ta carbides and carbonitrides in high-speed arc discharge plasma jet. *J Alloys Compd* 2025, **1010**: 177178.
[284] Li W, Shen ZH, Liu RL, *et al.* Generative learning facilitated discovery of high-entropy ceramic dielectrics for capacitive energy storage. *Nat Commun* 2024, **15**: 4940.
[285] Bunpang K, Singkammo S, Cann DP, *et al.* Titanate-based high-entropy perovskite oxides relaxor ferroelectrics. *Sci Rep-UK* 2024, **14**: 6017.
[286] Herbert-Galarza C, Durán A. Structural stability, optical and dielectric properties of the $(Ba_{1/5}Pb_{1/5}Sr_{1/5}RE_{1/5}K_{1/5})TiO_3$ high-entropy ceramic. *Int J Miner Metall Mater* 2025, **32**: 2821–2834.
[287] Zhu XW, Xiong SY, Zhu GB, *et al.* Dielectric properties and excellent energy storage density under low electric fields for high entropy relaxor ferroelectric $(Li_{0.2}Ca_{0.2}Sr_{0.2}Ba_{0.2}La_{0.2})TiO_3$ ceramic. *J Alloys Compd* 2024, **984**: 173987.
[288] Sun XF, Xu CP, Ji PQ, *et al.* The enhancement of energy storage performance in high-entropy ceramic. *Ceram Int* 2023, **49**: 17091–17098.
[289] Zhou JY, Zheng P, Bai WF, *et al.* Breaking the mutual constraint between polarization and voltage resistance with nanograined high-entropy ceramic. *ACS Appl Mater Inter* 2024, **16**: 2530–2538.
[290] Deng QH, Liu H, Wang YR, *et al.* Dielectric property optimization

of polymer nanocomposites using $BaTiO_3$ based high-entropy ceramic filler with Dirac-cone effect. *Physica B* 2024, **684**: 415992.
[291] Zhang X, Zhang F, Niu YW, *et al.* High energy storage performance of lead-free Nb-modified $(Bi_{0.2}Na_{0.2}Ca_{0.2}Ba_{0.2}Sr_{0.2})TiO_3$ high-entropy ceramics. *J Am Ceram Soc* 2024, **107**: 4864–4877.
[292] Qi JL, Zhang MH, Chen YY, *et al.* High-entropy assisted $BaTiO_3$-based ceramic capacitors for energy storage. *Cell Rep Phys Sci* 2022, **3**: 101110.
[293] Wu J, Tan H, Qi H, *et al.* High energy storage performance in $BiFeO_3$-based lead-free high-entropy ferroelectrics. *Small* 2024: 2400997.
[294] Peng HN, Wu TT, Liu Z, *et al.* High-entropy relaxor ferroelectric ceramics for ultrahigh energy storage. *Nat Commun* 2024, **15**: 5232.
[295] Ye WH, Yan B, Meng DD, *et al.* Excellent energy storage properties in $(Bi_{0.4}Na_{0.2}K_{0.2}Ba_{0.2})(Ti_{0.95}Zr_{0.05})O_3$-based high-entropy ceramics by introduction of $Sr(Mg_{1/3}Nb_{1/3}Ta_{1/3})O_3$ medium-entropy endmember. *J Energy Storage* 2024, **82**: 110546.
[296] Liu J, Ren K, Ma CY, *et al.* Dielectric and energy storage properties of flash-sintered high-entropy $(Bi_{0.2}Na_{0.2}K_{0.2}Ba_{0.2}Ca_{0.2})TiO_3$ ceramic. *Ceram Int* 2020, **46**: 20576–20581.
[297] Ma ZY, Yang QQ, Meng B, *et al.* Dielectric and energy storage properties of $(Ba_{0.2}Sr_{0.2}Na_{0.2}Ca_{0.2}La_{0.2})(Zr_xTi_{1-x})O_3$ high-entropy ceramics and thin films. *Int J Appl Ceram Tec* 2024, **21**: 3422–3434.
[298] Zhou SY, Pu YP, Zhao XY, *et al.* Dielectric temperature stability and energy storage performance of NBT-based ceramics by introducing high-entropy oxide. *J Am Ceram Soc* 2022, **105**: 4796–4804.
[299] Ning YT, Pu YP, Zhang XQ, *et al.* Remarkable energy-storage density together with efficiency of above 92% in high-entropy ferroelectric ceramics. *Mater Today Phys* 2024, **43**: 101418.
[300] Niu YW, Zhang F, Zhang X, *et al.* Enhanced energy storage properties of $(Bi_{0.2}Na_{0.2}Ca_{0.2}Ba_{0.2}Sr_{0.2})(Ti_{1-x}Zr_x)O_3$ high entropy ceramics by Zr doping at B-site. *Ceram Int* 2024, **50**: 230–237.
[301] Ning YT, Pu YP, Chen ZM, *et al.* High-entropy ceramics with excellent energy storage performance via screening sintering aids. *J Am Ceram Soc* 2025, **108**: 20205.
[302] Liu TY, Yan B, Chen KP, *et al.* Screening sintering aids for 0.88 $(Bi_{0.4}Na_{0.2}K_{0.2}Ba_{0.2})TiO_3$–0.12$Sr(Mg_{1/3}Nb_{2/3})O_3$ high-entropy dielectric ceramics. *J Am Ceram Soc* 2023, **106**: 836–840.
[303] Ning YT, Pu YP, Zhang Q, *et al.* Improved energy storage capacity of high-entropy ferroelectric perovskite ceramic via flash sintering. *J Power Sources* 2024, **618**: 235205.
[304] Li HT, Li X, Du YX, *et al.* Remarkable energy storage performance of $BiFeO_3$-based high-entropy lead-free ceramics and multilayers. *Chem Eng J* 2024, **499**: 156112.
[305] Zheng BL, Yuan QB, Lin Y, *et al.* High entropy-driven large capacitive energy storage in $BaTiO_3$-based multilayer ceramic capacitors. *Adv Energy Mater* 2026, **16**: 04126.
[306] Surdu VA, Marinică MA, Pătru RE, *et al.* High-entropy lead-free perovskite $Bi_{0.2}K_{0.2}Ba_{0.2}Sr_{0.2}Ca_{0.2}TiO_3$ powders and related ceramics: Synthesis, processing, and electrical properties. *Nanomaterials* 2023, **13**: 2974.
[307] Liu ZB, Liu TY, Zheng BF, *et al.* Enhanced energy storage performance of $(Bi_{0.4}Ba_{0.2}K_{0.2}Na_{0.2})TiO_3$–$NaNbO_3$ high-entropy ceramics under moderate electric fields. *Ceram Int* 2024, **50**: 21869–21877.
[308] Zeng XF, Lin JF, Shen J, *et al.* Giant capacitive energy storage in high-entropy lead-free ceramics with temperature self-check. *Adv Mater* 2024, **36**: 2409059.
[309] Wang XC, Zhang J, Ma XS, *et al.* Machine learning assisted composition design of high-entropy Pb-free relaxors with giant energy-storage. *Nat Commun* 2025, **16**: 1254.
[310] Zeng XF, Lin JF, Dong GL, *et al.* Polymorphic relaxor phase and defect dipole polarization co-reinforced capacitor energy storage in temperature-monitorable high-entropy ferroelectrics. *Nat Commun* 2025, **16**: 1870.
[311] Kong X, Yang LT, Meng FQ, *et al.* High-entropy engineered $BaTiO_3$-based ceramic capacitors with greatly enhanced high-temperature energy storage performance. *Nat Commun* 2025, **16**: 885.
[312] Wu J, Guo J, Ren YF, *et al.* High-entropy La–$(Bi_{0.2}Na_{0.2}Ba_{0.2}Sr_{0.2}Ca_{0.2})TiO_3$ ceramic with ultrastable dielectric performance within 327–689 K and up to 7 GPa. *Adv Electron Mater* 2024, **10**: 2400028.
[313] Shi P, Li H, Zhou Y, *et al.* Energy-storage performance of high-entropy $(NaBiBa)_{0.205}(SrCa)_{0.1925}TiO_3$–$La(Mg_{0.5}Zr_{0.5})O_3$ ceramic under moderate electric fields. *Energies* 2025, **18**: 5838.
[314] Sarkar A, Wang QS, Schiele A, *et al.* High-entropy oxides: Fundamental aspects and electrochemical properties. *Adv Mater* 2019, **31**: 1806236.
[315] Zheng W, Liang GM, Liu Q, *et al.* The promise of high-entropy materials for high-performance rechargeable Li-ion and Na-ion batteries. *Joule* 2023, **7**: 2732–2748.
[316] Ouyang B, Zeng Y. The rise of high-entropy battery materials. *Nat Commun* 2024, **15**: 973.
[317] Ding FX, Ji PX, Han Z, *et al.* Tailoring planar strain for robust structural stability in high-entropy layered sodium oxide cathode materials. *Nat Energy* 2024, **9**: 1529–1539.
[318] Wang B, Ma J, Wang KJ, *et al.* High-entropy phase stabilization engineering enables high-performance layered cathode for sodium-ion batteries. *Adv Energy Mater* 2024, **14**: 2401090.
[319] Gu ZY, Guo JZ, Cao JM, *et al.* An advanced high-entropy fluorophosphate cathode for sodium-ion batteries with increased working voltage and energy density. *Adv Mater* 2022, **34**: 2110108.
[320] Wang LH, You Y, Li Z, *et al.* Achieving highly reversible anionic redox and negligible voltage decay by a high-entropy strategy in Na-ion layered oxide cathodes. *J Colloid Interf Sci* 2026, **701**: 138686.
[321] Zeng Y, Ouyang B, Liu J, *et al.* High-entropy mechanism to boost ionic conductivity. *Science* 2022, **378**: 1320–1324.
[322] Lun ZY, Ouyang B, Kwon DH, *et al.* Cation-disordered rocksalt-type high-entropy cathodes for Li-ion batteries. *Nat Mater* 2021, **20**: 214–221.
[323] Sun Z, Zhao YJ, Sun C, *et al.* High entropy spinel-structure oxide for electrochemical application. *Chem Eng J* 2022, **431**: 133448.
[324] Ma GZ, Zheng Y, Meng FB, *et al.* Understanding the lithiation mechanism of Li_2O-doped spinel high-entropy oxides as anode materials for Li-ion batteries. *Energy Adv* 2023, **2**: 1685–1692.
[325] Wang XF, Liu GF, Tang C, *et al.* A novel high entropy perovskite fluoride anode with 3D cubic framework for advanced lithium-ion battery. *J Alloys Compd* 2023, **934**: 167889.
[326] Zheng DY, Zha JX, Wang YS, *et al.* $Co_{0.2}Sb_{0.2}Fe_{0.2}Mn_{0.2}Ni_{0.2}$ high-entropy alloy carbon nanofiber as anode for lithium/potassium ion batteries. *J Mater Sci* 2025, **60**: 3926–3939.
[327] Han SX, Wang ZQ, Ma Y, *et al.* Fast ion-conducting high-entropy garnet solid-state electrolytes with excellent air stability. *J Adv Ceram* 2023, **12**: 1201–1213.
[328] Umair M, Rana HTH, Yu SZ, *et al.* A medium-entropy Li-garnet solid electrolyte with ultrahigh ionic conductivity and outstanding electrochemical stability for solid-state batteries. *Energy Storage Mater* 2025, **81**: 104484.
[329] Wang PF, Sun ZH, Zhang K, *et al.* High-rate stability of $Na_3V_2(PO_4)_2F_3$ sodium-ion cathode materials enabled by an entropy-increasing strategy. *J Mater Chem A* 2025, **13**: 25855–25864.
[330] Zhan JJ, Huang JW, Li Z, *et al.* Air-stable high-entropy layered oxide cathode with enhanced cycling stability for sodium-ion batteries. *Nano Lett* 2024, **24**: 9793–9800.
[331] Chen TY, Wang SY, Kuo CH, *et al. In operando* synchrotron X-ray studies of a novel spinel $(Ni_{0.2}Co_{0.2}Mn_{0.2}Fe_{0.2}Ti_{0.2})_3O_4$ high-entropy oxide for energy storage applications. *J Mater Chem A* 2020, **8**: 21756–21770.
[332] Li QY, Ho HP, Zeng ZP, *et al.* Local structural distortion and energy gradient enhance lithium ionic conductivity in high-entropy oxide. *Mater Today* 2025, **89**: 26–34.
[333] Bakker E, Zhao LF, Khan K, *et al.* Comprehensive guide for the rational design of high-entropy layered transition metal oxide

cathodes for sodium-ion batteries. *Adv Energy Mater* 2026, **16**: 04677.
[334] Duan LP, Du YC, Liu YJ, *et al.* Recent advances in high-entropy materials for efficient alkali metal-ion batteries. *Chem Soc Rev* 2025, **54**: 11740–11826.
[335] Zheng QF, Ren ZH, Zhang YX, *et al.* Surface phase conversion in a high-entropy layered oxide cathode material. *ACS Appl Mater Inter* 2023, **15**: 4643–4651.
[336] Dang YZ, Xu Z, Yang HD, *et al.* Designing water/air-stable co-free high-entropy oxide cathodes with suppressed irreversible phase transition for sodium-ion batteries. *Appl Surf Sci* 2023, **636**: 157856.
[337] Xu JJ. High-entropy electrolytes in boosting battery performance. *Mater Futures* 2023, **2**: 047501.
[338] Albedwawi SH, AlJaberi A, Haidemenopoulos GN, *et al.* High entropy oxides-exploring a paradigm of promising catalysts: A review. *Mater Design* 2021, **202**: 109534.
[339] Hidalgo-Jiménez J, Akbay T, Sauvage X, *et al.* Mixed atomic-scale electronic configuration as a strategy to avoid cocatalyst utilization in photocatalysis by high-entropy oxides. *Acta Mater* 2025, **283**: 120559.
[340] Dadvari P, Hung WH, Wang KW. High entropy spinel oxide $(AlCrCoNiFe_2)O$ as highly active oxygen evolution reaction catalysts. *ACS Omega* 2024, **9**: 27692–27698.
[341] Zhang LJ, Fan FS, Song XM, *et al.* A novel septenary high-entropy (oxy)hydroxide electrocatalyst for boosted oxygen evolution reaction. *J Materiomics* 2024, **10**: 348–354.
[342] Yang CH, Li J, Li YT, *et al.* High-entropy perovskite air electrode with fluorine-induced Electron pair modulation strategy for stable and efficient reversible protonic ceramic cells. *Chem Eng J* 2025, **519**: 165139.
[343] Okejiri F, Fan JT, Huang ZN, *et al.* Ultrasound-mediated synthesis of nanoporous fluorite-structured high-entropy oxides toward noble metal stabilization. *iScience* 2022, **25**: 104214.
[344] Riley C, De La Riva A, Park JE, *et al.* A high entropy oxide designed to catalyze CO oxidation without precious metals. *ACS Appl Mater Inter* 2021, **13**: 8120–8128.
[345] Liu SX, Du MR, Ge YF, *et al.* Enhancement of high entropy oxide $(La_{0.2}Nd_{0.2}Sm_{0.2}Gd_{0.2}Y_{0.2})_2Zr_2O_7$ mechanical and photocatalytic properties via Eu doping. *J Mater Sci* 2022, **57**: 7863–7876.
[346] Liu S, Pao CW, Chen JL, *et al.* A general flame aerosol route to high-entropy nanoceramics. *Matter* 2024, **7**: 3994–4013.
[347] Pan YT, Liu JX, Tu TZ, *et al.* High-entropy oxides for catalysis: A diamond in the rough. *Chem Eng J* 2023, **451**: 138659.
[348] Ding ZY, Bian JJ, Shuang S, *et al.* High entropy intermetallic–oxide core–shell nanostructure as superb oxygen evolution reaction catalyst. *Adv Sustain Syst* 2020, **4**: 1900105.
[349] Sukkurji PA, Cui YY, Lee S, *et al.* Mechanochemical synthesis of novel rutile-type high entropy fluorides for electrocatalysis. *J Mater Chem A* 2021, **9**: 8998–9009.
[350] Fang SH, Yang TH, He W, *et al.* Solution combustion synthesis of Ce-free high entropy fluorite oxides: Formation, oxygen vacancy and long-term thermal stability. *Ceram Int* 2024, **50**: 7431–7440.
[351] Ho TYK, Pung KS, Lock DWH, *et al.* Direct vat-photopolymerization 3D printing of hierarchically porous SiC loaded with Co/Ni based catalysts by using Pickering emulsions. *Adv Funct Mater* 2024, **34**: 2406132.
[352] Pourmand Tehrani Z, Fromme T, Reichenberger S, *et al.* Laser fragmentation of a high-entropy oxide for enhanced photocatalytic carbon dioxide (CO_2) conversion and hydrogen (H_2) production. *Adv Powder Technol* 2024, **35**: 104448.
[353] Chiu CT, Teng YJ, Dai BH, *et al.* Novel high-entropy ceramic/carbon composite materials for the decomposition of organic pollutants. *Mater Chem Phys* 2022, **275**: 125274.
[354] Chiu IC, Chiang CY, Chang HY, *et al.* Advanced high entropy oxides for seawater splitting. *Sustain Mater Technol* 2025, **45**: 01515.
[355] Han B, Pan QH, Chen YH, *et al.* High-entropy perovskite oxide washcoated porous alumina ceramic as a superb catalyst for activating peroxymonosulfate to eliminate refractory organic pollutants. *Chem Eng J* 2023, **455**: 140828.
[356] Ouyang X, Zhang ZZ, Qin TT, *et al.* Macroporous high-entropy spinel oxide monoliths as efficient oxygen evolution electrocatalyst. *J Am Ceram Soc* 2024, **107**: 8354–8366.
[357] Wang F, Monteverde F, Cui B. Will high-entropy carbides and borides be enabling materials for extreme environments. *Int J Extrem Manuf* 2023, **5**: 022002.
[358] Johnstone GHJ, González-Rivas MU, Taddei KM, *et al.* Entropy engineering and tunable magnetic order in the spinel high-entropy oxide. *J Am Chem Soc* 2022, **144**: 20590–20600.
[359] Mahmood A, Bai Z, Wang T, *et al.* Enabling high-performance multivalent metal-ion batteries: Current advances and future prospects. *Chem Soc Rev* 2025, **54**: 2369–2435.
[360] Gussev IM, O'Quinn EC, Tucker M, *et al.* Systematic study of short- and long-range correlations in RE_3TaO_7 weberite-type compounds by neutron total scattering and X-ray diffraction. *J Mater Chem A* 2023, **11**: 8886–8903.
[361] Du FH, Yang TN, Hao H, *et al.* Giant electrocaloric effect in high-polar-entropy perovskite oxides. *Nature* 2025, **640**: 924–930.
[362] Sharma Y, Musico BL, Gao X, *et al.* Single-crystal high entropy perovskite oxide epitaxial films. *Phys Rev Materials* 2018, **2**: 060404.
[363] Csanádi T, Castle E, Reece MJ, *et al.* Strength enhancement and slip behaviour of high-entropy carbide grains during micro-compression. *Sci Rep-UK* 2019, **9**: 10200.
[364] Feng L, Fahrenholtz WG, Brenner DW. High-entropy ultra-high-temperature borides and carbides: A new class of materials for extreme environments. *Annu Rev Mater Res* 2021, **51**: 165–185.
[365] Gild J, Wright A, Quiambao-Tomko K, *et al.* Thermal conductivity and hardness of three single-phase high-entropy metal diborides fabricated by borocarbothermal reduction and spark plasma sintering. *Ceram Int* 2020, **46**: 6906–6913.
[366] Zhao PB, Zhu JP, Zhang YL, *et al.* A novel high-entropy monoboride $(Mo_{0.2}Ta_{0.2}Ni_{0.2}Cr_{0.2}W_{0.2})B$ with superhardness and low thermal conductivity. *Ceram Int* 2020, **46**: 26626–26631.
[367] Yao Y, Yang F, Zhao XF. Multicomponent high-entropy Zr–Y–Yb–Ta–Nb–O oxides for next-generation thermal barrier coating applications. *J Am Ceram Soc* 2022, **105**: 35–43.
[368] Zhang XL, Bai Y, Liang WC, *et al.* Thermophysical and mechanical properties of $(La_{0.2}Nd_{0.2}Sm_{0.2}Eu_{0.2}Me_{0.2})_2Zr_2O_7$ (where Me = Gd, Y, Yb, Lu) high-entropy ceramics. *Ceram Int* 2025, **51**: 19282–19292.
[369] Batra R, Song L, Ramprasad R. Emerging materials intelligence ecosystems propelled by machine learning. *Nat Rev Mater* 2021, **6**: 655–678.
[370] Madika B, Saha A, Kang C, *et al.* Artificial intelligence for materials discovery, development, and optimization. *ACS Nano* 2025, **19**: 27116–27158.
[371] Zuccarini C, Ramachandran K, Jayaseelan DD. Material discovery and modeling acceleration via machine learning. *APL Mater* 2024, **12**: 090601.
[372] Vasudevan R, Pilania G, Balachandran PV. Machine learning for materials design and discovery. *J Appl Phys* 2021, **129**: 070401.
[373] Nam C. Prediction of mechanical properties of high-entropy ceramics by deep learning with compositional descriptors. *Mater Today Commun* 2023, **35**: 105949.
[374] Zhu XH, Zhang Y. Functional applications and data-driven design of high-entropy ceramics. *High Entropy Alloys Mater* 2024, **2**: 219–245.
[375] Zhou Q, Xu F, Gao CZ, *et al.* Machine learning-assisted mechanical property prediction and descriptor-property correlation analysis of high-entropy ceramics. *Ceram Int* 2023, **49**: 5760–5769.
[376] Zhang J, Xu B, Xiong YX, *et al.* Design high-entropy carbide ceramics from machine learning. *Npj Comput Mater* 2022, **8**: 5.
[377] Liu JC, Wang AZ, Gao P, *et al.* Machine learning-based crystal structure prediction for high-entropy oxide ceramics. *J Am Ceram Soc* 2024, **107**: 1361–1371.
[378] Mitra R, Bajpai A, Biswas K. Machine learning based approach for

phase prediction in high entropy borides. *Ceram Int* 2022, **48**: 16695–16706.
[379] ManchLI-GordchLAF, Panadero-Medianero P, Blázquez JS. Descriptors for predicting single- and multi-phase formation in high-entropy oxides: A unified framework approach. *Materials* 2025, **18**: 3862.
[380] Mitra R, Bajpai A, Biswas K. ADASYN-assisted machine learning for phase prediction of high entropy carbides. *Comp Mater Sci* 2023, **223**: 112142.
[381] Attari V, Arroyave R. Machine learning-assisted high-throughput exploration of interface energy space in multi-phase-field model with CALPHAD potential. *Mater Theory* 2022, **6**: 5.
[382] Guo LX, Huang SW, Li W, *et al.* Theoretical design and experimental verification of high-entropy carbide ablative resistant coating. *Adv Powder Mater* 2024, **3**: 100213.
[383] Zou JY, Tang L, He WW, *et al.* High-entropy oxides: Pioneering the future of multifunctional materials. *ACS Nano* 2024, **18**: 34492–34530.
[384] Wu XY, Li W, Huang ZH, *et al.* Dielectric and third-order nonlinear optical properties of high-entropy perovskite oxides $(La_{0.2}Ba_{0.2}Sr_{0.2}Ca_{0.2}Bi_{0.2})(Ti_{1-x}Sn_x)O_3$ (x = 0–0.5. *Ceram Int* 2025, **51**: 32090–32099.
[385] Luo J. From high-entropy ceramics to compositionally complex ceramics and beyond[J]. *Journal of Materiomics*, 2026: 101173.
[386] Qiu SH, Xiang HM, Dai FZ, *et al.* Medium-entropy $(Me,Ti)_{0.1}(Zr,Hf,Ce)_{0.9}O_2$ (Me = Y and Ta): Promising thermal barrier materials for high-temperature thermal radiation shielding and CMAS blocking. *J Mater Sci Technol* 2022, **123**: 144–154.
[387] Lin MT, Zu JH, Wang Y, *et al.* Novel $Zr_{1-3x}Y_xGd_xNb_xO_2$ medium-entropy oxide ceramics for advanced thermal barrier coatings. *Ceram Int* 2025, **51**: 53040–53046.
[388] Chen Q, Wu JZ, Xu J, *et al.* Thermophysical and mechanical properties of medium-entropy rare-earth zirconate ceramics. *Ceram Int* 2025, **51**: 54315–54324.
[389] Zhang XX, Yang X, Luo X, *et al.* Formation mechanism of (Ti,Zr,Hf)C medium-entropy carbide derived from polymer precursors and its modification on the ablative mechanism of C/C–SiC composites. *Corros Sci* 2024, **230**: 111935.
[390] Wang YW, Zhang XY, Yang MY, *et al.* A-site high entropy and B-site medium entropy double perovskite structure cathode material for solid oxide fuel cells. *J Alloys Compd* 2025, **1022**: 180002.
[391] Shen LY, Du ZH, Zhang Y, *et al.* Medium-entropy perovskites Sr$(Fe_\alpha Ti_\beta Co_\gamma Mn_\zeta)O_{3-\delta}$-as promising cathodes for intermediate temperature solid oxide fuel cell. *Appl Catal B Environ* 2021, **295**: 120264.
[392] Li XL, Shi CX, Zhang GJ, *et al.* A medium-entropy perovskite oxide $La_{0.7}Sr_{0.3}Co_{0.25}Fe_{0.25}Ni_{0.25}Mn_{0.25}O_{3-\delta}$ as intermediate temperature solid oxide fuel cells cathode material. *Ceram Int* 2023, **49**: 30187–30195.
[393] Sarker P, Harrington T, Toher C, *et al.* High-entropy high-hardness metal carbides discovered by entropy descriptors. *Nat Commun* 2018, **9**: 4980.
[394] Hossain MD, Borman T, Oses C, *et al.* Entropy landscaping of high-entropy carbides. *Adv Mater* 2021, **33**: 2102904.
[395] Fan W, Bai Y, Liu YF, *et al.* Principal element design of pyrochlore-fluorite dual-phase medium- and high-entropy ceramics. *J Mater Sci Technol* 2022, **107**: 149–154.
[396] Wang YH, Jin YJ, Wei T, *et al.* Size disorder: A descriptor for predicting the single- or dual-phase formation in multi-component rare earth zirconates. *J Alloys Compd* 2022, **918**: 165636.
[397] Huang TT, Liu YF, Fan W, *et al.* Investigations on the mechanical and thermal properties of multicomponent dual-phase rare-earth zirconate ceramics. *J Alloys Compd* 2024, **1007**: 176425.
[398] He JJ, He G, Wang PP, *et al.* Pyrochlore-fluorite dual-phase high-entropy $RE_2(Ce_{0.2}Zr_{0.2}Hf_{0.2}Sn_{0.2}Ti_{0.2})_2O_7$ ($RE_2HE_2O_7$, RE = La, Nd, Sm, Eu, Gd, Dy) ceramics with glass-like thermal conductivity. *J Mater Sci* 2022, **57**: 17563–17576.
[399] Li ZF, Bai Y, Hao JJ, *et al.* High-entropy $(La_{0.2}Nd_{0.2}Y_{0.2}Yb_{0.2}Lu_{0.2})_2Zr_2O_7$ ceramic: A novel dual-phase high-entropy ceramic. *J Eur Ceram Soc* 2025, **45**: 117361.
[400] Chen L, Luo KR, Li BH, *et al.* Mechanical property enhancements and amorphous thermal transports of ordered weberite-type RE_3Nb/TaO_7 high-entropy oxides. *J Adv Ceram* 2023, **12**: 399–413.
[401] Li BH, Wang JK, Chen L, *et al.* Breaking the trade-off relationship between thermal conductivity and toughness of ferroelastic oxide ceramics via a high-density dislocation strategy. *Adv Mater* 2026, **38**: 23083.
[402] Zhang Y, Ni BY, Liu Y, *et al.* Enhanced fracture toughness of high entropy boride by adding SiC. *Ceram Int* 2024, **50**: 37208–37216.
[403] Lu L, Du PC, Jiang TX, *et al.* Comparison of oxidation resistance of high-entropy $(Ti_{0.2}Zr_{0.2}Hf_{0.2}Ta_{0.2}Nb_{0.2})C$/SiC composites prepared by different methods at 1300–1600 °C. *J Eur Ceram Soc* 2025, **45**: 116885.
[404] Zhao JH, Fu YQ, Lv JS, *et al.* Insights into high entropy ceramics under extreme conditions: Ablation behavior and microstructure evolution of C/C–$(Ti_{0.2}Zr_{0.2}Hf_{0.2}Nb_{0.2}Ta_{0.2})C$ composites. *J Eur Ceram Soc* 2025, **45**: 117616.
[405] Ostovari Moghaddam A, Cabot A, Trofimov EA. Does the pathway for development of next generation nuclear materials straightly go through high-entropy materials. *Int J Refract Met H* 2021, **97**: 105504.
[406] Zhou L, Li F, Liu JX, *et al.* High-entropy thermal barrier coating of rare-earth zirconate: A case study on $(La_{0.2}Nd_{0.2}Sm_{0.2}Eu_{0.2}Gd_{0.2})_2Zr_2O_7$ prepared by atmospheric plasma spraying. *J Eur Ceram Soc* 2020, **40**: 5731–5739.
[407] Wei P, Bai H, Liu YW, *et al.* Improved CMAS corrosion resistance of high-entropy rare-earth monosilicates by multicomponent synergistic effects. *Ceram Int* 2025, **51**: 32175.
[408] Guo J, Xiao WR, Zhang XY, *et al.* Achieving excellent energy storage properties in fine-grain high-entropy relaxor ferroelectric ceramics. *Adv Electron Mater* 2022, **8**: 2200503.
[409] Zhu BH, Wang XC, Zhang J, *et al.* Designing Pb-free high-entropy relaxor ferroelectrics with machine learning assistance for high energy storage. *J Am Chem Soc* 2025, **147**: 27912–27921.
[410] Zhou YC, Zhao B, Chen H, *et al.* Electromagnetic wave absorbing properties of TMCs (TM = Ti, Zr, Hf, Nb and Ta) and high entropy $(Ti_{0.2}Zr_{0.2}Hf_{0.2}Nb_{0.2}Ta_{0.2})C$. *J Mater Sci Technol* 2021, **74**: 105–118.
[411] Chen DQ, Yan N, Cao XF, *et al.* Entropy regulation in $LaNbO_4$-based fergusonite to implement high-temperature phase transition and promising dielectric properties. *J Adv Ceram* 2023, **12**: 1067–1080.
[412] Feng L, Fahrenholtz WG, Hilmas GE, *et al.* Synthesis of single-phase high-entropy carbide powders. *Scripta Mater* 2019, **162**: 90–93.
[413] Mao HR, Dong ET, Jin SB, *et al.* Ultrafast high-temperature synthesis and densification of high-entropy carbides. *J Eur Ceram Soc* 2022, **42**: 4053–4065.
[414] Wei XF, Qin Y, Liu JX, *et al.* Gradient microstructure development and grain growth inhibition in high-entropy carbide ceramics prepared by reactive spark plasma sintering. *J Eur Ceram Soc* 2020, **40**: 935–941.
[415] Gu JF, Zou J, Sun SK, *et al.* Dense and pure high-entropy metal diboride ceramics sintered from self-synthesized powders via boro/carbothermal reduction approach. *Sci China Mater* 2019, **62**: 1898–1909.
[416] Song WY, Lu YJ, Yang LT, *et al.* Enhancement of densification and mechanical property of $(Hf_{0.2}Zr_{0.2}Ti_{0.2}Nb_{0.2}Ta_{0.2})N$ high-entropy bulk ceramic via silicon carbide addition. *J Adv Ceram* 2025, **14**: 9221004.
[417] Luo SC, Guo WM, Plucknett K, *et al.* Low-temperature

densification of high-entropy (Ti,Zr,Nb,Ta,Mo)C–Co composites with high hardness and high toughness. *J Adv Ceram* 2022, **11**: 805–813.

[418] Xia LS, Dong S, Wang LM, *et al.* Mechanisms for low temperature densification and enhanced mechanical properties of (Ti,Zr,Hf,Nb,Ta)(C,N) using $CrSi_2$ as an additive: Formation of $(Ti,Zr,Nb)_2Cr_4Si_5$ and grain boundary strengthening. *Sci China Mater* 2026, **69**: 361–373.

[419] Spiridigliozzi L, Dell'Agli G, Esposito S, *et al.* Ultra-fast high-temperature sintering (UHS) of $Ce_{0.2}Zr_{0.2}Y_{0.2}Gd_{0.2}La_{0.2}O_{2-\delta}$ fluorite-structured entropy-stabilized oxide (F-ESO). *Scripta Mater* 2022, **214**: 114655.

[420] Li B, Qian B, Xu Y, *et al.* Fine-structured CoCrFeNiMn high-entropy alloy matrix composite with 12 wt% TiN particle reinforcements via selective laser melting assisted additive manufacturing. *Mater Lett* 2019, **252**: 88–91.

[421] Jiang MD, Li R, Li BZ, *et al.* Lightweight and ultrastrong 3D nanoarchitected high-entropy ceramic metamaterials. *Sci Adv* 2025, **11**: 6632.

[422] Liu YH, Wang G, Zhao Y, *et al.* Joining of SiC using CoFeCrNiCuTi high entropy alloy filler by electric current field assisted sintering. *J Eur Ceram Soc* 2022, **42**: 1995–2003.

[423] Zhang P, Lou ZH, Gong LY, *et al.* High-entropy $MTiO_3$ perovskite oxides with glass-like thermal conductivity for thermoelectric applications. *J Alloys Compd* 2023, **937**: 168366.

[424] Wang SY, Chen TY, Kuo CH, *et al.* operando synchrotron transmission X-ray microscopy study on (Mg,Co,Ni,Cu,Zn)O high-entropy oxide anodes for lithium-ion batteries. *Mater Chem Phys* 2021, **274**: 125105.

[425] Vayer F, Decorse C, Bi.org/10.10et al. New entropy-stabilized oxide with pyrochlore structure: $Dy_2(Ti_{0.2}Zr_{0.2}Hf_{0.2}Ge_{0.2}Sn_{0.2})_2O_7$. *J Alloys Compd* 2021, **883**: 160773.

[426] Dai FZ, Xu YF, Wang YN, *et al.* A general deep neural network potential model for transition metal carbides. *J Am Ceram Soc* 2025, **108**: 20647.

[427] Mei ZG, Ye B, Yacout AM, *et al.* First-principles study of the surface properties of uranium carbides. *J Nucl Mater* 2020, **542**: 152257.